MIXING AND CIRCULATION OF LAKES AND RESERVOIRS WITH AIR PLUMES

by

Robert S. Torrest
John Wen

Department of Engineering

COMPLETION REPORT

Project A-030-NH

under Grant No. 14-31-0001-3829

WATER RESOURSE RESEARCH CENTER
UNIVERSITY OF NEW HAMPSHIRE
DURHAM, NEW HAMPSHIRE

MIXING AND CIRCULATION OF LAKES AND RESERVOIRS WITH AIR PLUMES

by

Robert S. Torrest
John Wen

Department of Chemical Engineering

COMPLETION REPORT

Project A-030-NH

under Grant No. 14-31-0001-3829

WATER RESOURCE RESEARCH CENTER
UNIVERSITY OF NEW HAMPSHIRE
DURHAM, NEW HAMPSHIRE

ACKNOWLEDGMENT

The work upon which this publication is based was supported in part by funds provided by the United States Department of the Interior, Office of Water Research and Technology, as authorized under the Water Resources Act of 1964, Public Law 88-379, through the Water Resource Research Center of the University of New Hampshire. The author wishes to thank Gordon L. Byers, Chairman of the Water Resource Research Center, University of New Hampshire for his assistance and encouragement and Mr. Ken Palmer, Chemical Engineering Department, University of New Hampshire who was instrumental in equipment construction.

PREFACE

The results presented here are based on experiments completed by May 1974. Unfortunately another year of planned work dealing with the effects of simulated wind-induced surface currents, initial stratification, bottom sediments, and dissolved oxygen buildup was not carried out since R. S. Torrest left the University.

There are a number of relatively minor inconsistencies in this report. They will not obscure the intended meaning. After nearly two years of manuscript preparation by mail between Houston and Durham the text is as clean as available time allows.

Robert S. Torrest

May 1976

CONTENTS

1. INTRODUCTION

The eutrophication of lakes and reservoirs is a growing world-wide problem. Increased nutrient levels due to the influx of organic and industrial wastes encourage the growth of a variety of micro-organisms. These, in turn, may lead to several undesirable conditions, ranging from "pea soup" type blue-green alga blooms coating the surface waters to unpleasant odor or taste of water for municipal supplies. Heavy blooms greatly reduce light penetration. As dead algae, fish, and other organic matter settle to the bottom, oxygen deficiencies are likely in the lower water layers which, with the possible release of toxins, may have substantial adverse effects on fish populations. These problems are intensified when thermal stratification is greatest, since only the surface layer or epilimnion is aerated due to winds and circulation. Below the epilimnion, the thermocline is the region of rapid temperature drop and reduction of dissolved oxygen (DO). The lowest layer of cold (most dense) water will tend to remain stagnant while decomposing organic material will deplete the D.O. Eventually iron and manganese will be reduced and go into solution, while sulfate reduction releases hydrogen sulfide. As carbon dioxide is produced, the pH is lowered, and organic material on the lake bottom will undergo anaerobic decay. The full scope of the nature and problems of eutrophication are discussed in the proceedings of a recent symposium of the National Academy of Sciences (1) and in the comprehensive literature review (2).

Control of excess nutrient input to lakes and reservoirs provides the most direct and effective means of prevention of artificial eutrophication. Unfortunately, in many cases, there is no immediate or economical alternative to the high level of nutrient input. Instead, some treatment is required to best minimize or alleviate the decline of water quality that would occur given no immediate remedial action. Available treatment techniques favored in the past include chemical additions (e.g., copper sulfate), dredging, and plant removal (e.g., see reference 13). However, such treatments may have undesirable immediate or long-term effects in addition to often being ineffective and costly.

More recently, there have been an increasing number of studies on the use of artificial circulation to mix and destratify lakes and reservoirs. Liquid pumping (3), an airlift pump (4), a floating mechanical aerator (5), and diffuse aeration from a manifold near the bottom of the reservoir (6), have been tried. Artificial circulation conveniently induced by aeration from the lake bottom brings up the cold bottom water that in summer might be depleted of D.O. The mixing tends to make temperature nearly constant with depth, while breaking up and distributing any surface algal bloom and delivering oxygen to lower levels within the zone of circulation.

Several of the early U. S. studies of mixing and destratification are conveniently available in reference (7), along with discussions and related material. Changes in temperature of D.O. are usually reported along with data for carbon dioxide, ionic concentrations, suspended solids and algal counts. Limnological changes due to aeration and destratification have been described by Wirth and Dunst (8), Johnson (9), and Fast et al (10). Haynes (11) has presented comprehensive results for Kezar Lake, a small eutrophic lake in North Sutton, New Hampshire. This 182 acre lake was aerated to control algal bloom after copper sulfate treatments caused substantial fish kills with little effect on the algae. Procedures and discussion of the aeration treatment are discribed in reference (12) which also includes a good reference list on artificial circulation studies and related topics. More recent detailed aeration studies are available in references (14), (15), (16), (17), and including mechanical pumping in (18). Fast (6) has presented detailed results for the aeration of El Capitan Reservoir near San Diego. He also described the various air injection techniques that have been proposed and used. Economic benefits, particularly with regard to improved taste and odor of aerated reservoir water and reduced chlorine requirements and evaporation are also discussed. A similar study at Lake Wohlford, California was presented by Koberg and Ford (19).

The extent of the literature cited suggests the widespread and growing interest in mixing and destratification by aeration. The studies in general tend to be descriptive. That is, the effect of aeration for a specified time in a given lake on a variety of parameters such as temperatures or D.O., were measured. There is usually little or no experimentation with, for example, air input rate, aerator location or intermittent operation in a given situation because of limited time, money, or objectives. Hence, although much work on artificial mixing by aeration or mechanical pumping has been performed and is currently underway, (see, for example, recent Water Resources Research Catalogs) treatment effectiveness in terms of the variation of D.O. or temperature distribution with time and position cannot generally be assessed in advance. Guidelines for required air input are based on previous experience in what was hopefully a similar situation. Where quantitative design is considered, it is usually based on the comparison of stability changes to the total energy input, with stability estimated from the existing stratification, (see, for example, references (18), (19) and paper (9), (10) and (12) of reference (7)). Unfortunately the technique is cumbersome and subject to misinterpretation.

A measure of the state of design in reservoir mixing is provided by a report of the AWWA's Quality Control in Reservoirs Committee (20). Almost all respondents to a questionnaire considered their mixing projects a success in terms of improved water treatment or raw-water quality. However, operating costs were found to vary from $0.01 to $14/mil gal/yr while initial costs varied from $0.15 to $60/mil gal. Diffused-aeration accounted for 55 percent of the installations (with typical rates of 1 scfm per foot of manifold) but the "Air-Aqua" System (Hinde Engineering Company) used in 33 percent of the cases, has an aeration rate of about 0.02 cfm/ft.

The wide variation in costs will determine whether and to what extent mixing will be carried out. Since overall success varies from case to case and is not clearly related to system cost, the difficulties in choosing the "proper" or "most effective" or optimum" system are evident. Fortunately, a large literature describing the fluid mechanics of air-screens or "point" sources is available as cited in the next section. When this material is supplemented with the experimental results developed during this study, it is possible to predict velocities in the zone of circulation as well as the cell size and efficiency (defined as the induced water flow rate compared to the aeration rate) for the full range of aeration rates and water and manifold depths. The relative efficencies of aeration and mechanical pumping may also be evaluated.

A simple mass transfer model with one parameter dependent primarily on the aeration rate, is shown to provide a good description of D.O. build-up in the primary circulation cell. Some experiments to investigate the influence of initial stratification on aeration induced mixing are also described. Although another year of study was to be spent largely on the influence of initial stratification, it may be possible to make estimates of the time required to eliminate stratification on the basis of available theoretical and experimental studies of different but related problems. These estimates may then be compared to the results of lake and reservoir studies to evaluate their utility.

2. BACKGROUND

The fluid mechanics of lake aeration can be conveniently split into two parts. They are (1) the entrainment and upwelling of fluid carried along immediately over the site of air injection, and (2) the overall circulation developed due to aeration. The first part has been studied in some detail and may also be compared to the problem of buoyancy input, for example, from a heated line source to the surrounding fluid. The overall circulation is more complex and has not been successfully analyzed, although with this study substantial experimental results are now available. The circulation will depend not only on the rate of air injection and type and location of the injection system, but also on lake geometry and any natural drift or flow within the lake as well as that caused by winds. We will, for now, ignore the complications caused by initial stratification and assume that density does not vary with height.

Air "curtains" or "screens" composed of a horizontal line source of air injected below the water surface were first analyzed by G.I. Taylor in 1942. His results were later published (21) in conjunction with an experimental study by J.H. Evans (22) in 1955 to show how the surface current due to an air curtain could be used to damp waves. This "pneumatic breakwater" technique has since been studied in some detail (e.g., 23 to 26) as has the equivalent hydraulic breakwater.

Other applications, including use as barriers to reduce salt intrusion through locks (27), to prevent ice formation (28) and to protect dredges (29), have been described. More recently, the surface currents generated by air screens have been studied as a means of oil-spill containment (30-32).

There are now a variety of studies of varying complexity dealing with the fluid mechanics of air screens and related flows. These studies provide much of the required information for the first part of our consideration of lake and reservoir aeration. They will be cited here from the simplest to the most detailed to provide the background with which to evaluate and compare the experimental results described later and to aid in system design. We will concentrate on line sources for now. Similar material for point sources will be introduced later as needed.

The simplest analysis of the flow due to air screens is that which assumes the air screen may be approximated as that due to buoyancy alone, neglecting the compressibility of the air, manifold characteristics, and the differential velocity between rising air bubbles and the water. The flow is then equivalent to the free convection produced by a heated line source (wire or rod) and has been analyzed in detail by Rouse, Yih and Humphreys (33) and many others (e.g., 34 to 39).

Following Rouse et al (33) consider the two dimensional flow over a line source at the origin of coordinates. The local mean velocity in the vertical direction y is denoted by u and that in the lateral direction x is denoted by v.

The mean local change in weight density $\Delta\gamma$ is assumed sufficiently great to produce vertical acceleration although the corresponding change in mass density may be neglected in comparison with the density itself, ρ, (Boussinesq assumption). Then, with the usual assumptions made for free turbulent flows, the differential equation of momentum conservation integrates to

$$d/dy\int_0^\infty \rho u^2 dx = -\int_0^\infty \Delta\gamma dx \qquad 2\text{-}1.$$

so that the vertical gradient of momentum flux is equal to the buoyancy of a layer of unit thickness.

Integration of the diffusion equation for $\Delta\gamma$ shows that the buoyancy flux (Kinematic weight flux) per unit length of source is constant

$$d/dy\int_0^\infty u\Delta\gamma dx = 0 \qquad 2\text{-}2.$$

With the assumption of dynamic similarity at all elevations such that dimensionless velocity and $\Delta\gamma$ depend only on (x/σ) where σ is a linear characteristic of the velocity profile (e.g., the half width) the conservation equations cited with that for energy show that

$$U_{max} \simeq X^0 \qquad 2\text{-}3.$$
$$\Delta\gamma_{max} \simeq X^{-1}$$
$$\sigma \simeq X$$

Then the constancy of the buoyancy flux ω above a source of length L is

$$\omega = W/L = 2\int_0^\infty u\Delta\gamma dx = q_o\rho g \qquad 2\text{-}4.$$

and is simply a measure of the output of the source where q_o is the volume flux per unit length of the source.

$\Delta\gamma$ is related to the temperature variation, ΔT as $\Delta\gamma/\gamma = -\Delta T/T$ and the rate of heat output from a line source is given by

$$H/L = 2C_p\rho\int_0^\infty u\Delta T dx \qquad 2\text{-}5.$$

Comparison of equations 2-4 and 2-5 shows that

$$W = Hg/C_pT \qquad 2\text{-}6.$$

With

$$u = u_{max}f(x/y) \qquad 2\text{-}7.$$

Taylor (21) used Schmidt's result (40) for a heated wire that

$$u_{max} \propto (Hg/\rho C_pT)^{1/3} \qquad 2\text{-}8.$$

also evident from dimensional analysis (33).

With the constant of proportionality found from experiment to be 1.9, Taylor estimated that

$$u_{max} = 1.9(q_o g)^{1/3} \qquad 2\text{-}9.$$

as may be verified using equations 2-4 and 2-6 since $q_o = H/\rho C_p T$ for bubble. release to produce a flow in water equivalent to that produced in air by release of H. Rouse et al (33) in their tests with heated air found the experimental results to scatter about the curve given by

$$u = 1.80\left(\frac{W/L}{\rho}\right)^{1/3} \exp(-32x^2/y^2) \qquad 2\text{-}10.$$

While the general form of equation 2-9 does indeed describe the variation in vertical velocity with aeration rate per unit length the constants in equation 2-9 (even in the lower value in equation 2-10) are upper limits to those observed for aeration from a manifold: that is, the analogy between air input and heat release is not exact.

In 1968, the first detailed analytical and experimental study of the flow induced by air-bubble systems was presented by Kobus.[44] He included bubble expansion by assuming the average rise velocity of the bubble stream $\bar{u}_b$, to be independent of elevation. Then, the momentum flux at y is given by the sum of the initial momentum flux and buoyancy force as

$$M(y) = C_D U_o q_a - \frac{P_{atm} q_a}{\bar{u}_b} \ln\left(1 - \frac{y}{h^*}\right) \qquad 2\text{-}11.$$

where q_a is the volumetric aeration rate per unit length of manifold, u_o is the exit velocity, C_D is a discharge coefficient and h* is given by

$$h^* = h + P_{atm}/\gamma_w \qquad 2\text{-}12.$$

where h is the manifold depth, $\gamma_w = \rho_w g$ and Patm is the atmospheric pressure. Since the buoyancy term grows rapidly with increasing y the contribution due to the initial momentum flux soon becomes negligible. Even for the relatively small water depths of about three feet, for the tests to be described, the initial momentum flux is only a few percent of the total value and the expected variations are observed.

Kobus went on to show that for Gaussian velocity profiles similar with respect to an analytical origin at y_o, with

$$u(x,y)/um(y) = e^{-x^2/2C'^2(y+y_o)^2} \qquad 2\text{-}13.$$

and Gaussian density profiles with C' replaced by C'α', the centerline velocity was given by

$$um(y) = \left(\frac{-Patm(qa)\ln(1-\frac{y}{h^*})}{\sqrt{\pi}\rho w \bar{u}_b C'(y+y_o')} \right)^{1/2} \qquad 2\text{-}14.$$

in which y_o is the position of the analytical origin while the volume flux ratio is

$$q(y)/qa = \left(\frac{-2\sqrt{\pi}PatmC'(y'+y_o')}{\rho w \bar{u}_b qa} \ln(1-\frac{y}{h^*}) \right)^{1/2} \qquad 2\text{-}15.$$

and the momentum flux ratio is

$$M(y)/M_o = -(P_o/Patm)\frac{gRTb_o}{u_b qa}\ln(1-\frac{y}{h^*}) \qquad 2\text{-}16.$$

where b_o is the slot width. Equation 2-14 predicts a slow increase in centerline velocity with distance above the manifold. Kobus shows the variation of C and $\bar{u}_b$ with aeration rate. A $(qa)^{1/3}$ dependence in agreement with Taylor's prediction was also observed. The volume flux ratio varied as $qa^{-1/2}$ and with a somewhat less than linear dependence on distance from the manifold. More recently, Cederwall and Ditmars extended the analytical treatment as described later, but with little advantage over Kobus' analysis in view of increased complexity.

There is relatively little published material on the size of the circulation cell induced by lake or reservoir aeration. In a discussion of flows induced by pumping, Hogan et al (89) used a potential flow analysis to conclude that the cell diameter for a point source was approximately four times the water depth. Hamilton and Baines (49) had earlier presented some limited data for point source aeration that shows the surface velocity had decreased about 50 percent of its initial value at ≈3.3 ft in an eight foot square tank with a depth of 5 1/2 feet. These results are evidently in question due to the influence of the tank walls on the flow.

There is somewhat more data on the extent of the circulation cell induced by aeration from a manifold or perforated straight pipe. Bulson (90) shows a few data points indicating a surface current to about eight times the water depth for depths to 34 feet, and even beyond at smaller depths, although Bulson notes some inconsistencies. Basco (31) later presented data with considerable scatter out to about 2.6 times the depth with extrapolation to zero surface velocity at three times the depth. Jones (30) shows surface velocity falling rapidly from about X = 2D, but the data extends out only to somewhat less than three times the depth.

The detailed and consistent results presented in the following sections shows circulation cell sizes and velocity profiles for a wide range of aeration rates and geometries and should help to define and clarify the trends indicated in past studies.

3. LINE SOURCE AIR PLUMES

Previous studies with linear manifolds have already been cited (e.g., references 22, 26, 30 and 31). Provost (42) examined in more detail some of the flow characteristics of aeration induced circulation from a perforated pipe set across tanks that were one foot wide, eight feet long, and either two or four feet high. Wen (43) later extended Provost's work to include the influence of manifold characteristics, a wider range of aeration rates and a larger scale channel to one and one-half or two feet and 12 feet long. Wen was supported as a research assistant on the OWRR project while Provost had only limited summer support. Both studies are in essential agreement in their results which are presented below.

A sketch of aeration induced flow patterns with defining notation is presented in Figure 3-1. The water depth is d, and the distance from the aerator to the surface D. For manifold aeration (i.e., a linear source) the vertical coordinate is y and the horizontal distance from the manifold is x. The air plume entrains surrounding water as it rises to develop a velocity profile U with maximum velocity U_m. This flow is deflected at the free surface to form horizontal (lateral) currents of thickness δ and maximum velocity V_s at the surface and a velocity profile V(y). The return current which must equal the mass flow of the surface current is also sketched.

Figure 3-1. Definition Sketch of Induced Flow Patterns

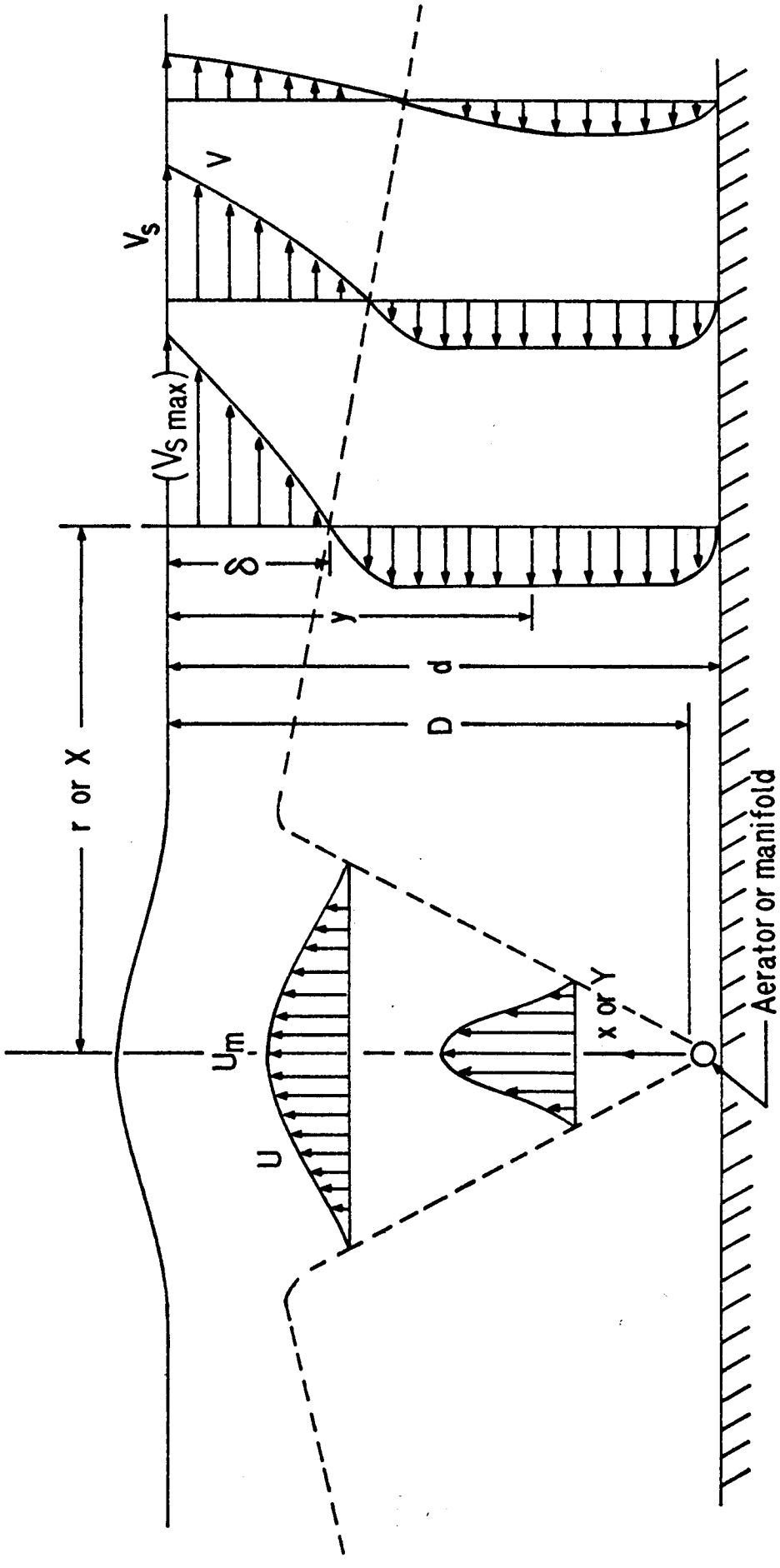

Taylor (21) by analogy with the flow field induced above a horizontal line source of heat, considering aeration to be equivalent to pure buoyancy input, showed that the maximum vertical velocity, U_m produced by a volumetric aeration rate per unit length, q_a, was given by

$$U_m = k(q_a g)^{1/3} = V_{smax} \qquad 3\text{-}1$$

where g is the acceleration of gravity and the constant k was taken to be 1.9 as noted previously. If no energy is lost when the rising flow is deflected by the free surface, then the maximum horizontal velocity $(V_s)_{max}$ would be equal to U_m. From the measured angle of the rising plume, Taylor suggested that the depth of the horizontal current would be 0.28D. Taylor, of course, recognized the idealization implied in his model; in particular, that real bubble rise velocities will be more rapid than that of a bubble swarm that is simply a buoyancy source, and on the basis of some aeration experiments by Evans (22) knew that the proportionality constant k in equation 3-1 was less than 1.9.

A variety of experiments cited earlier have since confirmed the general form of equation 3-1 but with k varying from about 1.1 to 1.9 apparently depending on manifold design, water depth, and aeration rate, and correction of aeration rates to standard conditions. The more detailed studies found k = 1.47 to 1.6 for typical aeration rates.

In the following sections we will examine the detailed characteristics of aeration induced circulation. It will, however, be worthwhile to remember that equation 3-1 provides a convenient first estimate to system characteristics (i.e., water circulation) when combined with some information on the size and shape of the surface current.

THE VERTICAL PLUME

Rouse et al (33) and others have shown that for a buoyant plume the rise of velocity is independent of distance from the source while the convection zone expands linearly with y. However, by allowing for expansion of the air bubbles as they rise, Kobus (44) was able to show that the rise velocity was given by equation 2-14. Kobus (44) found that y_o = 0.8 m in his experiments with a manifold depth of 4.5 m. y_o was independent of aeration rate. Both the rate of spread C, and $\bar{U}_b$ were found to be weak functions of the aeration rate, both increasing with $q_a^{0.15}$. The overall variation of U_m with x is a general agreement with equation 2-14 and $U_m(y)$, while almost constant over much of the depth, actually increases at a decreasing rate until the influence of the free surface is felt at about 80% of the distance from the manifold. Kobus found his assumed Gaussian distribution curves were in good agreement with measured profiles.

Cederwall and Ditmars (41) developed a more elaborate model for the vertical air-bubble plume by allowing for the differential velocity between the rising bubbles and water; the assumption that the rate of entrainment was directly proportional to the centerline velocity, and the use of a turbulent Schmidt number to characterize the bubble lateral spread. By allowing the slip velocity to go to zero, the case of small bubbles at the source, that is, an approach to "pure buoyancy input" or "ideal design" is simulated. Kobus' experimental results were used to assign values to parameters such as the entrainment coefficient. Lateral spreading of bubbles is slow relative to plume expansion with a spreading ratio $\lambda = .2$ and constant throughout the plume rise (calculations were not sensitive to λ variation from 0.1 to 0.3). The turbulent Schmidt number $Sc_t = 1/\lambda^2 \simeq 25$. With variation of $\bar{U}_b$ and α a rough agreement of numerical prediction with experiment was obtained. Unfortunately, α is a strong function of airflow rate q_a at low flow rates with possible approach to an asymptotic value of 0.16 at a high q_a, the value Cederwall and Ditmars chose to match the data. The slip velocity $\bar{u}_b = 0.3$ m/sec is based on rise velocities of single bubbles in still water over a wide range of sizes. The authors suggest that it is appropriate except at low discharge rate per orifice (as in the case of a porous tube). The plume is most effectively generated when bubbles are very small, their "ideal design". Other considerations will be presented later to show why this "ideal" may not be an optimum design.

In our experiments (42 and 43) only limited measurements of the rising plume were made because of the relatively limited depth (i.e., the structure is not fully developed based on Kobus[4] data) and local non-uniformities due to the incomplete decay and merging of the individual point sources that made up the line source. Still, symmetical profiles were observed, although longer than usual averaging was required because of oscillations of the plume. Velocities were observed to increase with distance from the manifold until $y \simeq 0.6D$ and were then approximately constant until $y = 0.3$ to $0.4D$ before decreasing due to the stagnation zone at the free surface. Maximum vertical velocity was observed to increase with depth from D = 20 until about D = 60cm after which it became independent of depth, as discussed later. The vertical velocities above the manifold was also observed to be uniform over at least the middle 75% of the tank width (for the shallow water tests with D = 25cm for which measurements were made). The significance of this uniformity is only to provide a measure of uniformity of air discharge from the main fold.

THE SURFACE CURRENT

The aim of aeration is to set up bulk circulation and increase the dissolved oxygen concentration. The important characteristics are the maximum surface velocity, velocity profile, and depth of surface current, the velocity decay and overall lateral extent of the circulation.

While the surface velocity close to the plume has been investigated in some detail, less work has been done on the decay of the surface velocity and profile shape with distance x from the manifold. Jones (30) on the basis of experiments in a recirculating open channel six feet wide, eight feet deep and 40 feet long using a 3" pipe with eleven orifices at 6" intervals found that the maximum surface velocity was given by

$$V_{smax} = 1.47(gq_a)^{1/3} \qquad 3\text{-}2$$

for flow rates of about 3.5 to 16 scfm/ft. V_s began to decay at (x/D) = 0.4 to 0.5 as $V_s/V_{smax} \sim X^{-1/2}$ until (x/D) $\simeq$ 2 where $V_s/V_{smax} = 0.5$. With much more rapid decay thereafter $V_s/V_{smax} = 0.2$ at (x/D) = 3. Jones noted that the $X^{-1/2}$ decay was the same for a two dimensional jet where here the free surface corresponds to the jet centerline. On this basis, he takes the increase in depth of the surface current to be linear in x. The velocity distribution for a two-dimensional jet

$$V = V_{max}(1-\tanh^2 y_d) \qquad 3\text{-}3$$

where $y_d + \sigma_y/x$ and σ is free constant, is found to fit Jones' limited data and some previous results although the most accurate higher velocity part of the profiles is just as accurately described as linear. The problem with equation 3-3 is that the curvature at the low velocity end is inconsistent with the return flow as shown later.

Our measurements were made as close as 1 cm from the still water surface and surface velocities were determined by extrapolation of measured profiles or as $V_{s_{max}} = (1.05 \pm .02)V(y = 1\ cm)$. Details of the experimental procedures for velocity measurement are presented in the Appendix. Figure 3-2 shows surface decay for three shallow water depths all at $q_a = 2.5$ scfm/ft. $V_s = V_{s_{max}}$ from x/D = 0.4 to 0.6 or 0.7 before decay as $(x/D)^{-.5}$ out to (x/D) = 2 in agreement with Jones. Figure 3-3 shows the decay is independent of flow rate from 1.65 to 3.9 scfm/ft and actually extends somewhat beyond (x/D) = 2 before the velocity falls off more rapidly in the one foot wide by eight feet long channel. The influence of water depth and higher aeration rates on surface velocity decay was examined in a 1 1/2 x 12 x 4 foot channel with the results shown in Figure 3-4. Here it was possible to measure $V_{s_{max}}$ from (x/D) = 0.3 and it was found to be constant to (x/D) = 0.6. The $x^{-1/2}$ decay law is seen to hold to (x/D) = 2.5 after which at least limited region of x^{-2} decay is observed. Manifold characteristics are summarized in the Appendix and Table A-1. Manifold A-2 (from Figure 3-4) had a single row of four 1/16 inch diameter orifices per inch of length in a 7/8 inch OD plastic pipe (i.e., a 1/2" standard pipe). When not otherwise indicated, manifold A-1, identical to A-2, except for length, was used.

Figure 3-2. Surface Velocity Decay for Three Water Depths
(with qa = 2.5 scfm/ft)

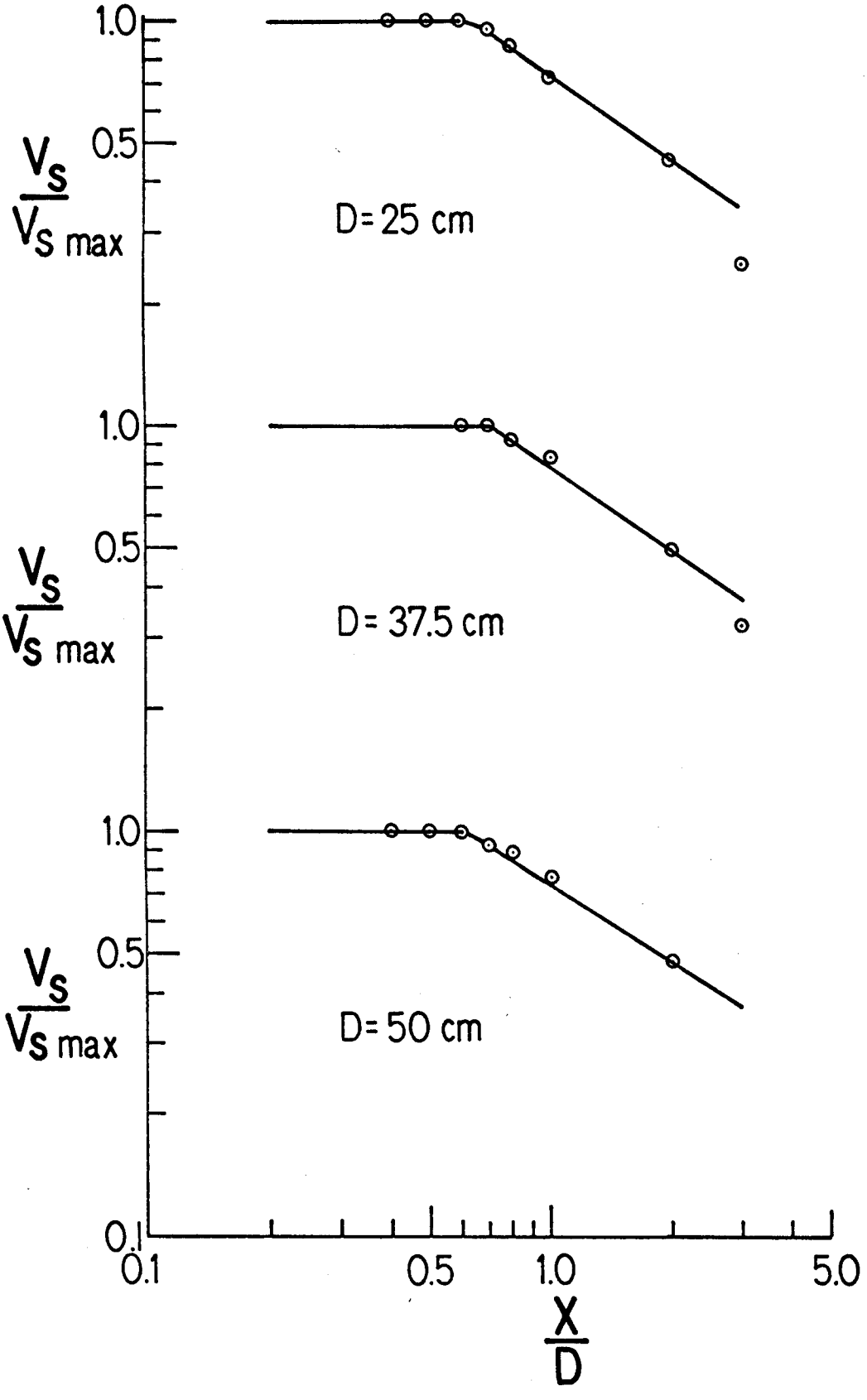

Figure 3-3. Surface Velocity Decay with Varying Aeration Rates

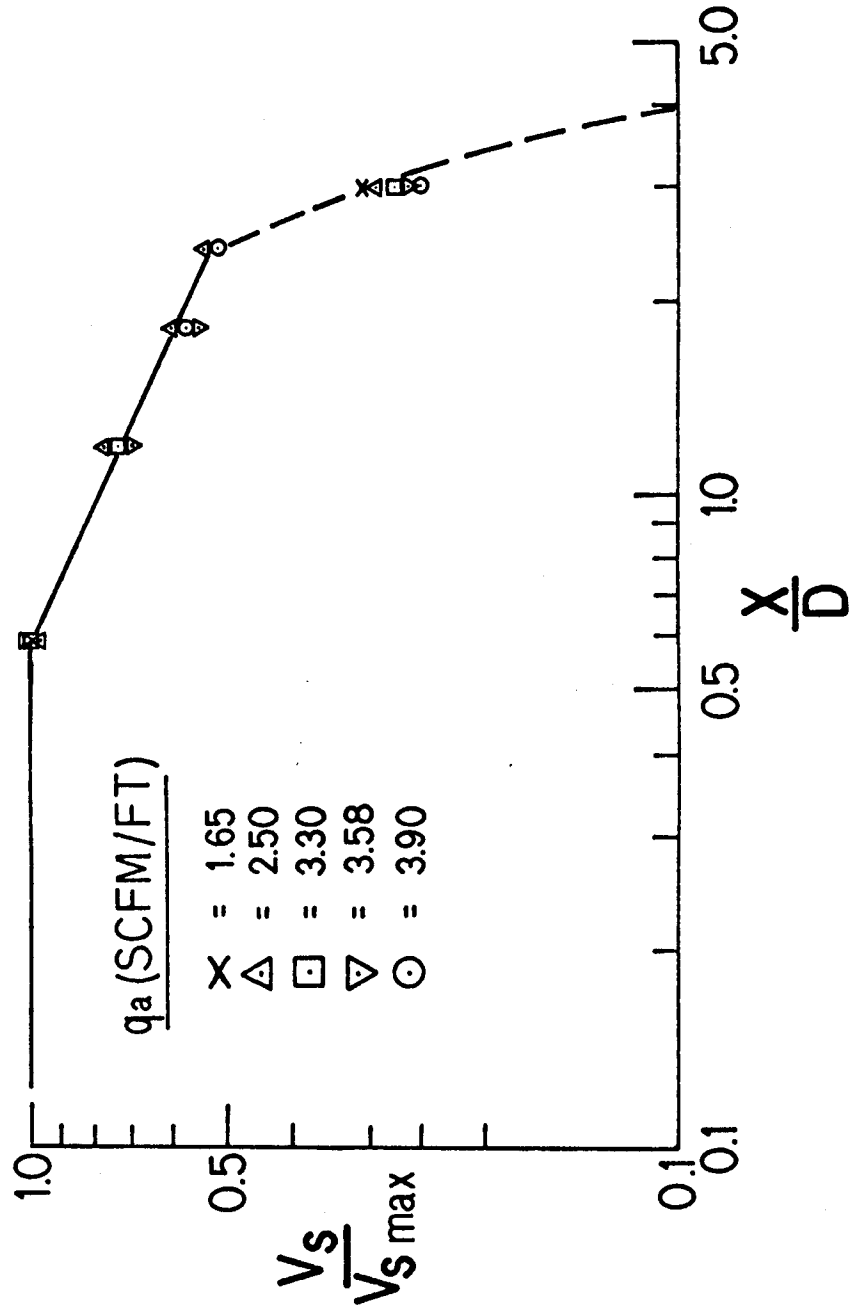

Figure 3-4. Surface Velocity Decay at Higher Aeration Rates at Three Depths

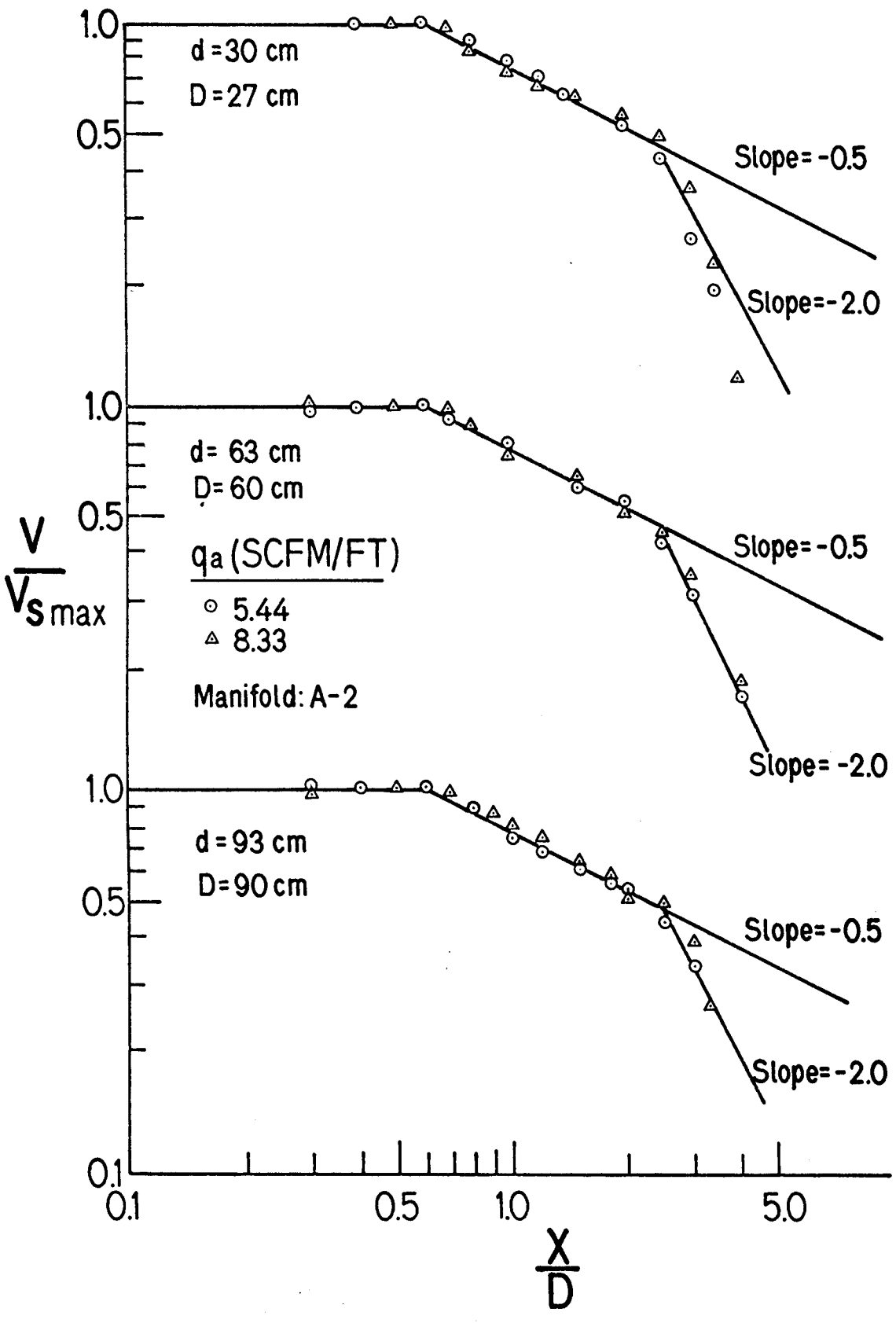

The influence of water depth on V_s is shown in Figure 3-5. Clearly the surface velocity becomes essentially independent of depth at about two feet. As mentioned previously, the same effect was observed for the vertical velocities, since there was insufficient depth to observe the weak depth dependence indicated by Equation 2-14 and observed Kobus.

VELOCITY PROFILES

We know that V_s is a function only of aeration rate for fixed depth and manifold and is, in fact, essentially independent of depth beyond a few feet. V_s is also independent of manifold design as will be shown. The jet like character of the surface current and related studies suggest that the dimensionless velocity profile surface velocity should be independent of aeration rate. Figures 3-6 and 3-8 show this to be true with d = 28 cm in our preliminary experiments. The slight curvature of the surface velocity profile becomes less pronounced with increasing (x/D) location. The jet velocity profile used by Jones (30) and given in Equation 3-3 is clearly inappropriate near the bottom of the surface current. A smooth transition from the surface to the bottom or return current is obviously required. For more than half of the depth of the return current for (x/D) < 2.4, the profile is flat over its central section. This is quite unlike a turbulent wall jet (e.g., 46, 47) and the bottom currents induced in wind driven circulation in channels (48).

Figure 3-5. Surface Velocity Variation with Water Depth

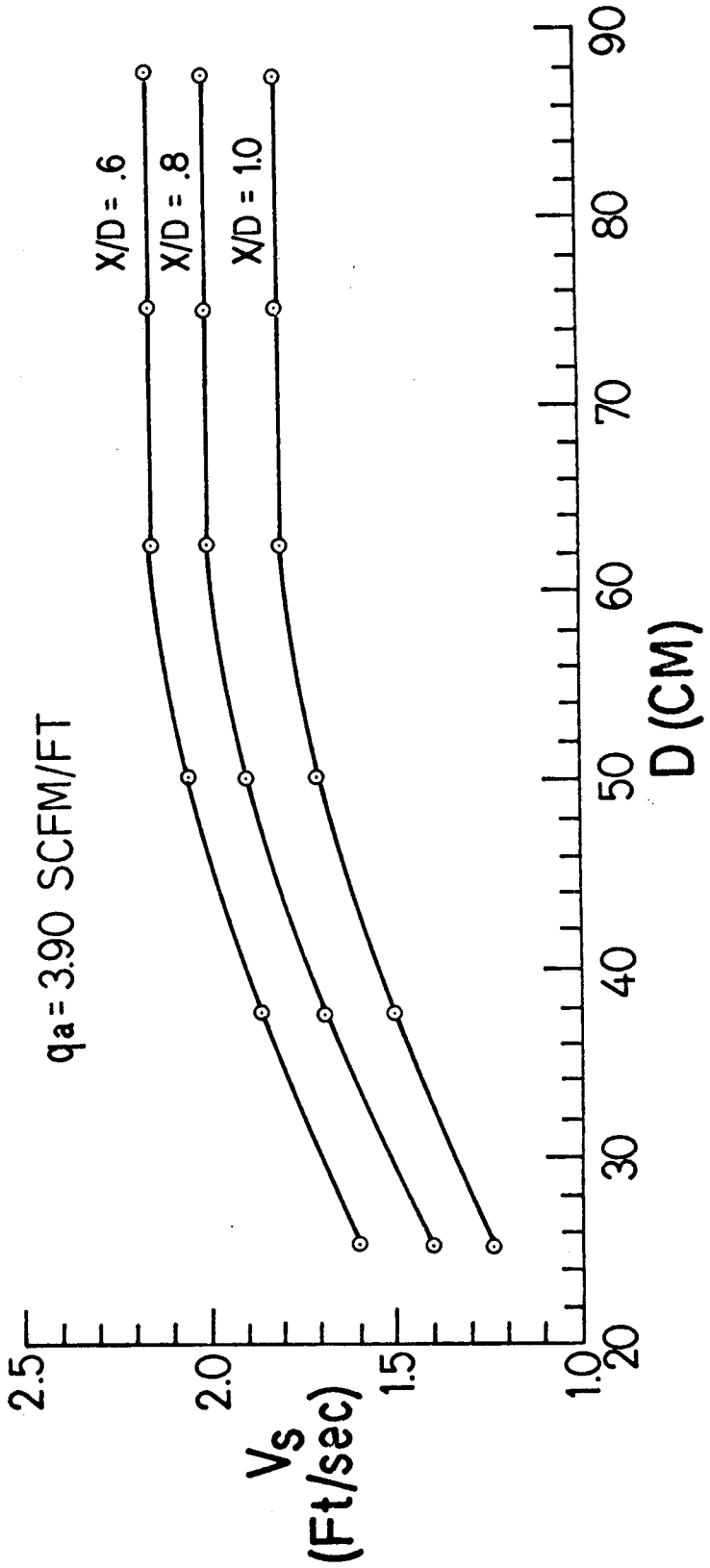

Figure 3-6. Dimensionless Velocity Profiles at x/D = 0.6 for Several Aeration Rates

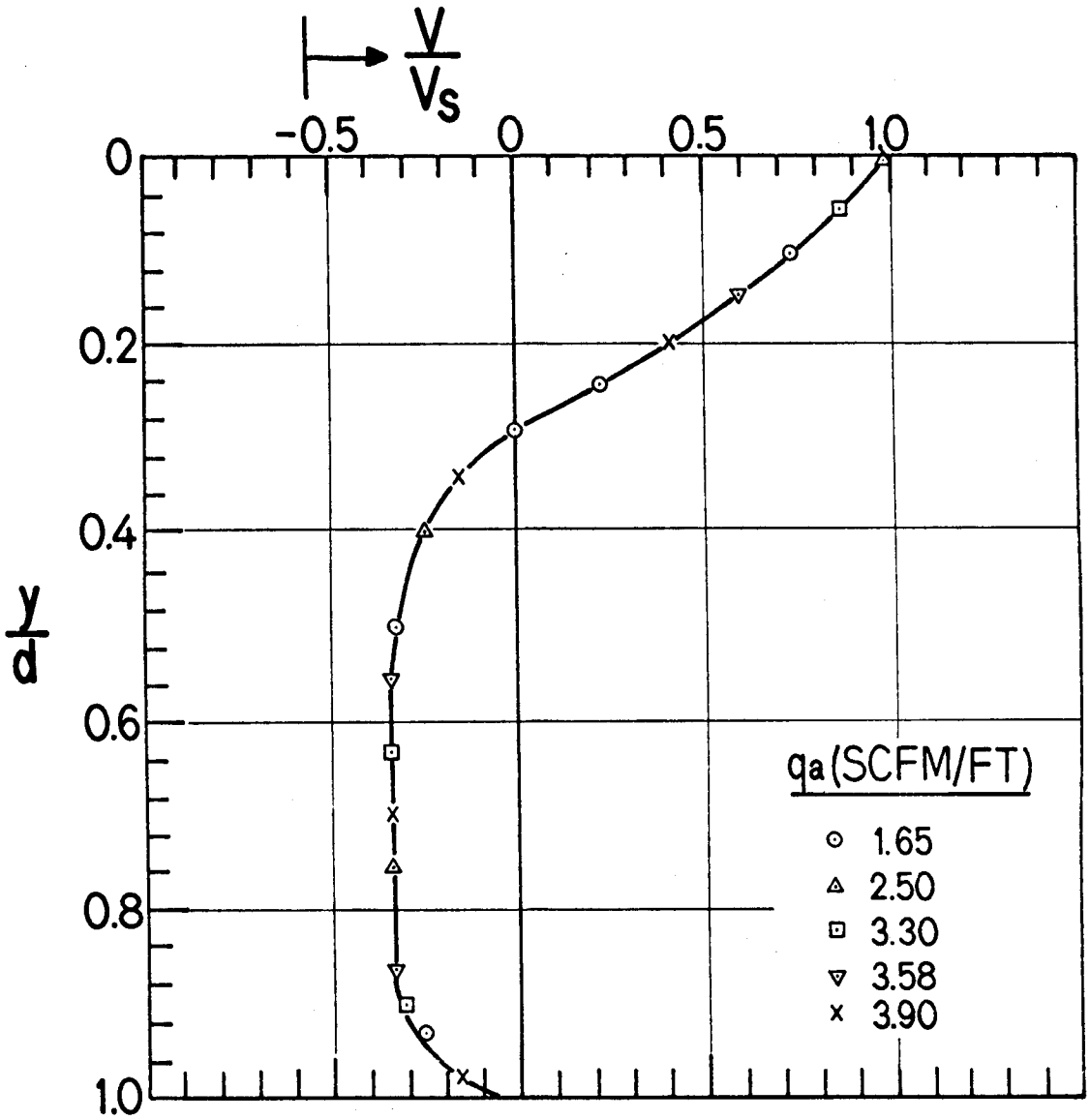

Figure 3-7. Dimensionless Velocity Profiles at x/D = 1.2 for Several Aeration Rates

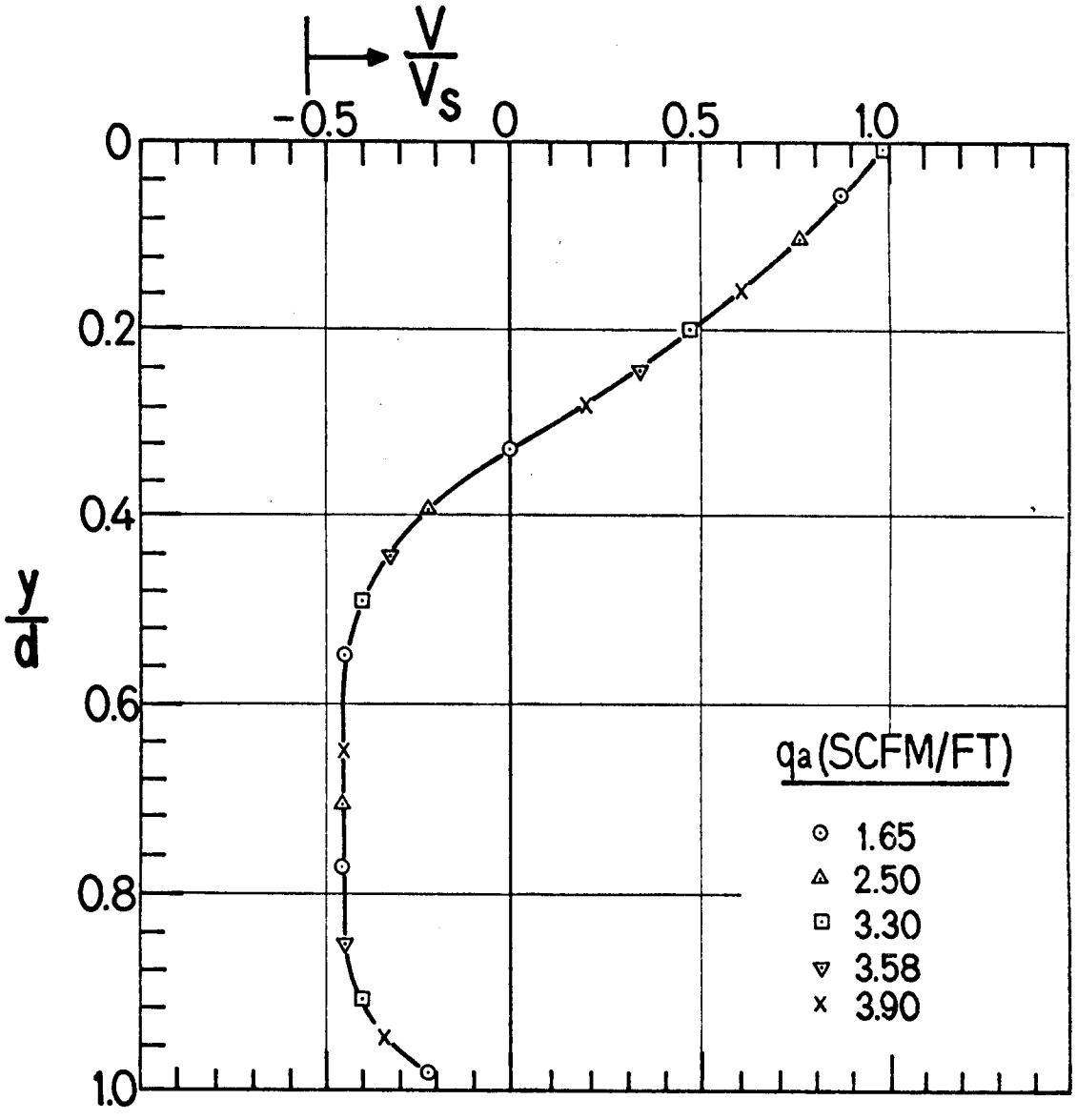

Figure 3-8. Dimensionless Velocity Profiles at x/D = 2.4 for Several Aeration Rates

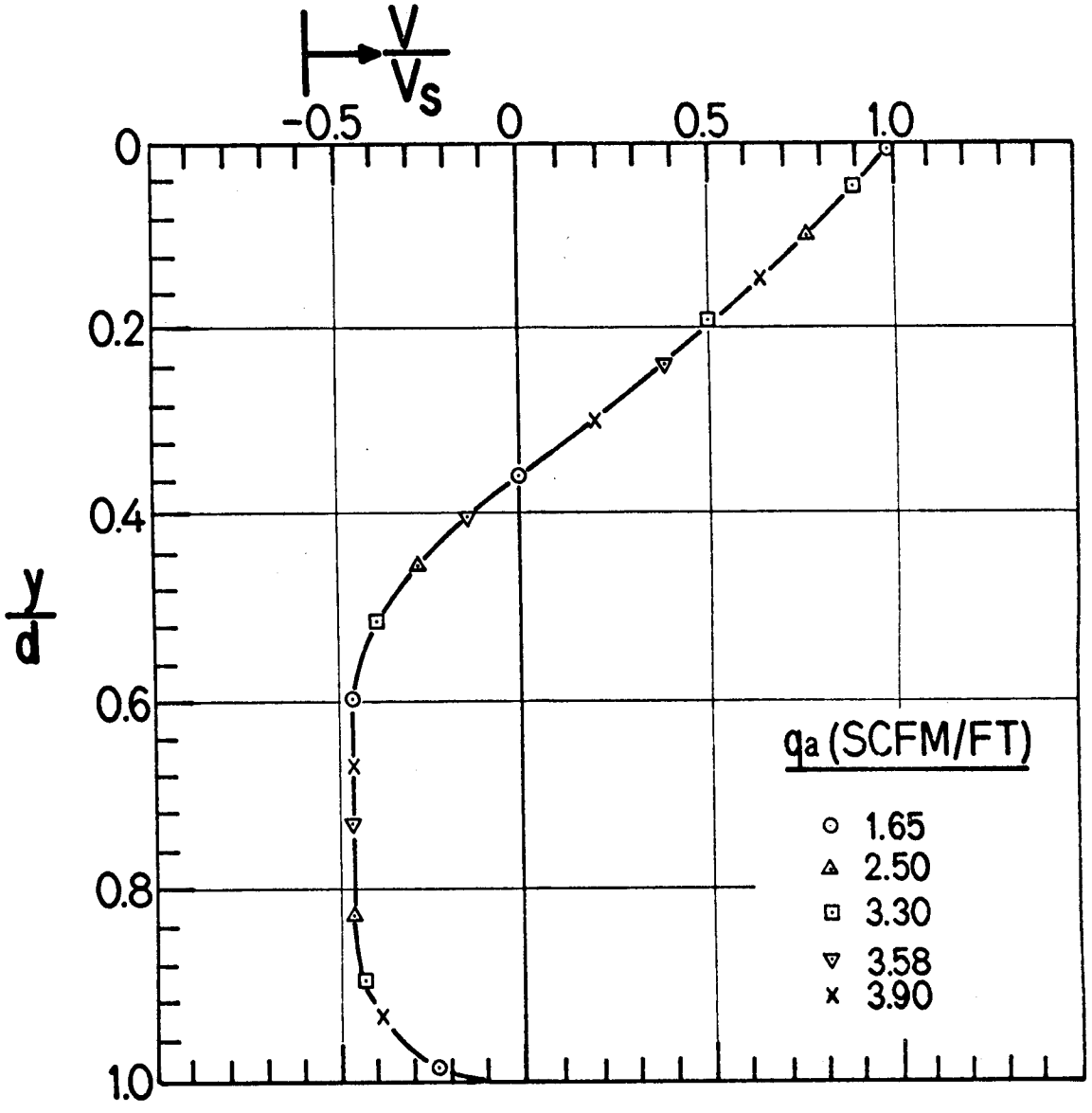

For an ideal two dimensional system the surface and return current must be of equal flow rate. Integration of these profiles at various lateral location then not only provides a check on the consistency of the measured velocities, but also gives a measure of the deviation from a simple two dimensional flow. For the profiles of Figures 3-6 to 3-8 and also at (x/D) = 1.8 and 3.0, Table 3-1 shows the volumetric flow rates for the surface q_s and return q_r and currents and their ratio which is seen to increase smoothly with increasing (x/D).

TABLE 3-1

Comparison of Surface and Bottom Current Flow Rates from Integration of the Velocity Profiles

X/D	q_s (It^3/sec)	q_r(It^3/sec)	q_s/q_r
.6	.236	.266	.887
1.2	.230	.248	.927
1.8	.192	.203	.946
2.4	.168	.169	.994
3.0	.144	.136	1.06

Note that in the mid-range of the circulation the flows are in good agreement, with the largest deviation closest to the manifold as expected.

On the basis of the results presented, so far, Provost found the surface current thickness δ, increases with X as

$$\delta/D = 0.05\ (X/D) + .308 \qquad 3\text{-}4$$

based on data for D = 25, 37.5 and 62.5 cm with measurements for $0.5<(X/D)<3.6$. Note that $\delta/D = .5$ at $X/D = 3.6$. Remember that Taylor estimated $\delta = .28D$ while others give $\delta/D = .25$ to .33. These results are for the position of maximum surface velocity at $X/D \simeq .5$ which from Equation 3-4 gives $\delta/D = 0.33$. There do not seem to be other detailed results for $\delta(X)$. Variation of q_a from 1.65 to 3.90 did not change $\delta(X)$ as is evident from Figures 3-6 to 3-8.

The jet velocity profile of Equation 3-3 is clearly incompatible with a smooth variation from surface to return flow. For the data presented, so far, within $0.6<X/D<2$ where surface decay $\sim X^{-1/2}$, the quadratic equation

$$V/V_{max} = -0.3(y/\delta)^2 - 0.7(y/\delta) + 1.0 \qquad 3\text{-}5$$

provides a good fit of the data for $1.65<q_a<3.9$ scfm and up to three feet of water. In fact, linear surface velocity profiles are reasonable for some of these results and will be further discussed later.

INFLUENCE OF MANIFOLD DESIGN

Results presented so far are primarily for Manifold A-1. While it has been shown that V_s is independent of orifice size, spacing, and arrangement within certain limits, because our shallow water results do not allow full development of the vertical flow patterns as mentioned previously (e.g., 44), the effect of varying manifold characteristics was studied briefly. Manifold A-4 was identical to A-1 but had five rows of orifices. A-6 was of twice the diameter, but more significantly, was a 0.3 micron porous tube. The results of Figure 3-9 reveals no significant influence of manifold characteristics, at least for q_a = 1.66 scfm/ft even in our shallowest water tests where any variation would be expected to be most pronounced. A slight trend to slightly higher surface velocities with A-6 was observed. These surface profiles are now linear. For a large series of measurements, k, the proportionality constant in Equation 3-1 was about 5% greater for the porous tube A-6 than for A-1, the standard perforated tube. There is also an apparent 5% increase in k with d increasing from 28 to 93 cm for each tube which is at least in part due to the simplicity of Equation 3-1 which does not allow for the influence of depth as does Equation 2-14. For d = 63 cm, k = 1.61 for A-1 and 1.69 for A-6, while for d = 93 cm, k = 1.65 for A-1 and 1.73 for A-6. It should be noted that the use of a porous tube here was merely intended to highlight the influence of manifold design. The small gains achieved with the porous tube will not compensate for its additional expense and increased probability of plugging in actual large scale aeration projects.

Figure 3-9. Velocity Profiles at x/D = 1.8 for Three Different Aeration Manifolds

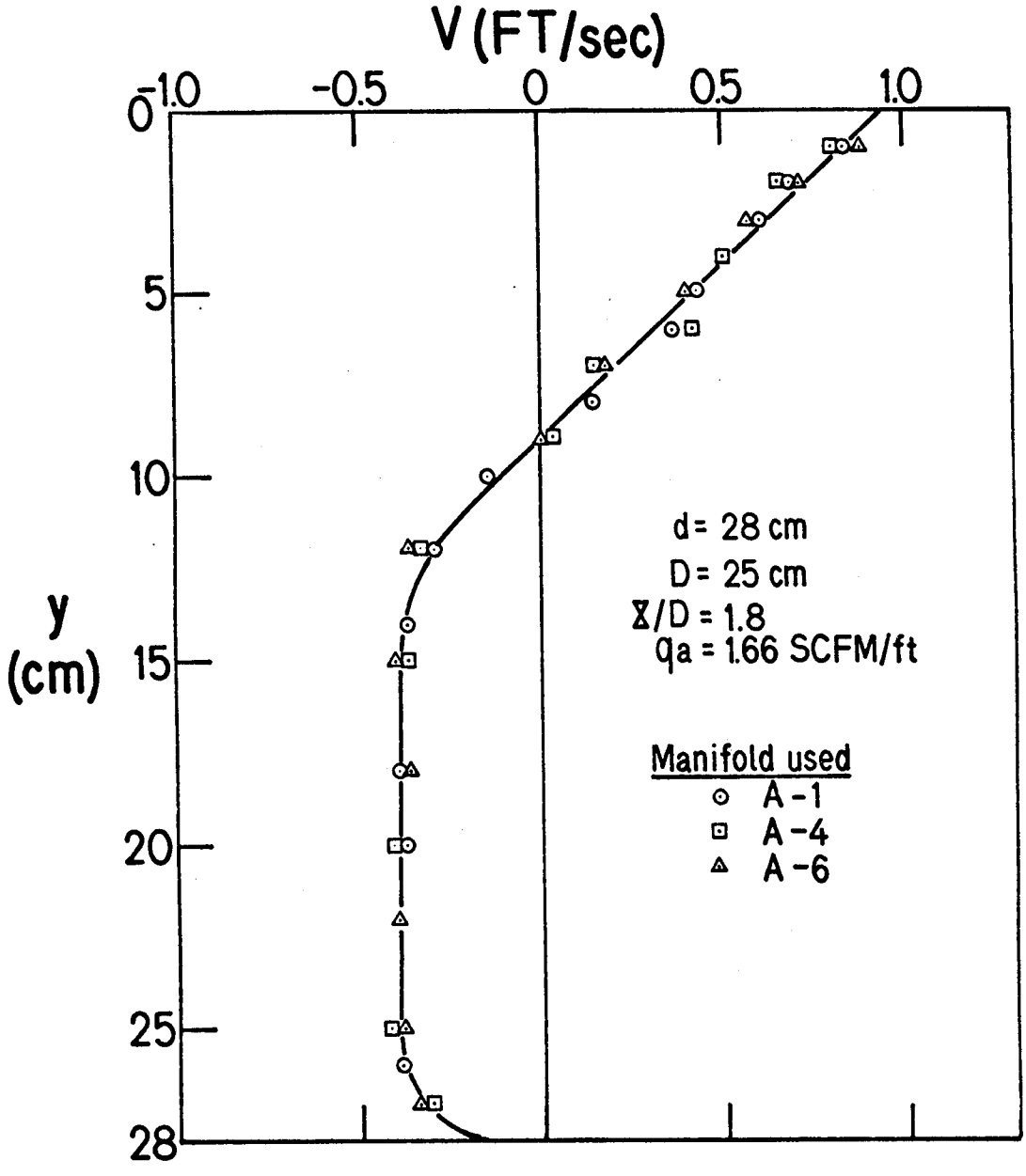

It is not surprising that the fine bubbles produced by A-6 lead to increasing k values which begin to approach Taylor's early estimate of 1.9 on the basis of the analogy with thermal convection. A uniform layer of fine bubbles appear to surround the sides of A-6. These bubbles converge to a plume above the tube of about 1/3 the diameter of the tube before spreading as they continue to rise.

Because the original set of experiments was performed in a channel, one foot wide, it was of interest later to compare those results with the results of otherwise identical experiments in a 1 1/2 foot wide channel. Figures 3-10 to 3-12 show that for the shallowest water, channel width has no significant effect on the measured velocities. Manifold A-2 in the 1 1/2 foot channel was identical to A-1 in orifice size and spacing (See Table). The profile for X/D = 3.6 in Figure 3-12 shows the changed shape of the bottom profile near the end of the circulation zone. Figure 3-13 shows that dimensionless velocity profiles are identical and independent of aeration rate for both channels. Note that the aeration rate per foot of manifold in the 1 1/2 foot channel has been more than doubled over the maximum possible rate of 3.90 scfm/ft for the one foot channel beyond which measurements became difficult or impossible due to waves and plume oscillations. Identical profiles for the two channels were also observed for greater water depths. There were no scale-up variations for larger channels, so that some of the more detailed results for the one foot channel were not further checked in the larger channel.

Figure 3-10. Similarity of Velocity Profiles at x/D = 0.6 for Channel Widths of 1 and 1 1/2 feet

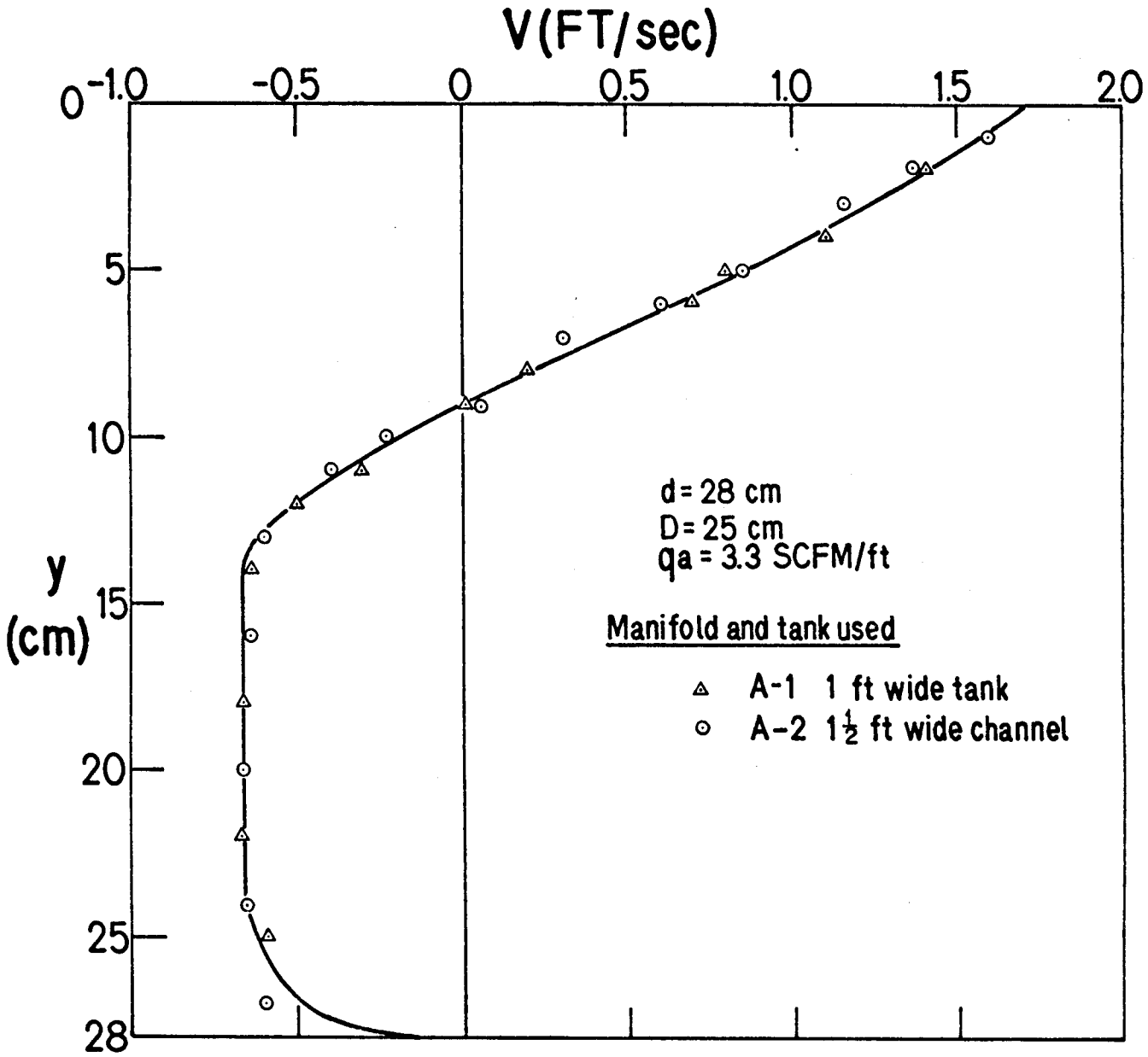

Figure 3-11. Similarity of Velocity Profiles at x/D = 1.8 for Channel Widths of 1 and 1 1/2 feet

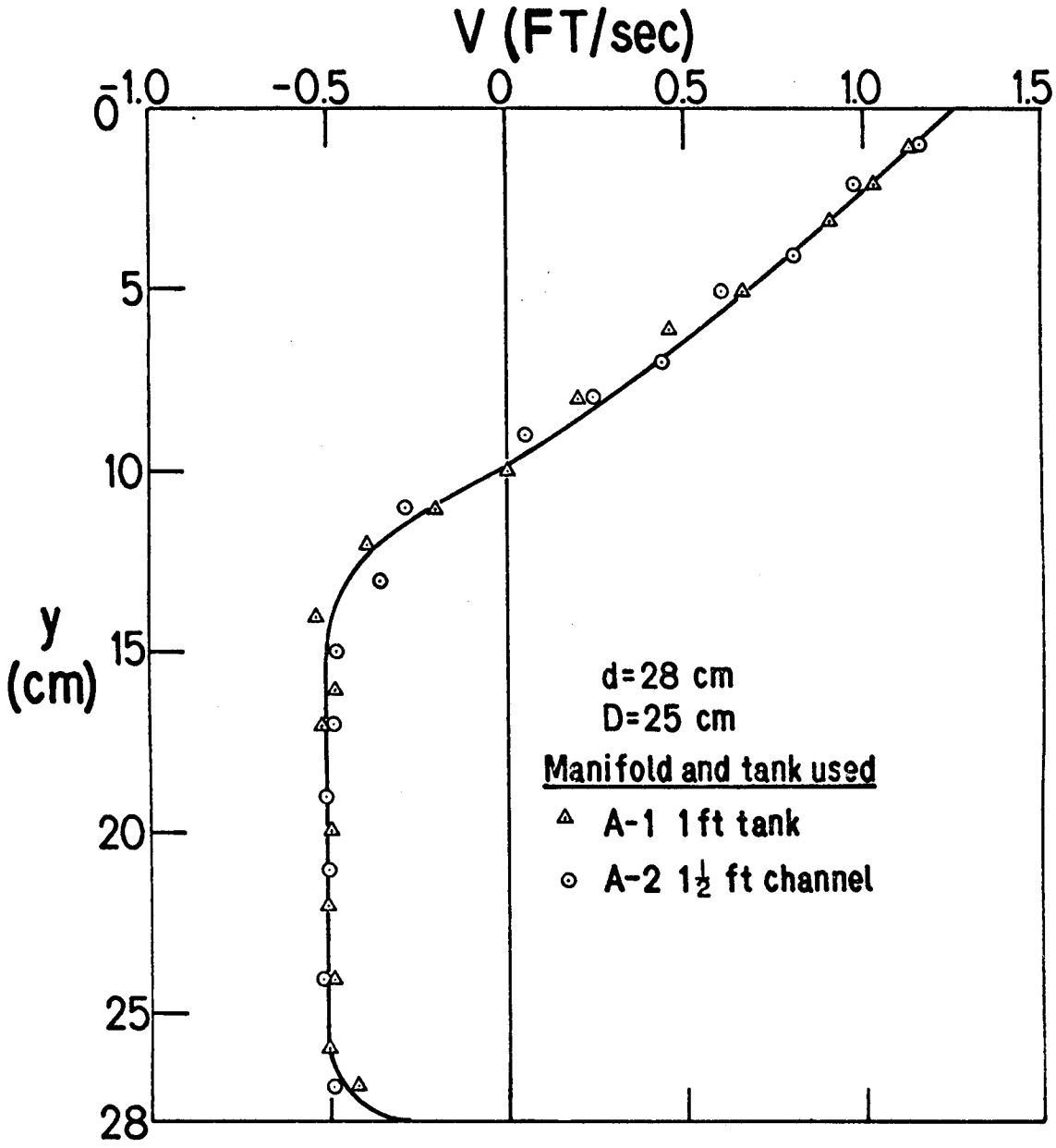

Figure 3-12. Similarity of Velocity Profiles at x/D = 3.6 for Channel Widths of 1 and 1 1/2 feet

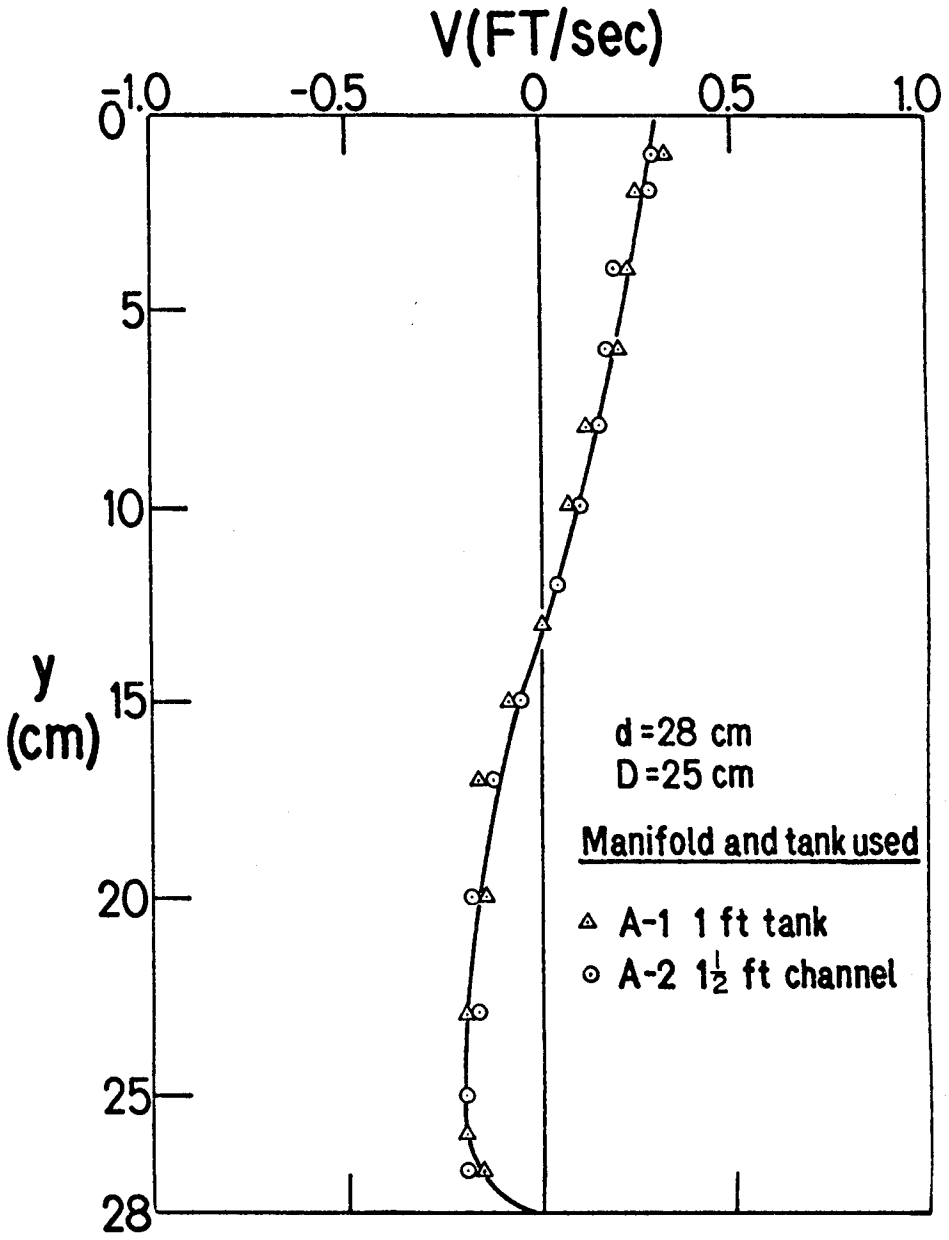

Figure 3-13. Dimensionless Velocity Profiles at x/D = 1.8 for Several Aeration Rates and Channel Widths of 1 and 1 1/2 feet

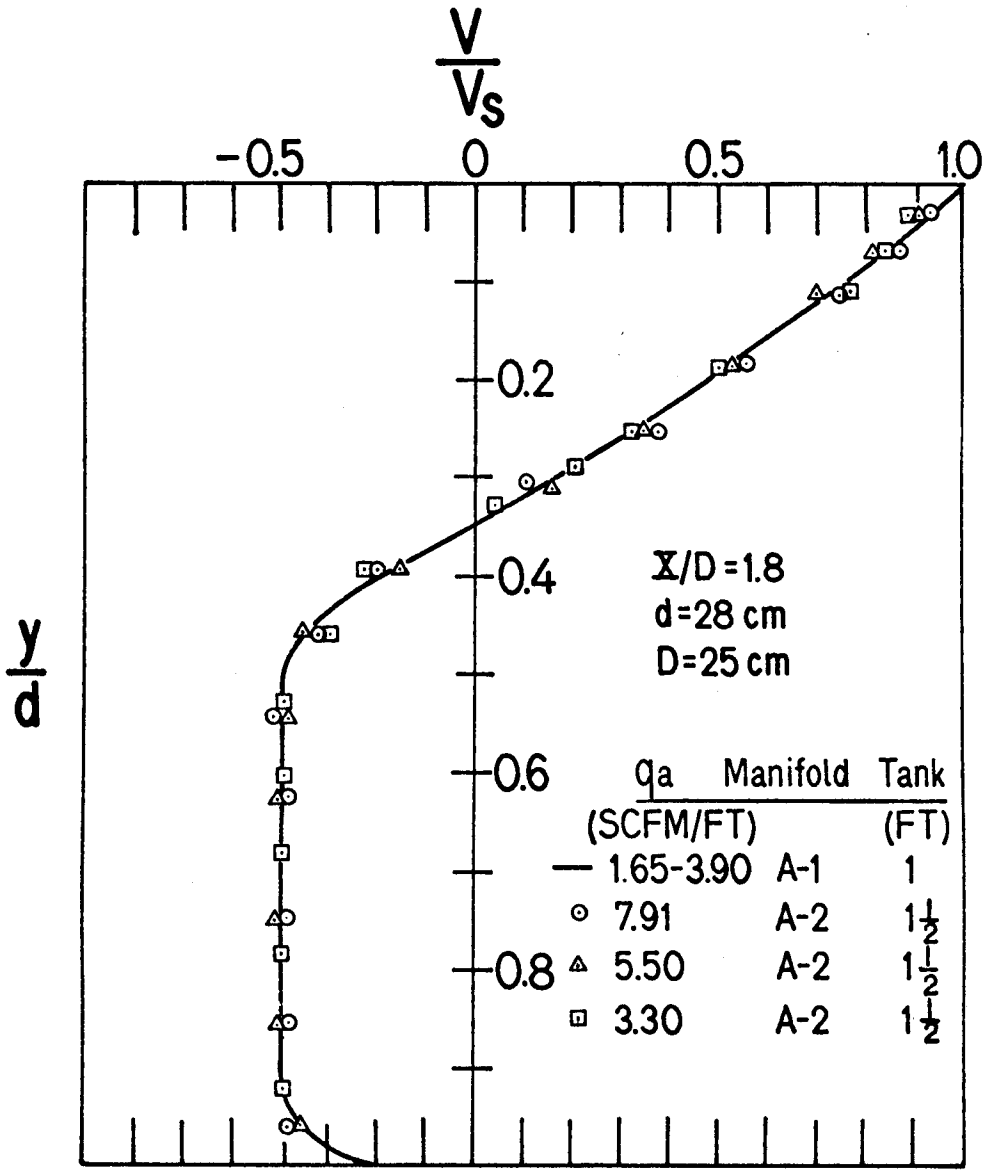

THE INFLUENCE OF HIGHER AND LOWER AERATION RATES

Although the preliminary experiments were limited to aeration rates of 1.65 to 3.9 scfm/ft we have already shown results at higher rates that were consistent with the original data. For example, Figure 3-4 shows that the decay of surface velocity at high rates was identical with that for moderate values of Figure 3-2. However, the shape of the surface velocity profile is dependent on aeration rate as shown in Figure 3-14 with the profiles most nearly linear for mid-range and higher aeration rates. Profile curvature becomes progressively more pronounced with decreasing aeration rates. A similar trend at the lower rates is observed in Figure 3-15 which is identical to Figure 3-14 except for the use of a porous tube aeratior (A-7) rather than the perforated tube. This is also reflected in the higher averaged values for k for manifold A-7 listed on Figure 3-15. The concave profiles for low to very low aeration rates are presented in Figure 3-16 for d = 63 cm. Concave profiles are observed at any depth for sufficiently low aeration rates. Note that the lowest rates require the use of a small porous manifold, A-5, for a uniform initial plume appearance. While previously a trend to increasing k was noted as q_a decreased from high to moderate or low values, further decrease in aeration rate to very low values leads to a decrease in k. For example, from Figure 3-16 as q_a varies from .26 to .034 scfm/ft k decreases from 1.82 to 1.14.

Figure 3-14. Velocity Profiles for the Standard Aeration Manifold A-2 and a Wide Range of Aeration Rates

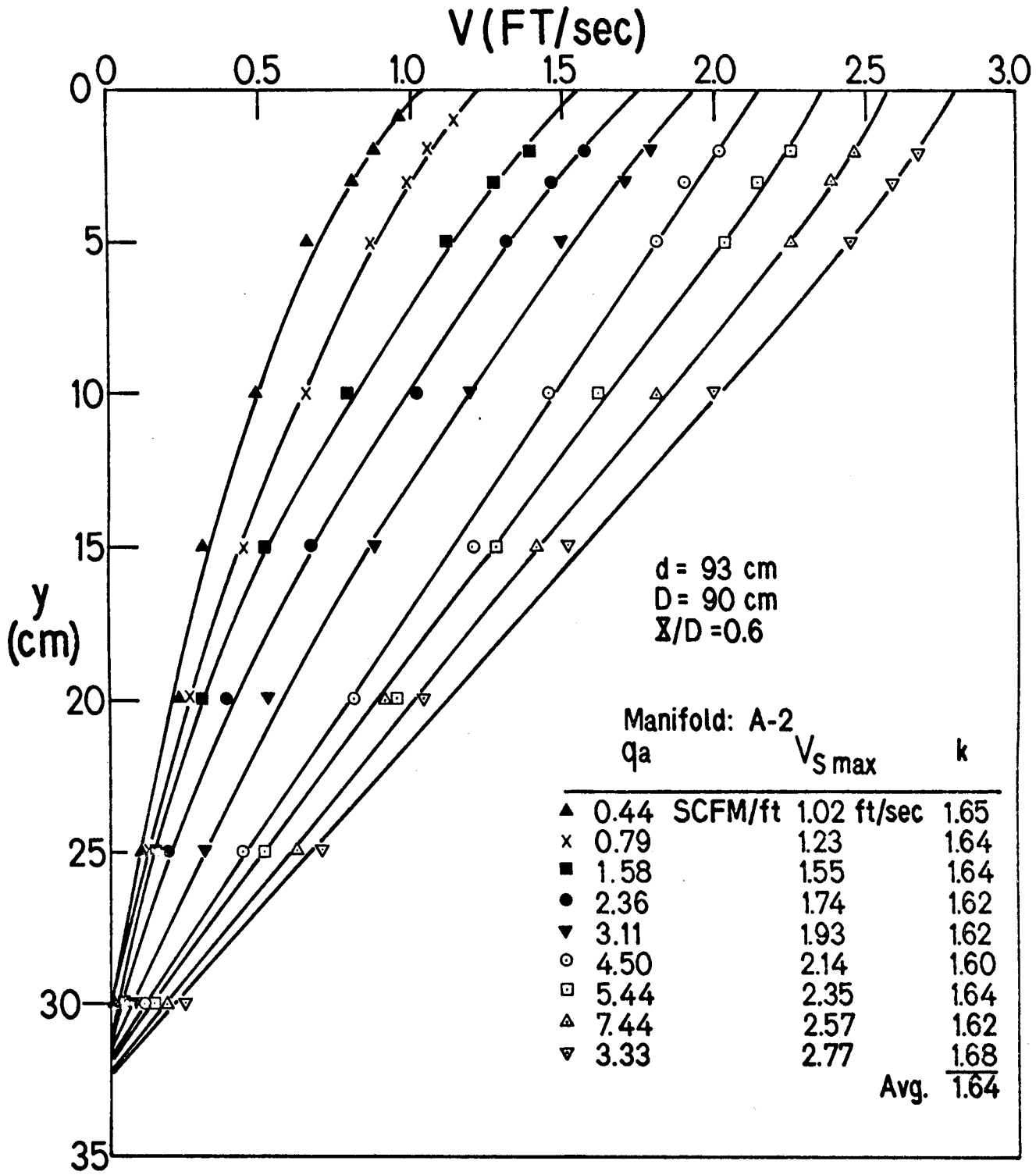

Figure 3-15. Velocity Profiles for the Porous Tube A-7 and a Wide Range of Aeration Rates

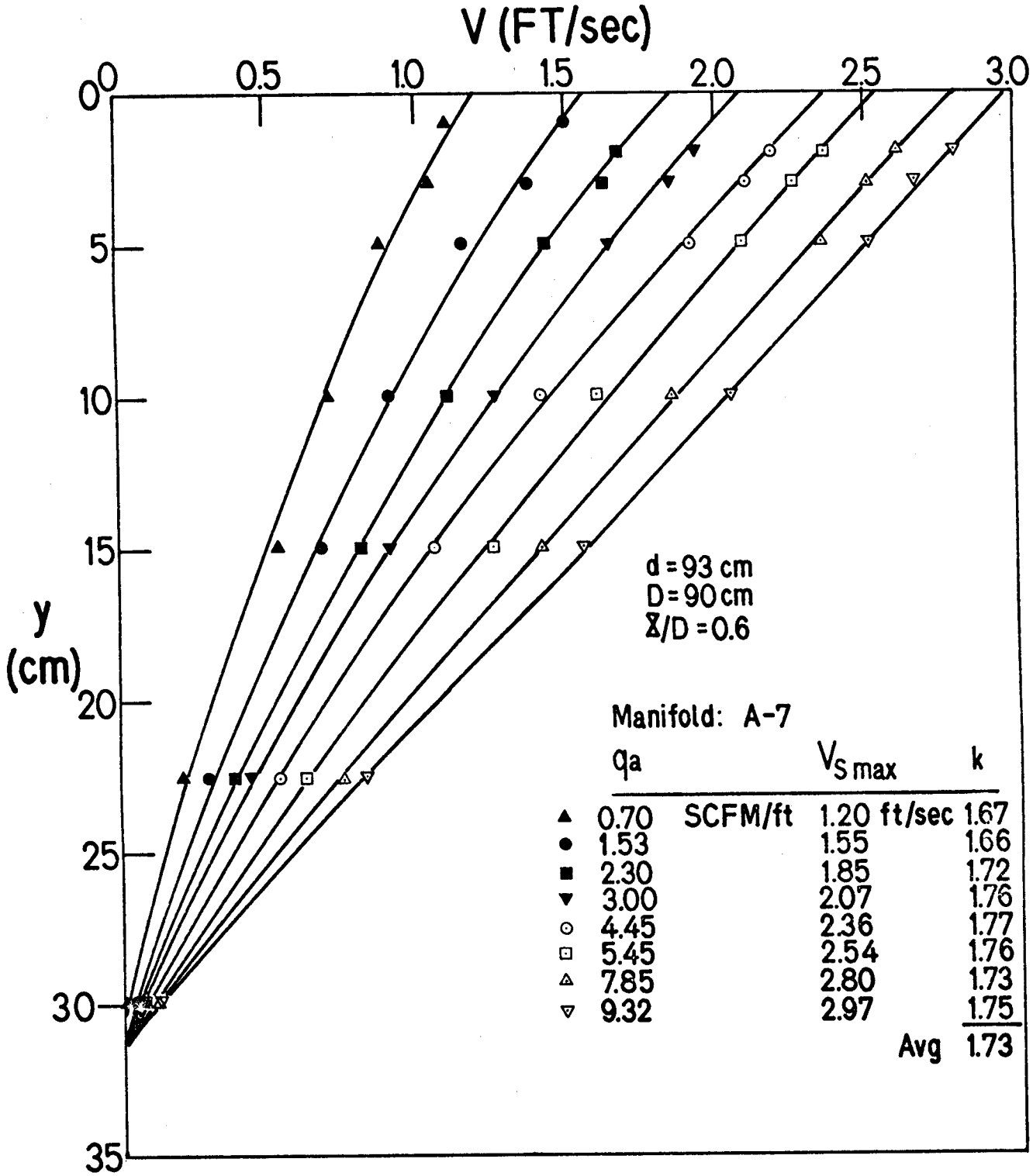

Figure 3-16. Surface Current Velocity Profiles at Low and Very Low Aeration Rates

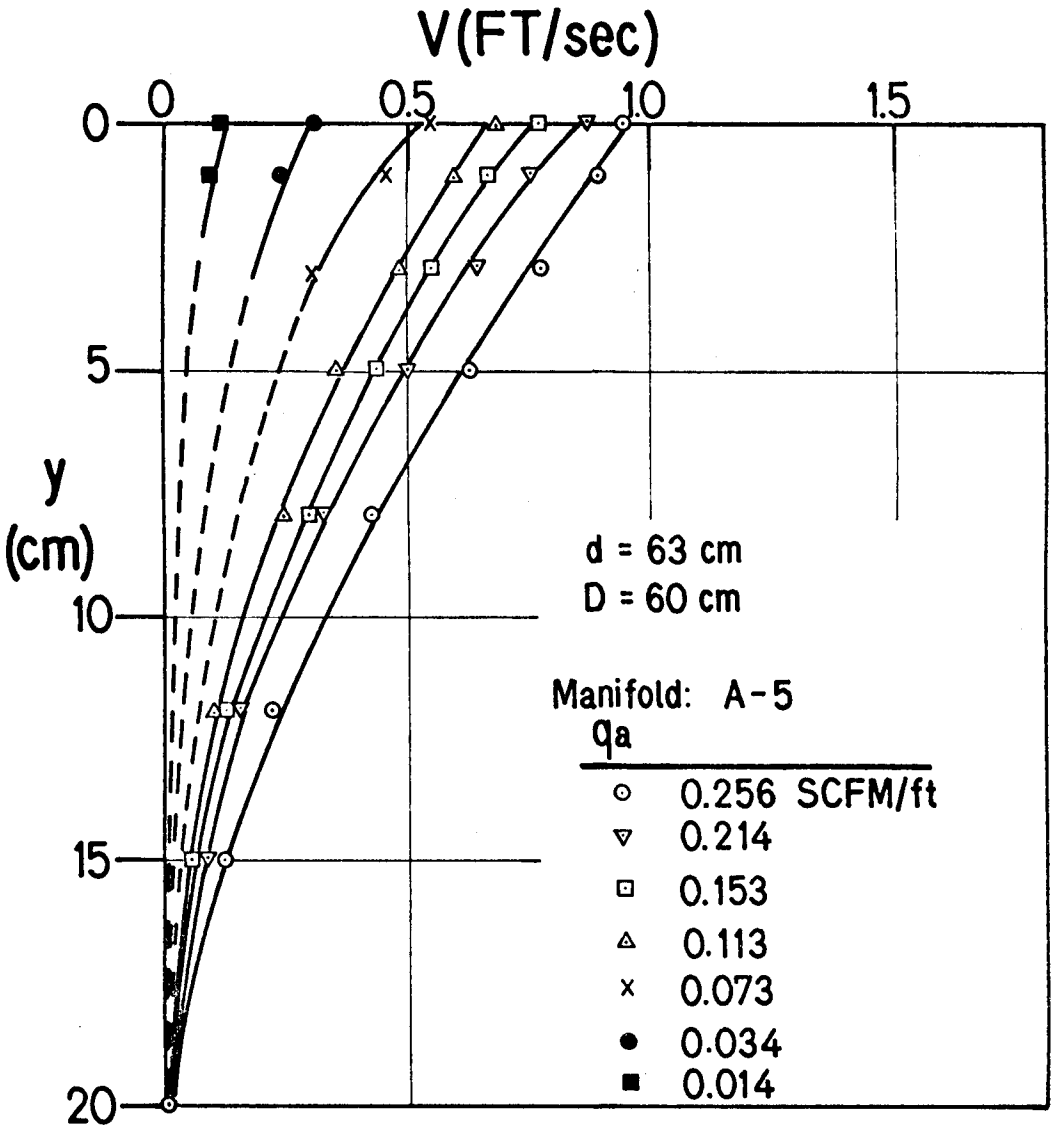

Surface velocity decay also varies at the very low aeration rates. Figure 3-17 shows that for low rates with $0.30<q_a<1.13$ scfm/ft the decay is as previously described for moderate rates (e.g., Figures 3-2 to 3-4). However, for the lower aeration rates of 0.256 and 0.113 scfm/ft the extent of the $X^{-1/2}$ decay is sharply reduced as is the overall extent of the circulation.

CIRCULATION CELL SIZE

The surface decay results presented serve to define a circulation cell which extends a distance of 4D from the manifold. Velocity measurements were possible down to $\sim$0.1 ft/sec and there is little doubt that these measurements provide a good overall measure of cell size. However, the more rapid surface velocity decay near the end of the cell coupled with increasing deviation from two dimensional flow and the desire to photograph the flow patterns led to additional methods for cell size determination. Dye injection was the most convenient and flexible. Injection at different positions in the region of $X \simeq 4D$ could, on averaging several results, pinpoint the edge of the circulation cell. Multiple measurements with neutrally buoyant plastic spheres were also useful, as were observation of the flow of the minute air bubbles. All of these measurement techniques gave cell sizes of 4.0 to 4.2 times the water depth independent of depth and aeration rate except as noted here. From Figure 3-17, cell size apparently decreased at the very low aeration rates.

Figure 3-17. Surface Velocity Decay at Low Aeration Rates

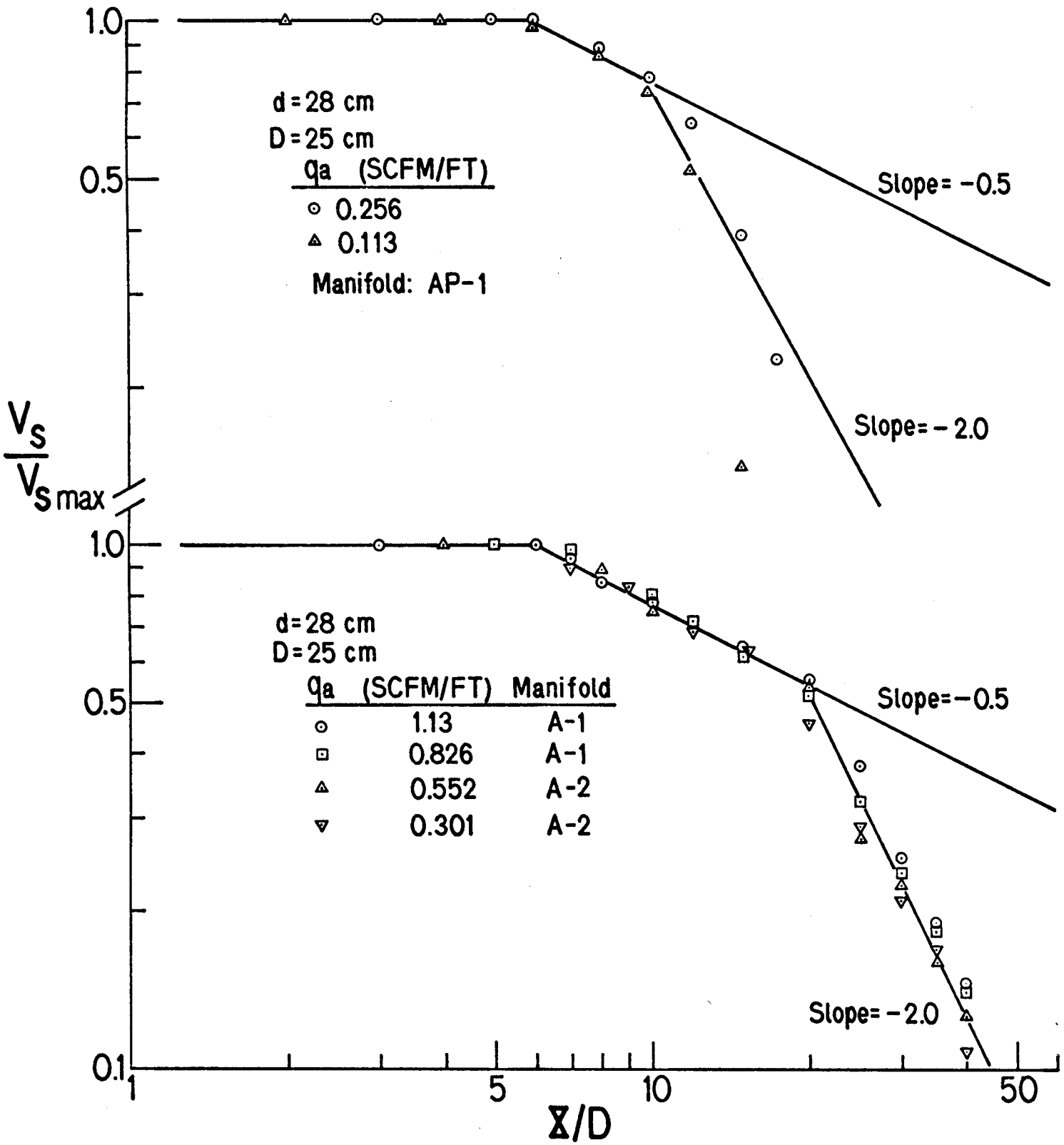

Using dye injection, for aeration rates of less than 0.3 scfm/ft in Figure 3-18, the cell size is seen to decrease smoothly from X = 4d at qa_c = 0.3 scfm/ft, a "critical" aeration rate, to about half that value at about $0.1qa_c$ Of course for these very low aeration rates profiles shapes have already been shown to change and it becomes progressively less accurate to speak of the weak circulation as a "cell".

The clockwise circulation to the right of the manifold must, of course, induce a counter circulation beyond the cell edge. While the velocities in this secondary cell were too low to measure and tank ends limited development, dye injection clearly revealed their existence.

MANIFOLD OFF CENTER

Since cell size was four times the water depth (on each side of the manifold) it is evident that with only one foot of water in the smallest tank (eight feet long) circulation extends to the ends of the tank. To test for possible end effects with d = 28 cm the manifold position was varied from the center to a position two feet from the end with no effect on cell size or velocities. In fact, the only influence noted was with the manifold near the end for small (X/D) values. For example, with the manifold one foot from the end a slight velocity increase was noted.

Figure 3-18. Circulation Cell Size Variation at Low Aeration Rates

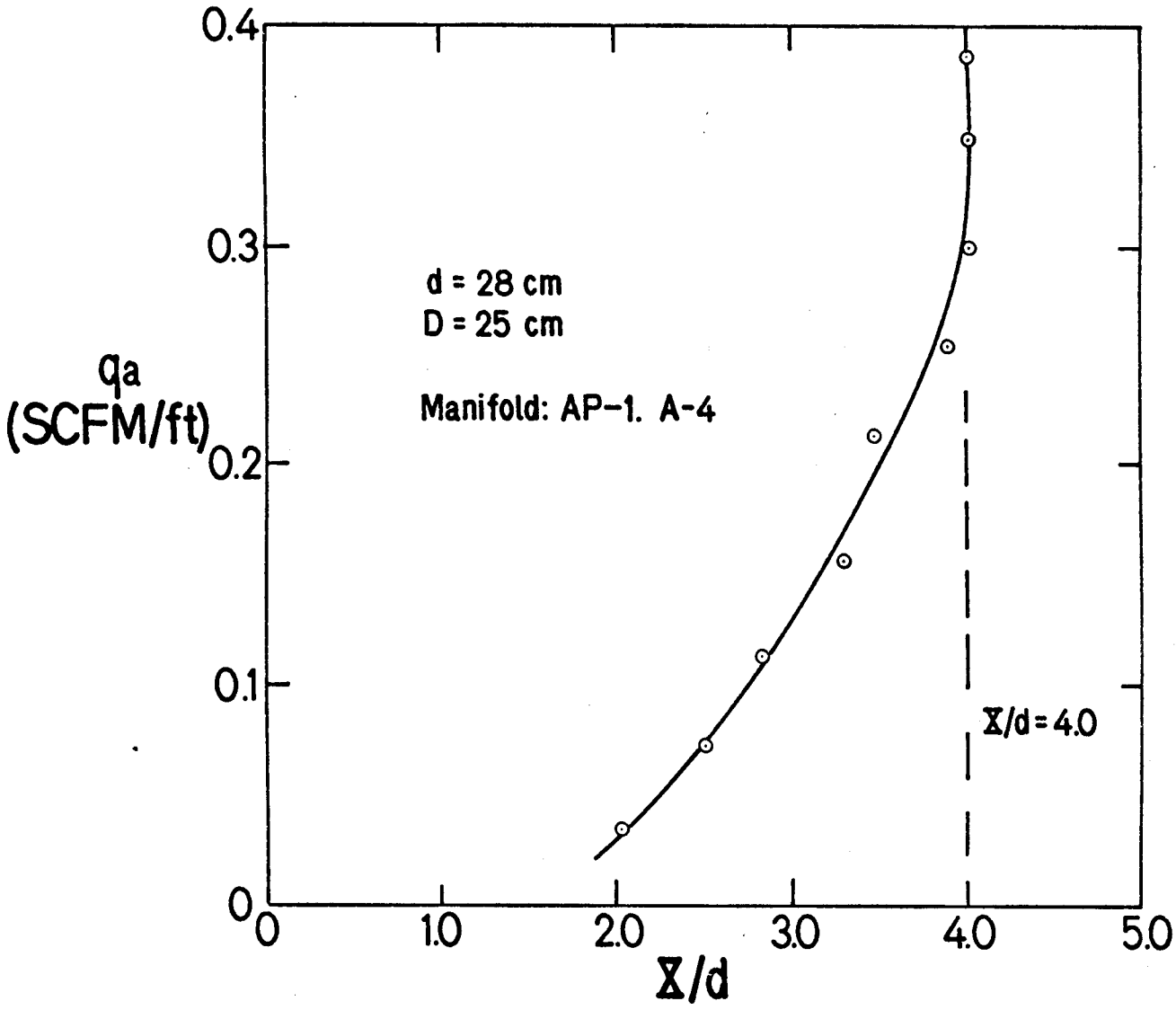

This velocity increase was a maximum for the manifold at about 20 cm from the end, where a 20% increase near the manifold was observed. Moving the manifold closer to the end caused the velocity to decrease to a value about 5% high with the manifold at the wall. Figure 3-19 shows the influence of manifold position on the velocity profile for measurement at X/D = 1.2.

The appearance of the plume also changes as the manifold is moved towards the end of the tank. At 35 cm from the end the plume is still symmetrical while at 25 cm air entrainment at the wall carries larger bubbles under. For standard rates of ≃2 scfm/ft, at 15 cm from the end, the air entrainment is still intense but the plume bends away from the wall. At 10 cm, the plume bends towards the wall and hugs the wall in the upper third of the depth. At 5 cm from the end, the air bubbles hug the wall over most of the depth. While additional measurements are available (42), the results indicate that wall effects were not important in the results presented here and are in any case a minor influence on the flow pattern and velocities even when the manifold is very close to the wall (i.e., within a distance of one water depth from the wall).

Figure 3-19. Velocity Profile Variation at x/D = 1.2 with Aeration Position

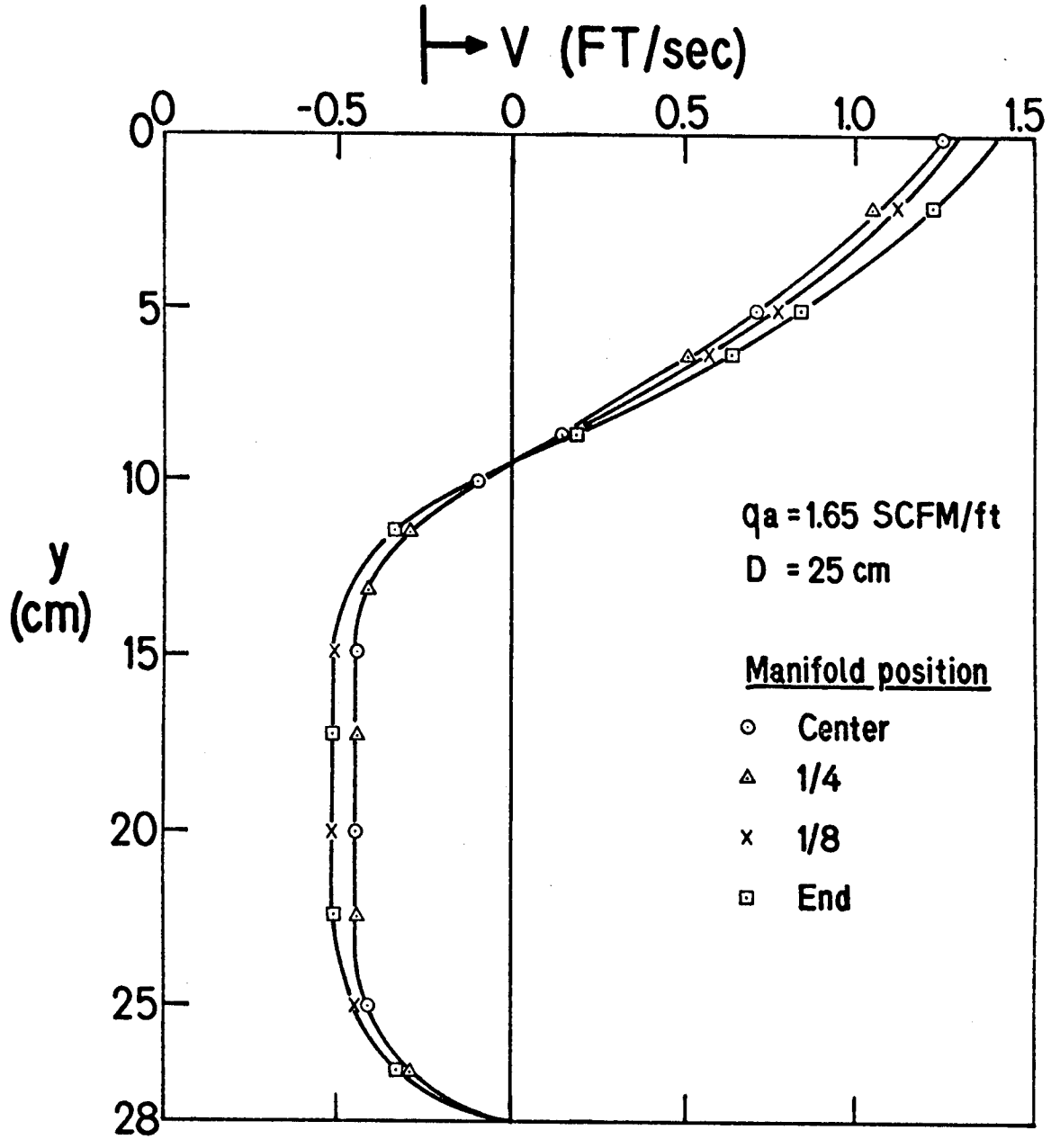

EFFECT OF MANIFOLD DEPTH

Compression costs are an important component in the overall costs of aeration systems. If, for example, the surface velocity and circulation rate and cell size at a specified aeration rate are independent of manifold depth over some range, then reduction in operation costs may more than balance the possibility of increased cost of manifold suspension at some distance above the bottom.

Figure 3-20 shows the velocity profile for the manifold set at 25 cm in 40.5 cm of water for q_a = 2.50 scfm/ft. When this is compared with the corresponding curve for the manifold at the bottom, the surface current velocities are in agreement as they are over the full cell. Of course, the maximum bottom current velocity is reduced for the raised manifold as expected from continuity. A series of results for the same aeration rate are shown in Figures 3-21 to 3-23 with the manifold still at 25 cm, but with water depths of 70 cm. The bottom currents are remarkably flat over most of their extent. Figure 3-22 shows the actual difference in profiles when the manifold is at the bottom and raised. Note that if y was "normalized" with D, the zero velocity points are at y/D = 0.34 for each profile and with the velocities normalized with V_s the surface current profiles overlap.

The influence of water depth for the manifold at 25 cm is shown in Figure 3-24. The data for d = 90 cm was taken by Wen sometime after the other results were obtained by Provost. The surface current profile is clearly independent of d, and the return current velocities are remarkably constant over the most of the range for larger d values. Figure 3-25 shows the influence of doubling D to 50 cm with conditions otherwise essentially identical to those of Figure 3-24. Again the surface velocity profiles are seen to overlap while the zero velocity positions occur of the same (y/D) for Figures 3-24 and 3-25.

Figure 3-20. Velocity Profile at x/D = 1.8 with Aeration Manifold Raised from Bottom

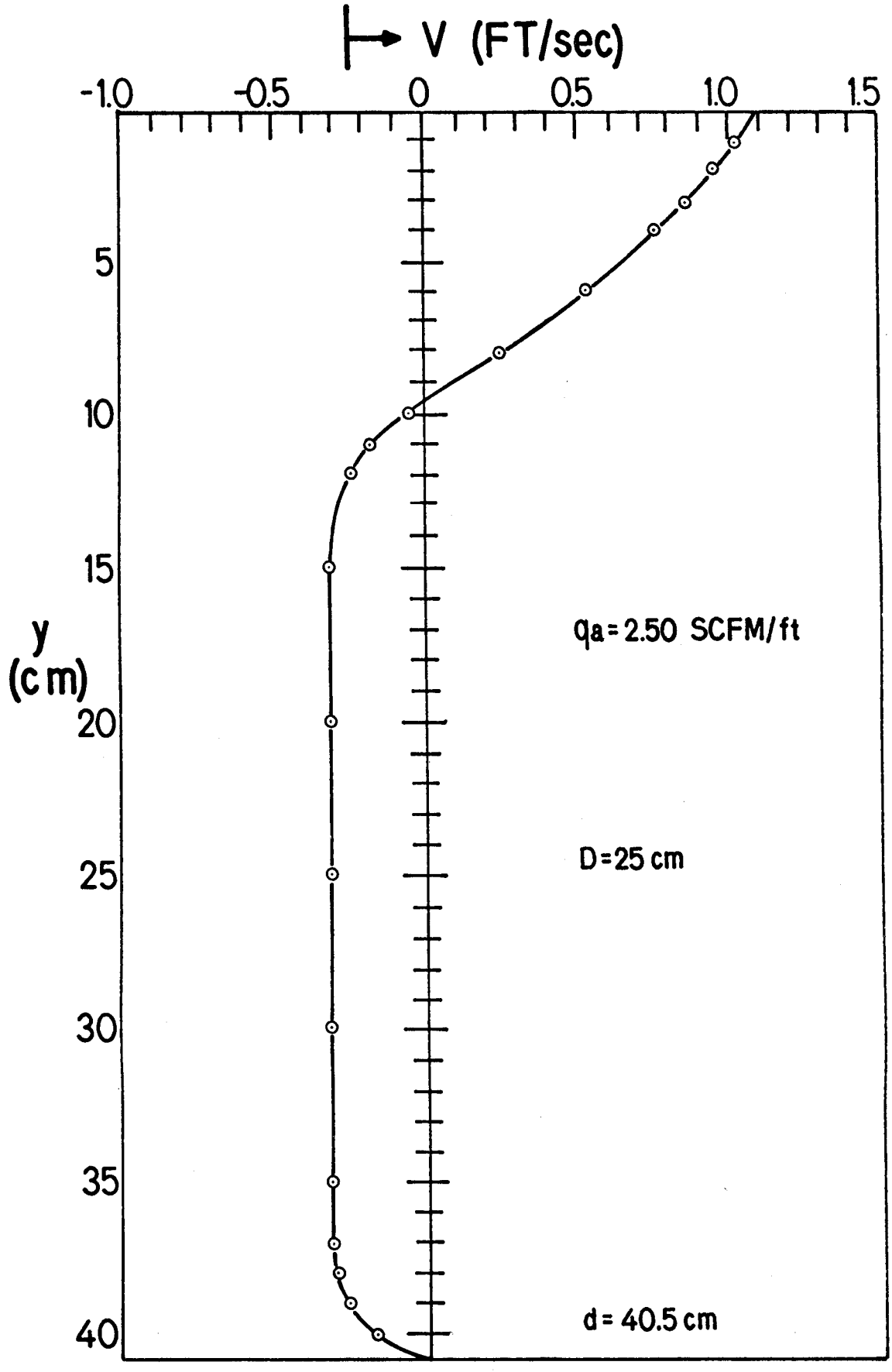

Figure 3-21. Velocity Profile at x/D = 0.3 with Raised Manifold

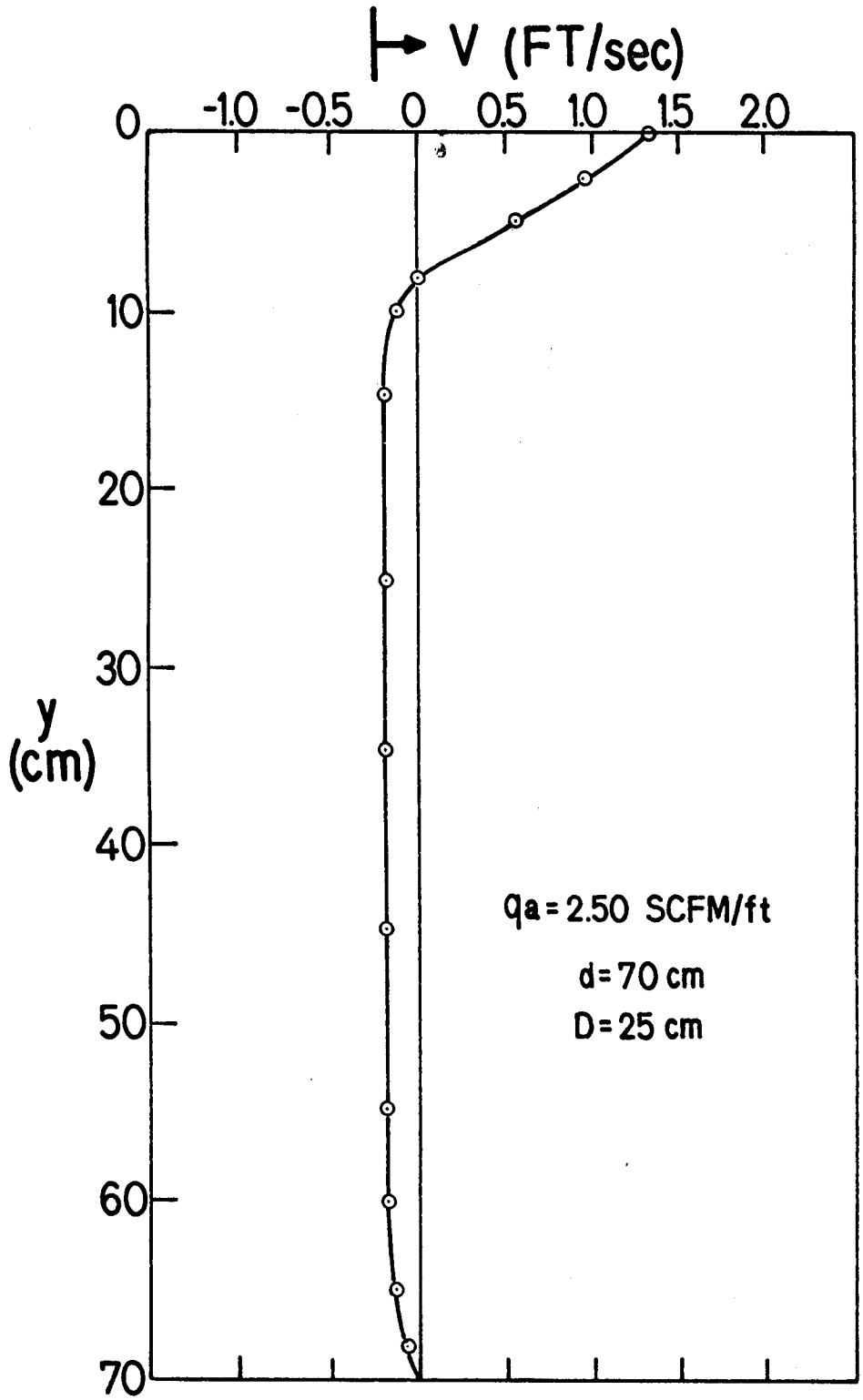

Figure 3-22. Velocity Profiles at x/D = 0.6 with Manifold Raised and on Bottom

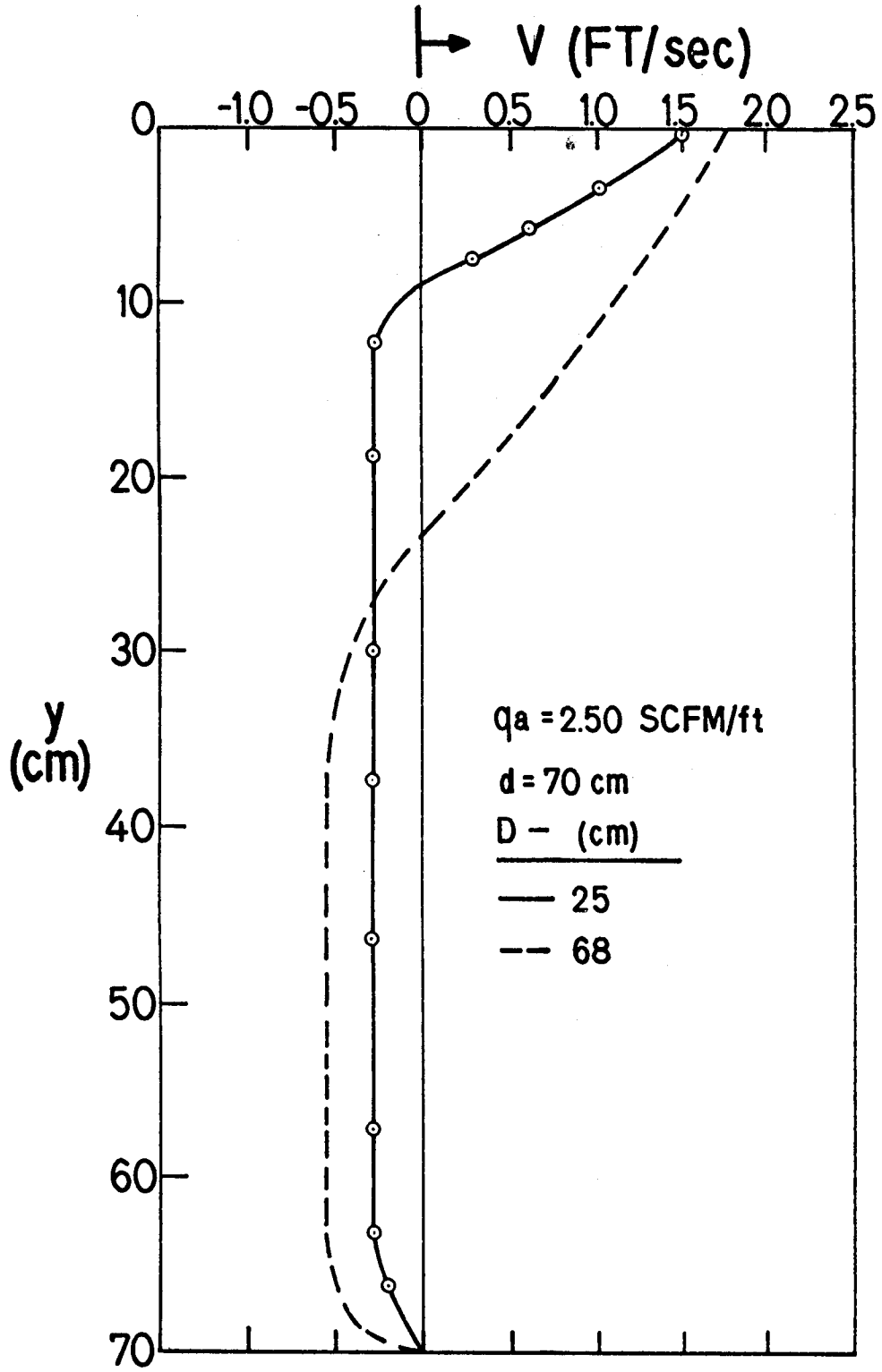

Figure 3-23. Velocity Profile at x/D = 0.9 with Raised Manifold

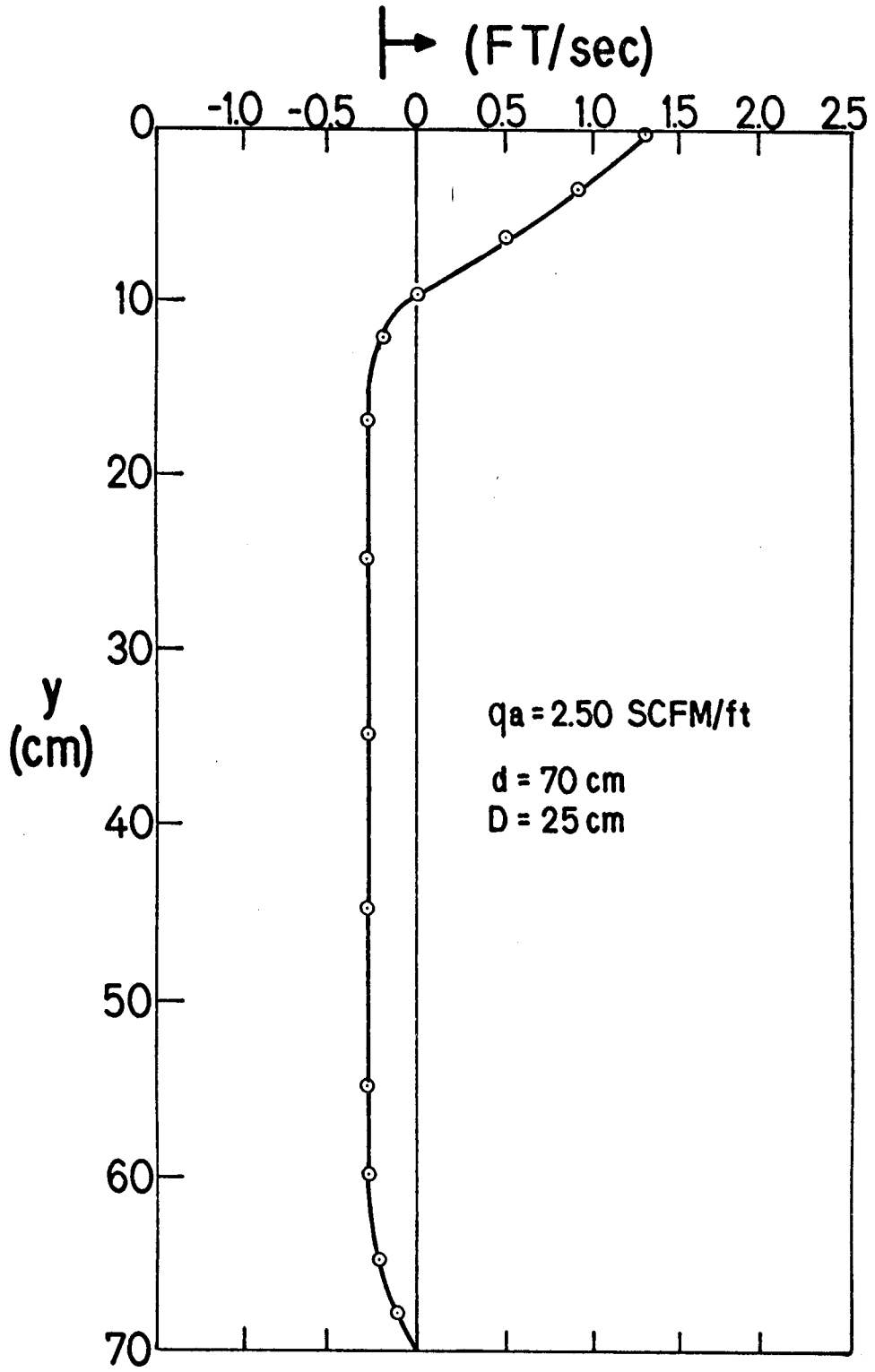

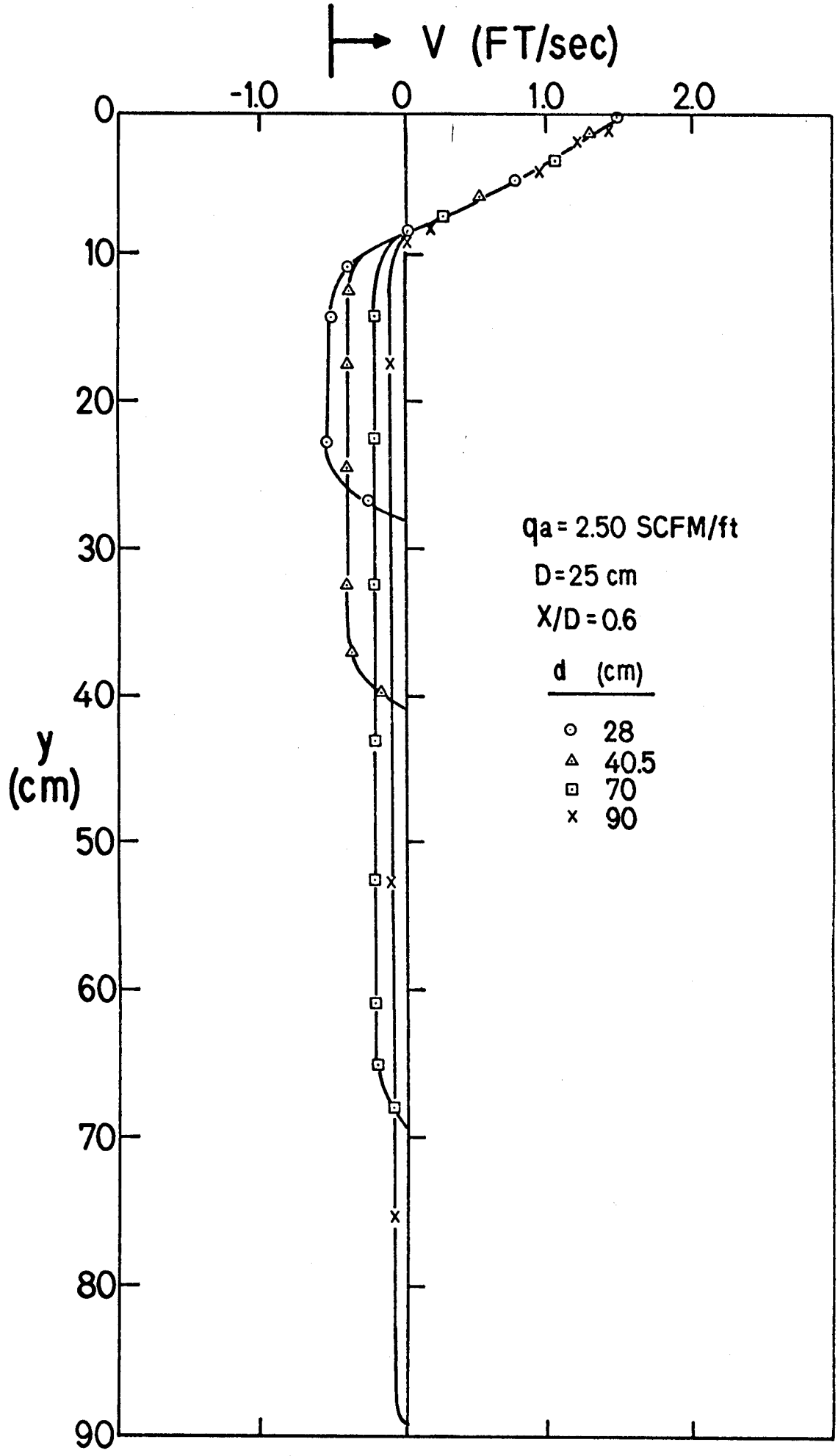

Figure 3-24. Comparison of Velocity Profiles at x/D = 0.6 with Several Water Depths and Fixed Manifold Depth, D = 25 cm

Figure 3-25. Comparison of Velocity Profiles at X/D = 0.6 with Several Water Depth and Fixed Manifold Depth, D = 50 cm

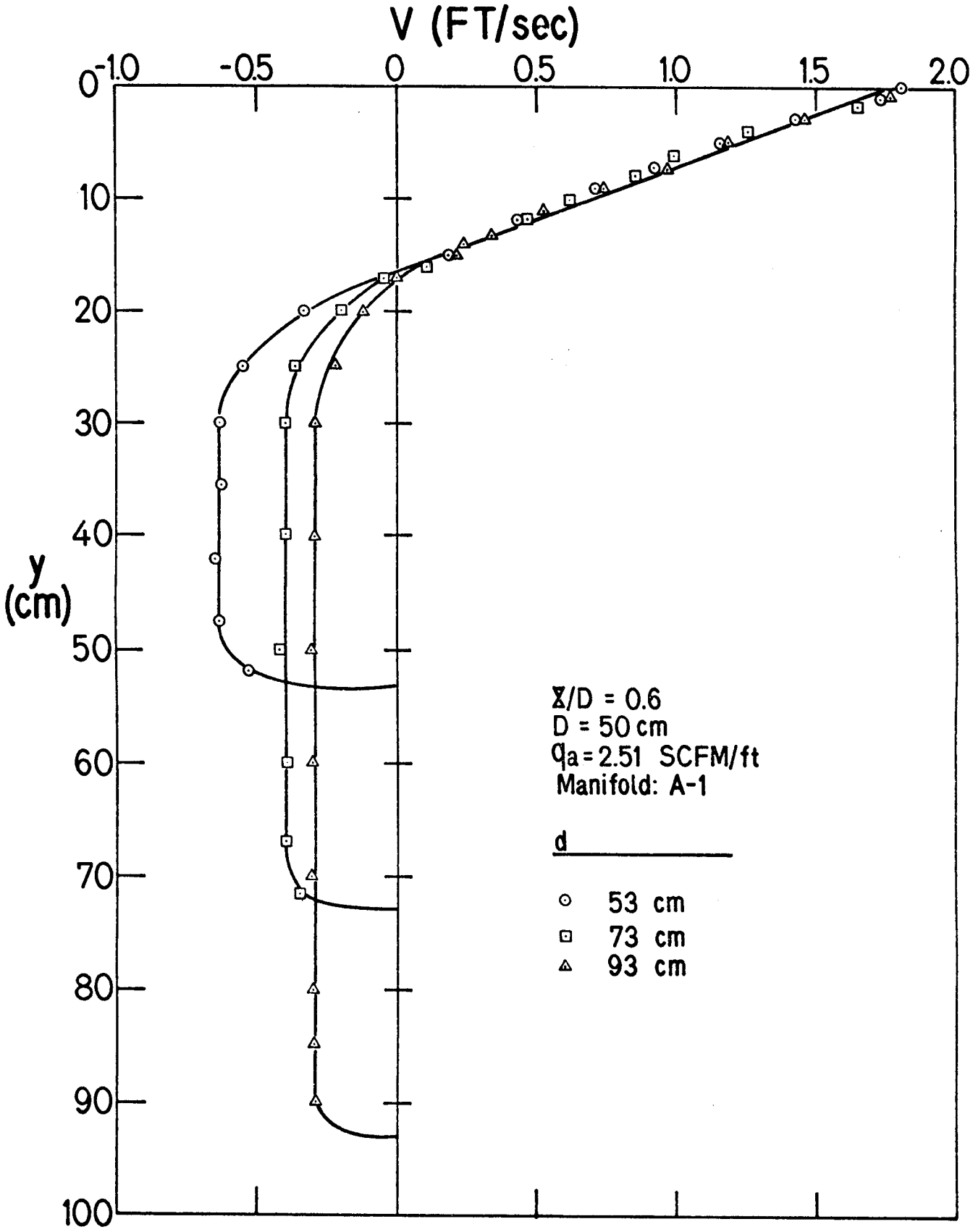

AERATION EFFICIENCY

When at least part of the reason for aeration is to generate overall circulation a useful measure of efficiency of an aeration system is given by the ratio of the flow rate of water in the surface current to the air discharge rate. Calling this the mass efficiency ratio η_m

$$\eta_m = \int_A v dA / Q \qquad 3\text{-}6$$

where v is the variable water velocity in the cross-section area A and Q is the total air discharge rate equal to Lq_a where L is manifold length. Neglecting the slight curvature in the surface current velocity profiles, it is appropriate to use a linear velocity profile

$$V/V_s = 1-(y/\delta) \qquad 3\text{-}7$$

where δ is the surface current thickness. Although we know V_s as a function of distance X from the manifold from Figure 3-6 the constant maximum surface velocity (constant over a limited (x/D) range) is the most logical measure for efficiency and to a good first approximation is a function only of the air discharge rate per unit length as given by Equation 3-1. Then, combining Equations 3-1 and 3-7, η_m can be evaluated from Equation 3-6 (assuming two dimensional flow) as

$$\eta_m = (V_{smax}/q_a) \int_o^\delta (1-y/\delta)dy = k(gq_a)^{1/3}(1/q_a)\ (\delta/2) \qquad 3\text{-}8$$

or

$$\eta_m = (1/2kg^{1/3})\delta q_a^{-2/3}$$

With $\delta = 0.33D$ at $(x/D) = 0.6$ and $k \simeq 1.60$ over the important range of aeration rates, then

$$\eta_m = 0.264g^{1/3}Dq_a^{-2/3} \qquad 3\text{-}9$$

and the mass ratio is about 770 times this volume ratio (for 25°C, 1atm). This result is compared with η_m's evaluated by graphical integration of the actual curved velocity profiles of Figures 3-14 to 3-16 on Figures 3-26 and 3-27 for the manifold on the bottom and three different water depths. The agreement is seen to be good even, surprisingly, to the very low range of aeration rates to 0.35 scfm/ft. In fact, at very low aeration rates the over-estimate in the surface flow rate inherent in using linear profiles for profiles that are actually concave would be balanced by the decreasing values of k for the very small aeration rates (that is, for less than 0.07 scfm/ft). It is important to remember that for aeration rates lower than about 0.2 scfm/ft the cell size decreases (see Figure 3-18) and the comparison begins to lose its significance since the flows are progressively less comparable. Provost found that over the mid-range of flow rates in shallow water, velocity profiles while almost linear, were better represented by the quadratic Equation 3-5. Using this result, integration with Equation 3-6 gives a numerical factor of 0.55 rather than 1/2 as shown for the linear profile. Of course, in practice, small variation in k on the order of 10% and the weak depth dependence of the surface flow rate will somewhat modify the results given here.

Figures 3-26 and 3-27 seem to suggest that very low rate aeration is most sensible in terms of the cost effectiveness of compressor expenses. We have already emphasized that at low rates circulation cell size decreases. Since the surface velocity is proportional to $q_a^{1/3}$, just to counterbalance a wind induced surface velocity of 1 ft/sec, $q_a \simeq 1.65$ scfm/ft. In addition, dissolved oxygen buildup depends on aeration rate as shown later. Equation 3-9 also shows that $\eta_m \alpha D$. However, increasing η_m by increasing D will also increase compressor costs. Further comment on these points will be presented later.

Figure 3-26. Aeration Efficiency Variation with Aeration Rate and Manifold Depth

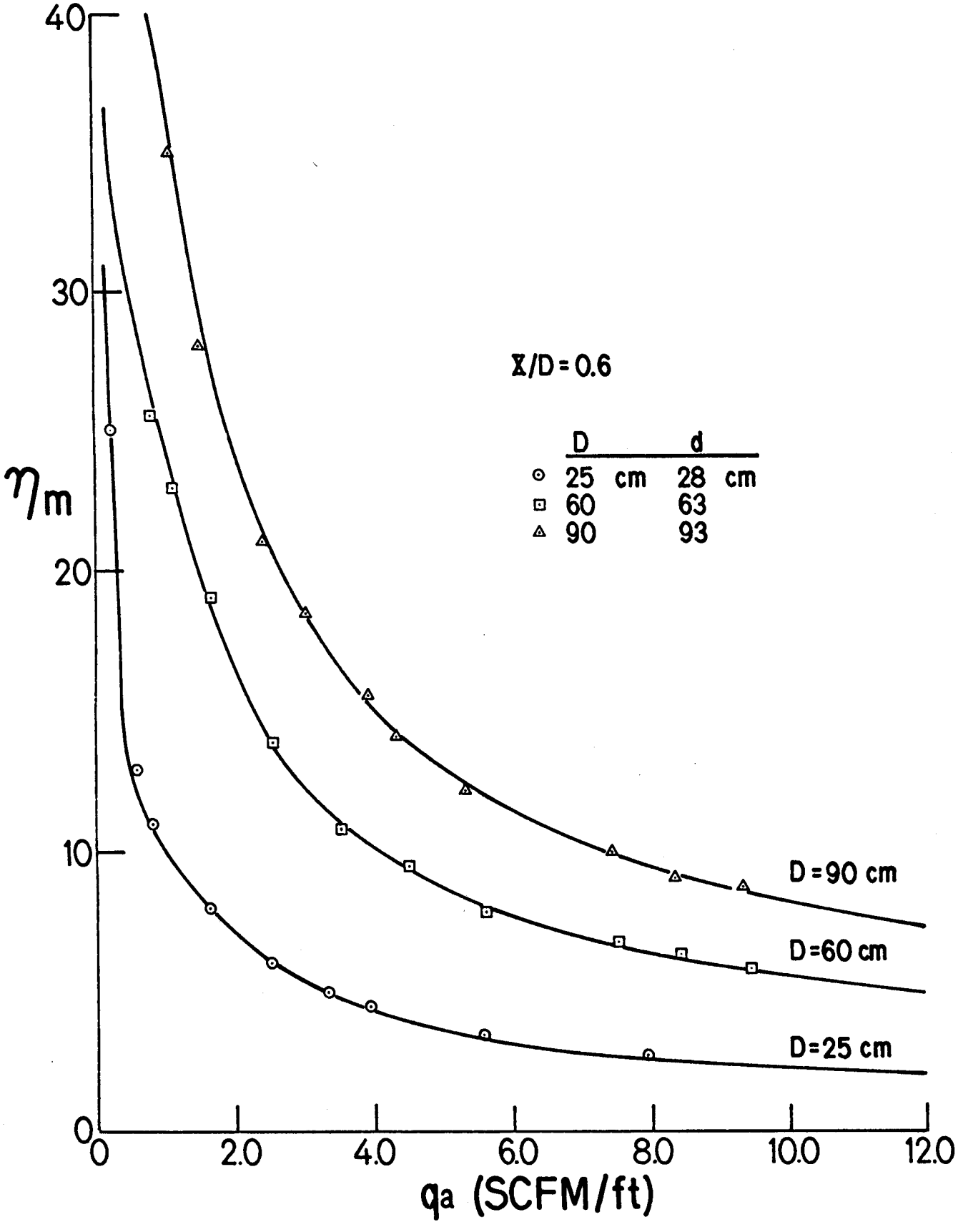

Figure 3-27. Aeration Efficiency Variation at Lower Aeration Rates

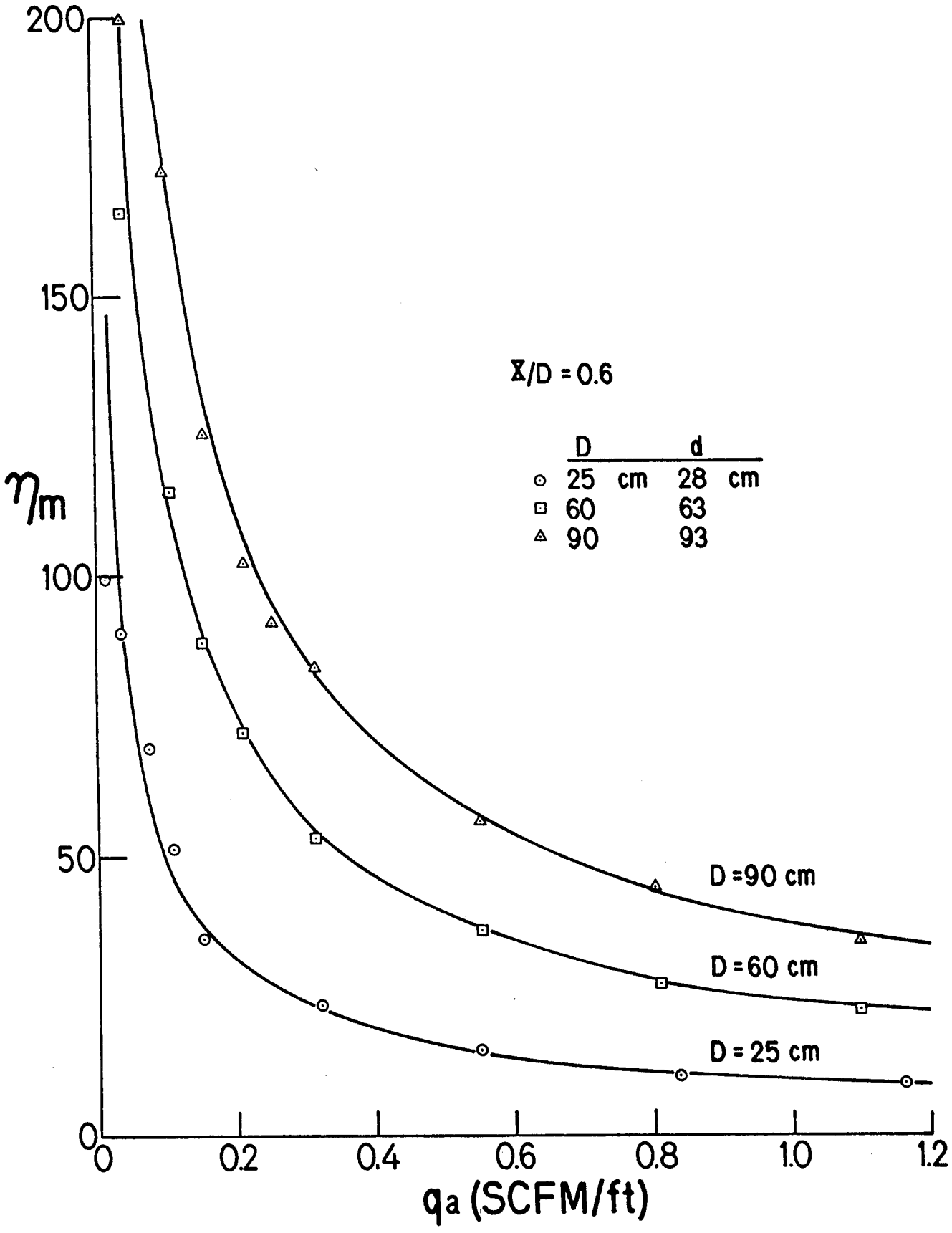

4. CIRCULATION WITH A PLANE WATER JET

Several studies have suggested or used water injection from manifolds for destratification and mixing. The primary differences between mixing with water or air are a) water jets can be directed at any angle from the vertical and b) dissolved oxygen build-up with water jets is limited to that due to circulation of oxygen rich surface water.

With these differences in mind, it would be useful to have a comparison of the effectiveness of water jet and aeration-induced circulation to provide a rational basis for the choice of these systems and to, for example, maximize overall circulation at specified cost.

Iamandi and Rouse (50) presented a simplified comparison of water jet induced circulation and aeration using the basic characteristics of the two systems. This development will be summarized since the concepts will be used in the presentation of our results. For a two dimensional jet (a slot jet) the flux of momentum is conserved so that

$$m/\rho = q_{wo}V_o = b_oV_o^2 = \int_{-b/2}^{b/2} V^2 dx \qquad 4\text{-}1$$

where q_w is the flow rate per foot of manifold with V_o the velocity at the manifold of slot width b_o. The jet velocity varies inversely with the square root of distance y, from the source, while the spread in linear in y. The flow at any y (except very close to the origin) is given by

$$q = q_o(0.62)\ \sqrt{y/b} \qquad 4\text{-}2$$

which may be combined with Equation 4-1 to give

$$q = \int_{-b/2}^{b/2} V dx = 0.62\ \sqrt{(m/\rho)y} \qquad 4\text{-}3$$

If aeration-induced flow is assumed to be due to buoyancy and bubble changes are neglected, the buoyancy (kinematic) flux per unit length of source is

$$w/\rho = q_a g = (1/\rho)\int_{-b/2}^{b/2} V\Delta\gamma dx \qquad 4\text{-}4$$

From continuity w is taken as constant with y while the momentum flux is linear in y. From experiments with heated air (33)

$$q_a = 0.57\left(\frac{w}{\rho}\right)^{1/3} y \qquad 4\text{-}5$$

For a water depth D, equating Equations 4-3 and 4-5

$$(m/\rho)/(w/\rho)^{2/3} \simeq (0.57/0.62)^2 \simeq D \qquad 4\text{-}6$$

assuming the flow patterns are similar. The ratio of power input by the water jet and aeration is

$$E_j/E_a = 1/2V_o^3 A_o/q_a Dg \qquad 4\text{-}7$$

where A_o is the jet cross-section per unit length or b_o.

Then from Equations 4-1, 4-4 and 4-6

$$E_j/E_a = 1/2V_o/(w/\rho)^{1/3} = 1/2V_o/(q_a g)^{1/3} = 1/2\sqrt{D/b_o} \qquad 4\text{-}8$$

Since $V_o^2 b_o$ is constant while the energy input $\propto V_o^3 b_o$, from momentum conservation doubling V_o is equivalent to a four fold increase in b_o, but an eight fold increase in b_o for energy conservation.

Kobus (51) extended the above analysis, based on his work with air-bubble systems, to show that for equality of surface discharge

$$m_o/w_o\sqrt{g/D}\,f(D) = 1 \qquad 4\text{-}9$$

where

$$f(D) = \frac{0.11D^2}{D^*(D+X_o)\ln(D^*\gamma_w/P_{atm})}\,\frac{\bar{U}_b/c}{\sqrt{gD}}\,\alpha\sqrt{D}$$

with the notation as defined previously. This result includes compressibility and bubble rise velocity. Kobus also shows that because of compressibility the rate of momentum flux increase with height is not linear in y. In contrast to Iamandi and Rouse's approximation from the case of a "pure" buoyancy source, Kobus' result shows that higher aeration rates are required than predicted by the "idealization" of Equation 4-6. Equation 4-9 leads to the efficiency ratio

$$E_{oj}/E_{ob} = 1/2\,\left(D/b_o\right)^{1/2}\left(\frac{M}{\gamma_w}\right)^{1/2}\frac{1}{Df(D)} = 1/2\sqrt{\frac{D}{b_o}\phi} \qquad 4\text{-}10$$

no longer the simple geometric dependence of Equation 4-8.

Kobus notes that both equations predict water jet energy input far in excess of that required for aeration for typical values of b_o and D (for which $0.1 < \phi < 1.0$). In fact, $E_{oj} \simeq E_{ob}$ only for large slots in very shallow water such that $b_o/D \simeq 0.1$.

For a given rate of flow induction (i.e., specified momentum flux) increasing slot width will decrease the required energy for a water jet while it affects aeration only in so far as the nozzle pressure drop decreases. Kobus (51) has noted that whereas a water jet requires an ever increasing discharge for a larger slot widths and is limited by capacity of the supply system, bubble screen orifices can be increased in size without any increase in air demand, up to the point at which a continuous air discharge is barely possible.

EXPERIMENTAL RESULTS

Experiments were carried out in the smaller channel (1' x 2' x 8') with manifolds of perforated 1/2" schedule 80 PVC plastic pipe. Perforation size and density were varied so that the velocity along the manifold was as nearly uniform as possible. After some trial and error, the manifold with 8, 1/16" holes spaced evenly over its one foot length (the inlet end was a 90° elbow set flat on the bottom and perforated so that full foot of length was available) gave velocity profiles at about half the depth that were fairly well represented for flow rates of 3 to 11 gpm/ft by

$$U_m/U_{mc} = (1-\frac{z}{w/2})^{1/9} \qquad 4\text{-}11$$

where w is the tank width and $\bar{z}$ the distance from the center plane. With this profile $U \simeq 0.75U_c$ at $Z = 0.9(w/2)$ and the average velocity is about 90% of the maximum or centerplane velocity.

Dimensionless velocity profiles for an intermediate flow rate and several positions above the manifold are shown to agree with Tollmien's model (45) in Figure 4-1 to establish the slot jet behavior of our perforated manifold as close as 10cm away. The velocity profile has the form

$$U/U_m = f(x/b) \qquad 4\text{-}12$$

where b is the distance from the jet axis to the position where $U = U_m/2$. b is independent of the water supply rate q_w and varies with distance as $b = 0.121Y$ consistent with jet models. The decay of centerline velocity is given by (45)

$$U_m = 2.40\sqrt{my/\rho_w} = 2.40\sqrt{k/y} \qquad 4\text{-}13$$

where the constant momentum flux is defined in Equation 4-1. Figure 4-2 shows that the experimental results are in good agreement with Equation 4-13 to about $y = 0.7D$. Beyond this point the velocity decays more rapidly because of stagnation. The stagnation zone at a free surface, for vertically directed jets, has been studied by Murota and Muraoka (52) who proposed equations for the velocity decay in the stagnation zone. Our limited measurements are in agreement with their results.

Figure 4-1. Dimensionless Velocity Profile Data for the Water Jet Compared with Tollmien's Model

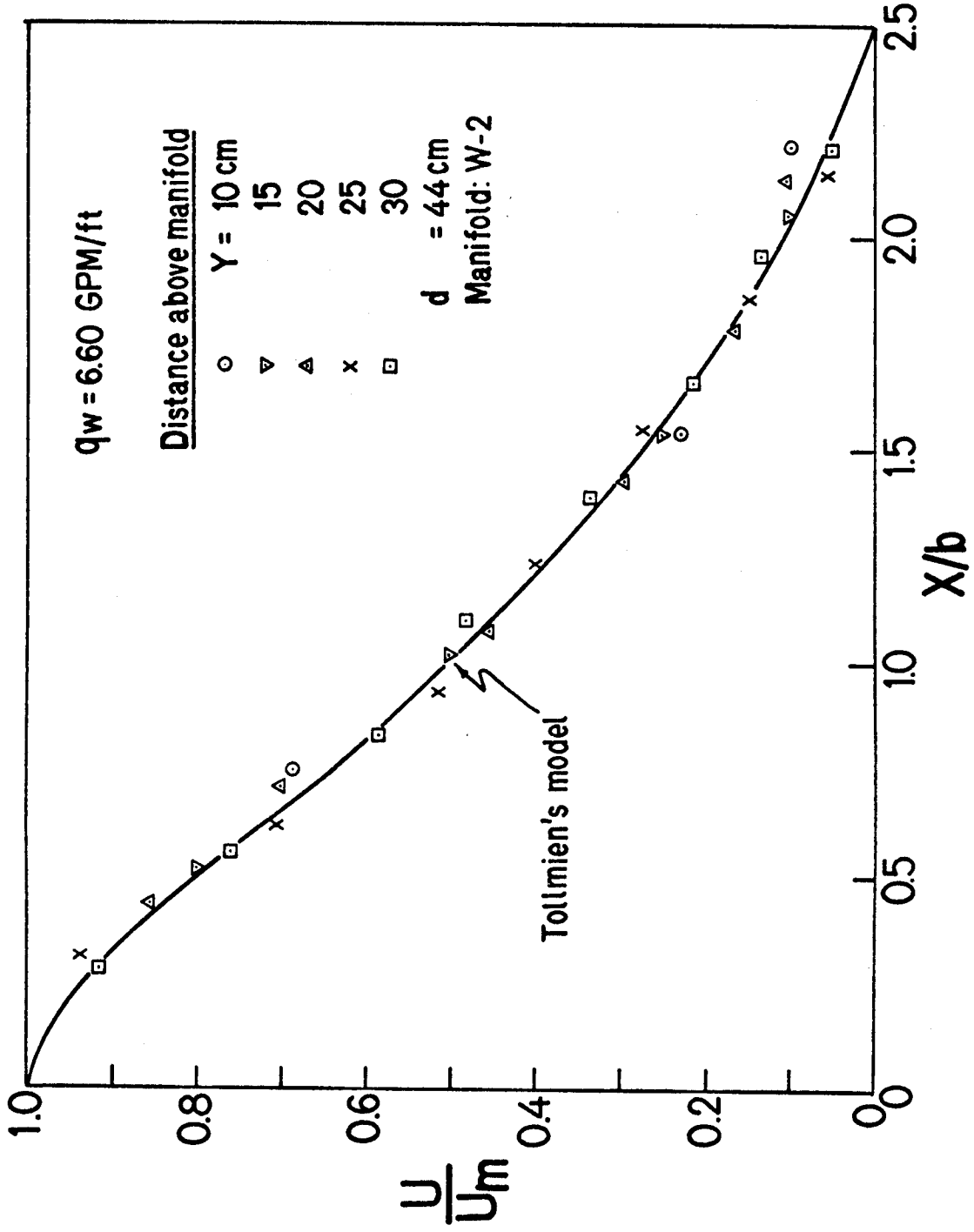

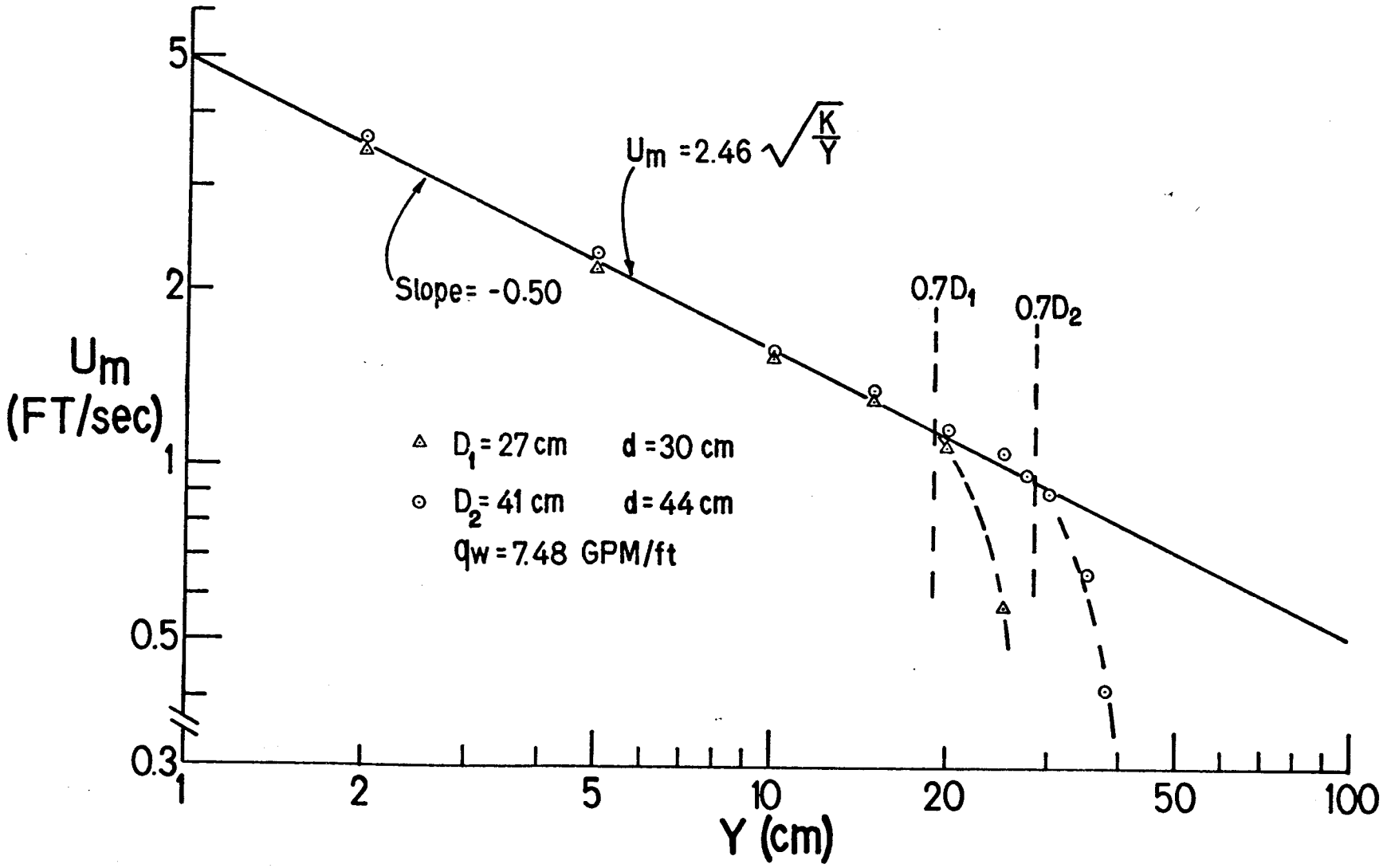

Figure 4-2. Jet Centerplane Velocity Variation with Distance from the Manifold

THE SURFACE CURRENT

Although the vertical jet velocity varies across the tank width according to Equation 4-11, the surface velocity was quite uniform over the central 10 to 11 inches of the one foot width, as shown in Figure 4-3. Surface velocity was obtained by extrapolation of measurement taken to 1/2 cm of the still water surface.

The surface velocity, V_s, reached its maximum at $x/D \simeq 0.5$ before decay began. From Equation 4-13, $V_s (\propto U_m)$, is strongly dependent on manifold depth D and characteristics (i.e., orifice size and density). Figure 4-4 shows that the Equation 4-13 describes the results for two different depths and two different manifolds. V_{smax} was found to be equal to U_m at a vertical distance $y = D$, as if the stagnation effect had not existed. Then

$$V_{smax} = 2.40\sqrt{k/D} = 2.40 q_w/\sqrt{A_o D} \qquad 4\text{-}14$$

where A_o is the total orifice area (or equivalent slot area) per unit width. While V_{smax} can be increased by reducing the orifice size or density at specified q_w and D, the pressure drop across the orifices will increase rapidly and may be a substantial part of the total system pressure drop. Note also that variation of d at fixed D and manifold does not effect the result.

Figure 4-3. Velocity Variation Across the Channel

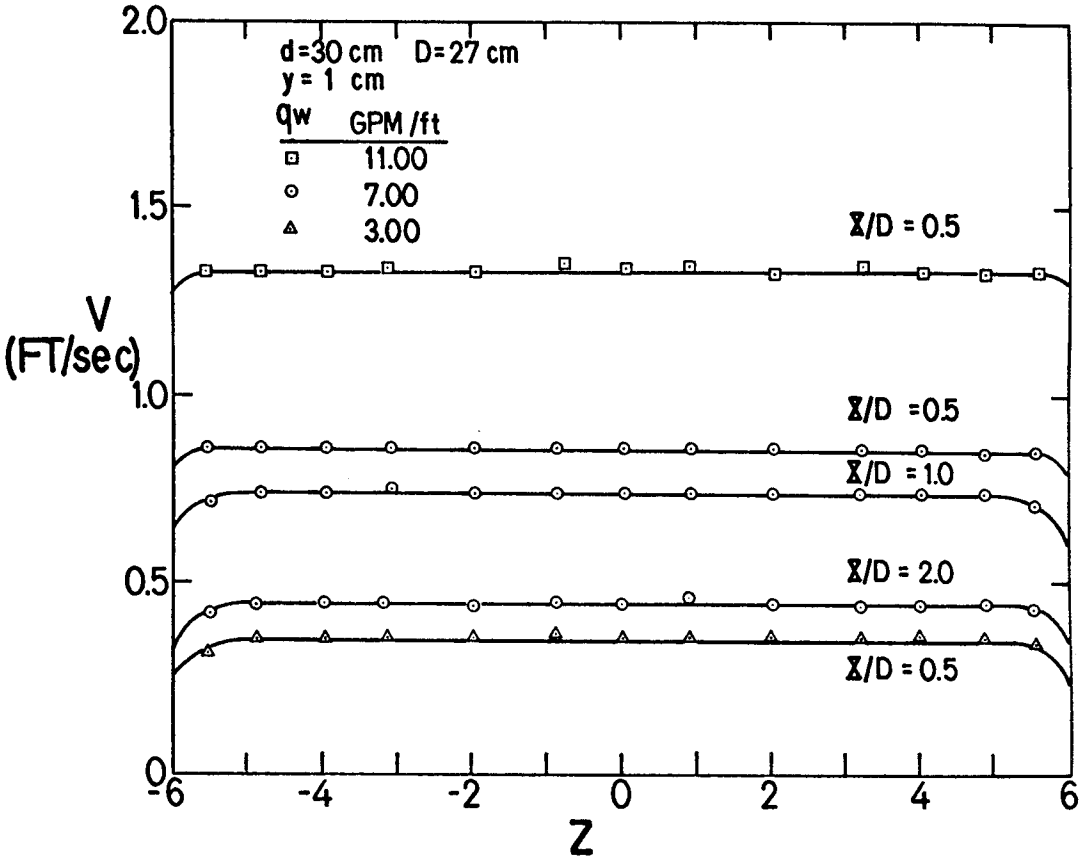

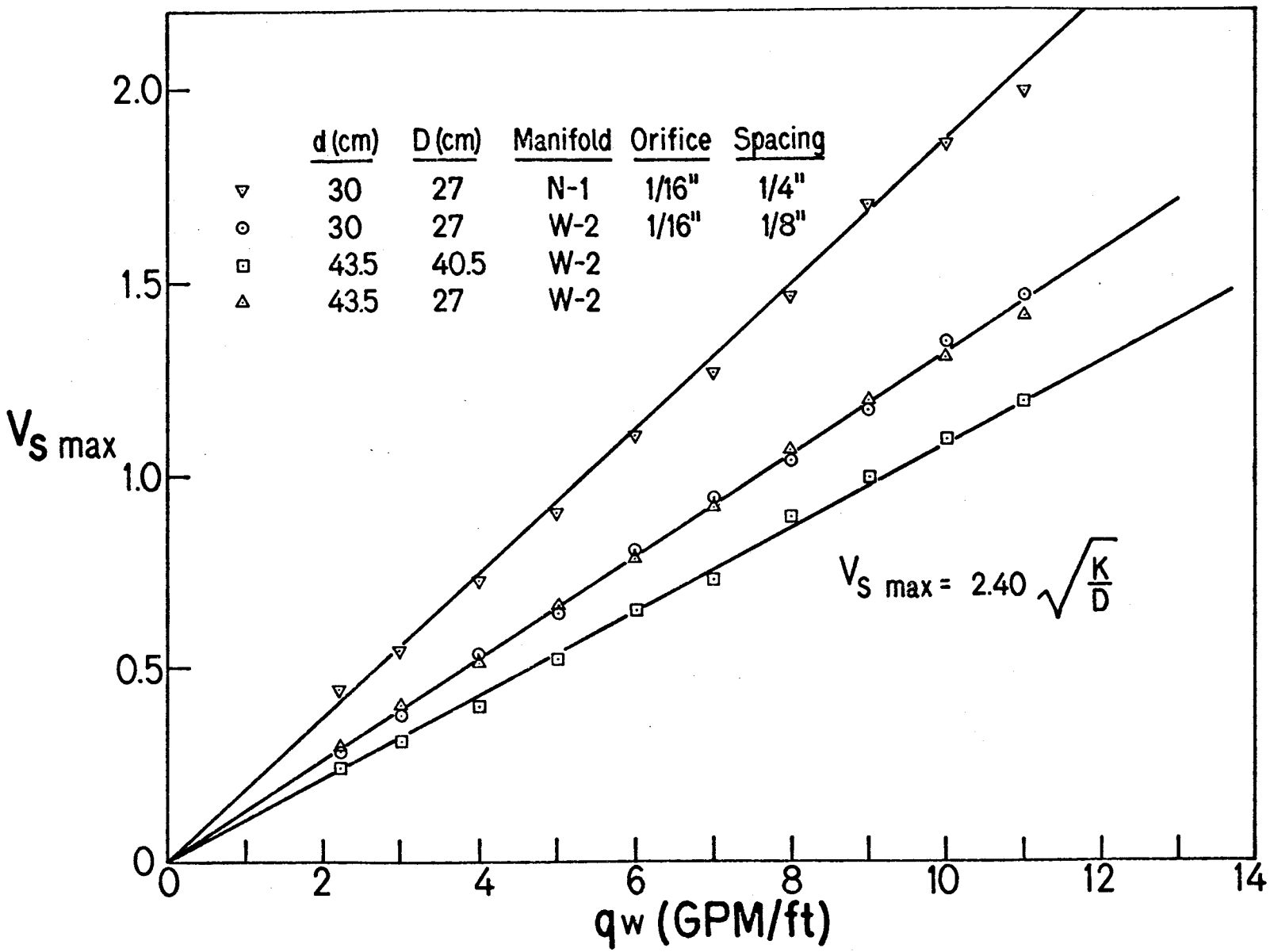

Figure 4-4. Maximum Surface Velocity Variation with Injection Rate and Manifold Characteristics

The surface velocity decay is shown in Figure 4-5. Unlike the aeration induced surface flow or a two dimensional jet, the decay is linear in X rather than proportional to $X^{-0.5}$. The data are well correlated, at least for $0.5 < x/D < 3.0$ to 3.5 by

$$V_s/V_{smax} = -0.286(x/D) + 1.14 \qquad 4\text{-}15$$

The overflow arrangement at the ends of the tank caused a measurable velocity at the end of the cell on the order of 0.05 ft/sec. However, Figure 4-5 shows a cell size of about 4d on extrapolation or just above 4d for measurements which show no clear trend of higher V_s with increasing q_w. Dye injection tests (with dye added to the water supply line) confirmed that the cell size was indeed 4.0d, and independent of q_w and manifold depth.

SURFACE CURRENT THICKNESS AND VELOCITY PROFILES

Figure 4-6 shows a series of velocity profiles which are similar to those induced by aeration and clearly establish the linear increase in surface current thickness, δ, with x. Figure 4-7 shows that the dimensionless current thickness δ/D is a function only of x/D and independent of injection rate and manifold water depth and, in fact, is the same as obtained for aeration systems:

$$\delta/D = 0.053(x/D) + 0.30 \qquad 4\text{-}16$$

Equation 4-16 predicts $\delta = 0.3D$ at $x = 0$, in agreement with the onset of the stagnation zone. Beyond $x/D = 3.6$, $\delta = 0.5d$.

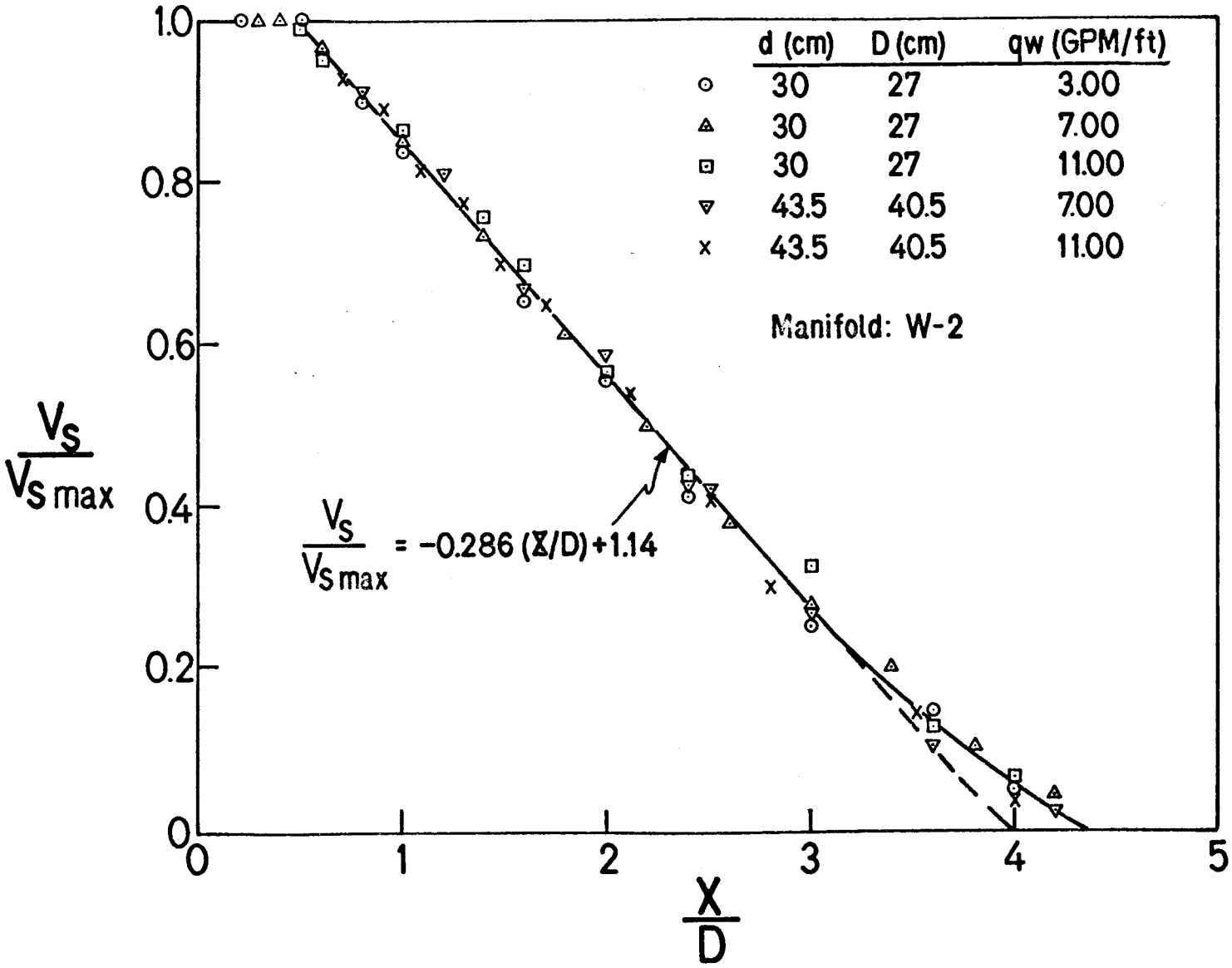

Figure 4-5. Surface Velocity Decay for a Variety of Conditions

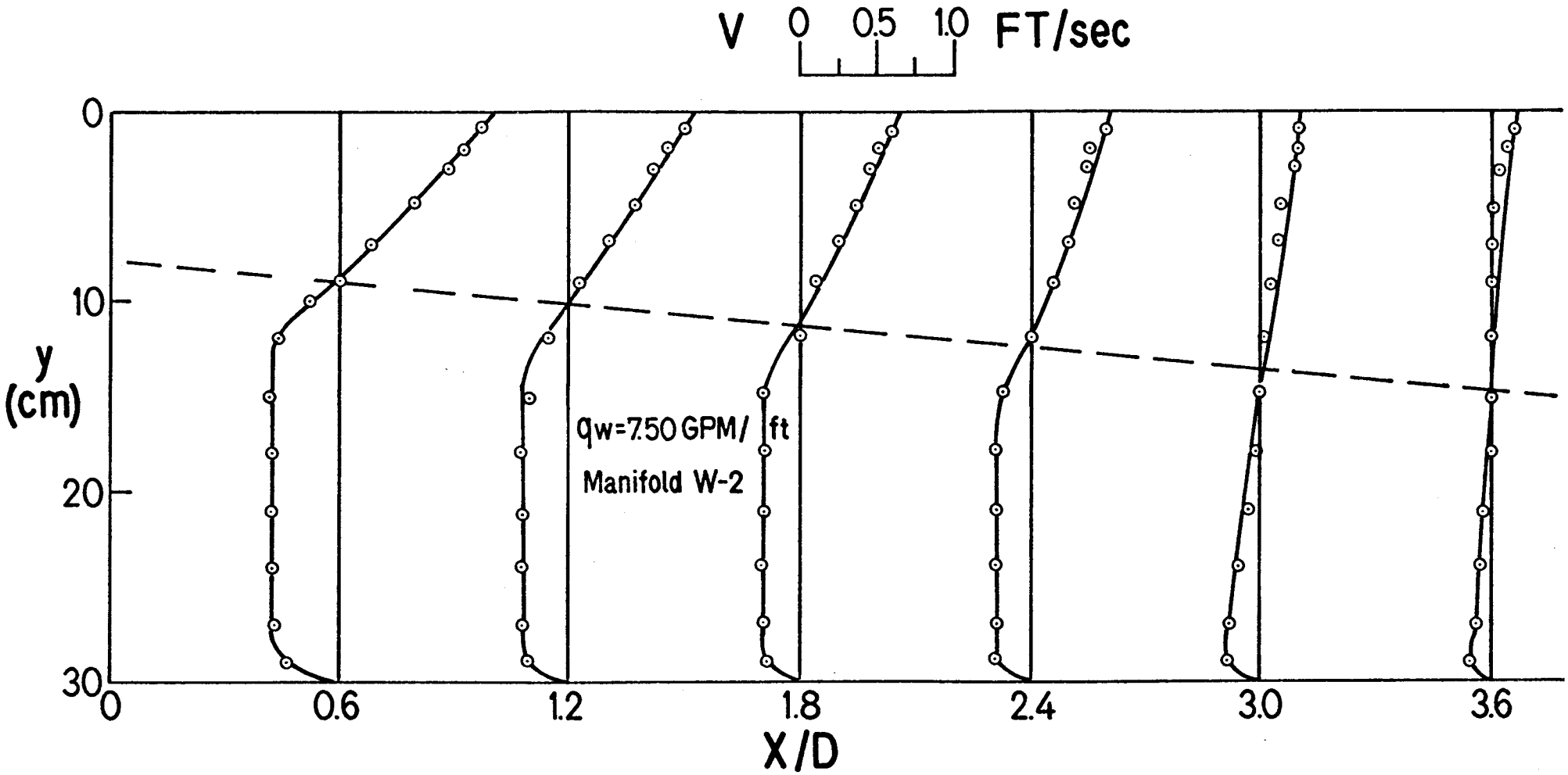

Figure 4-6. Velocity Profiles at Six x/D Positions

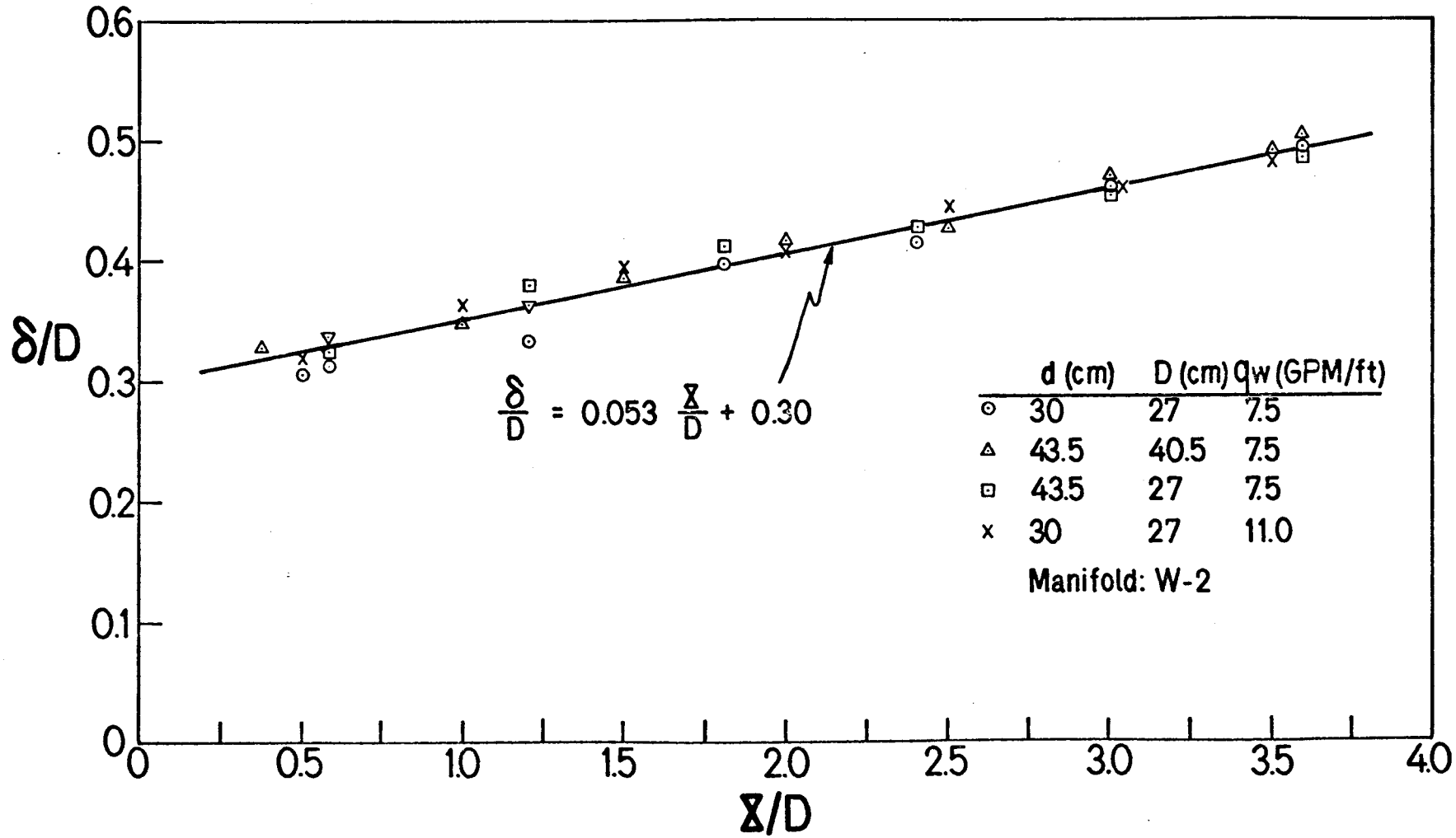

Figure 4-7. Surface Current Depth Variation with x/D

Figure 4-8 shows that the nondimensional velocity profile is independent of q_w over the range of 3 to 11 gpm/ft at x/D = 1.2, as was the case at other x/D values. The surface and bottom profiles are similar to those for aeration induced flows as expected, with slight curvature in the surface profile, and a large part of the return current at the constant velocity of $0.4V_{smax}$. When the manifold was raised off the bottom the surface current was found to depend on D and not total water depth d. Results for three tests were as expected based on aeration results described previously.

Since the surface water drawoff at the tank ends caused at least minor disturbance to the flow this effect was further explored with tests for which the manifold was located not only at the center of the tank (four feet from the end), but also at the end. A clear but small effect of manifold location on velocity profile was observed only when the manifold was adjacent to the ends of the tank (where the velocity was increased ~7%). As for aeration, end effects on the overall flow patterns and velocities were negligible.

Surface velocity profiles show a slight curvature. However, the linear profile

$$V/V_s = 1.0-(y/\delta),\ 0.6 < x/D < 3.0 \qquad 4\text{-}17$$

provides a good approximation for most of the data with the surface current thickness available from Equation 4-16.

Figure 4-8. Dimensionless Velocity Profiles at x/D = 1.2 for Several Injection Rates

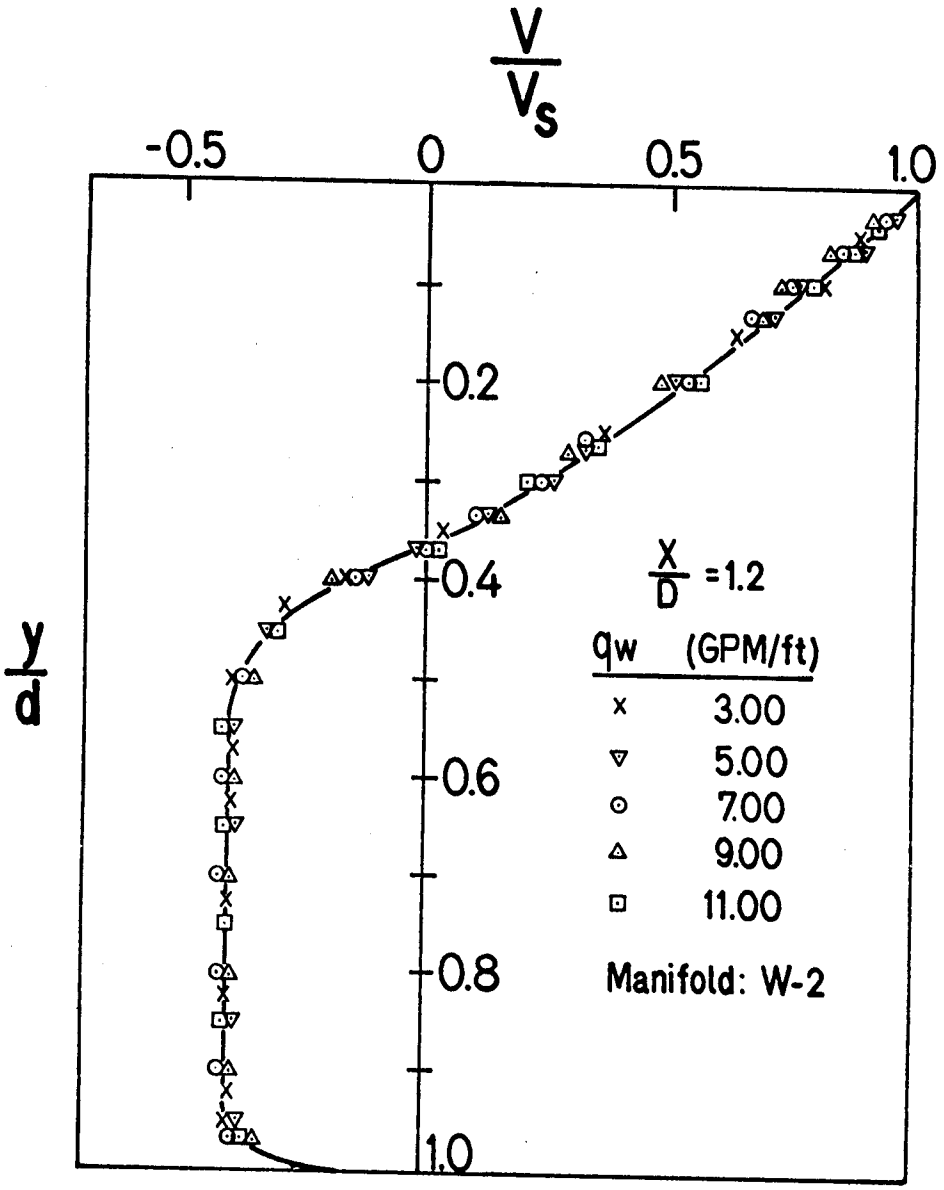

COMPARISON OF THE AERATION AND WATER JET SYSTEMS

Dimensionless velocity profiles for the water jet and air plume at $x/D = 0.6$ are compared in Figure 4-9 to re-emphasize the equivalence of shape and the nearly linear surface current profile. With this in mind, the maximum surface currents induced by aeration or water jets will be equal when the respective maximum surface velocities are equal. Then from Equations 3-1 and 4-13 with $k = 1.6$

$$2.4\sqrt{K/D} = 1.6(gq_a)^{1/3} \qquad 4\text{-}18$$

or when combined with Equation 4-6

$$K/(gq_a)^{2/3} = (m/\rho_w)/(w/\rho_w)^{2/3} = D/2.25 \qquad 4\text{-}19$$

Equation 4-19 is identical to that of Iamandi and Rouse, Equation 4-6, except for the factor of 2.25, which they take as unity (and is actually 1.18 from their development). Equation 4-19 is compared with Equations 4-6 (Iamandi and Rouse) and 4-9 (Kobus) on Figure 4-10 for $D = 10$ m with the manifold equivalent slot width taken as $A_o = .008$ mm (for ten 1 mm diameter holes per meter).

Figure 4-9. Comparison of Dimensionless Velocity Profiles at x/D = 0.6 for Aeration and the Water Jet

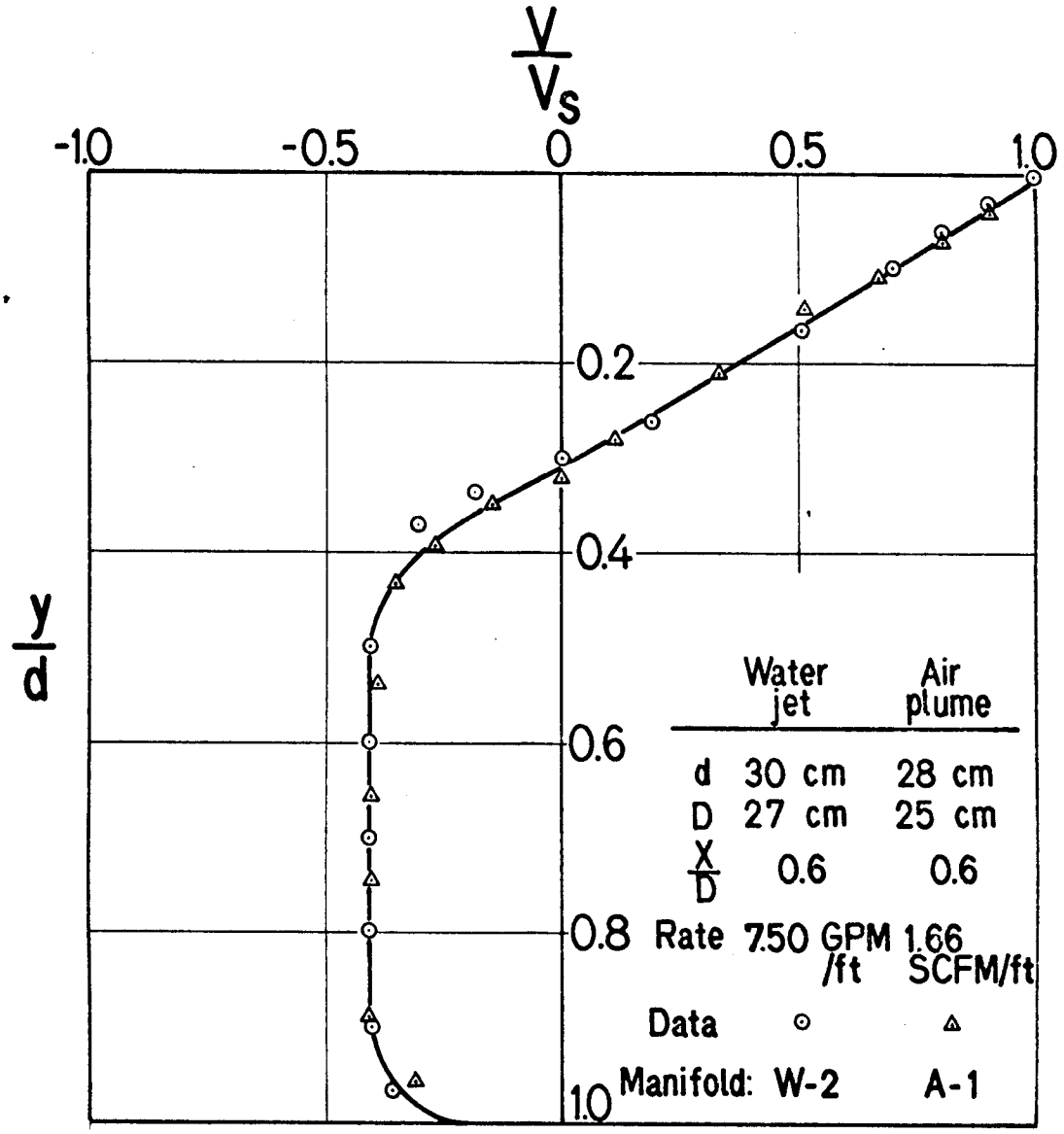

Figure 4-10. Water Jet Injection and Aeration Rates Generating the Same Surface Currents

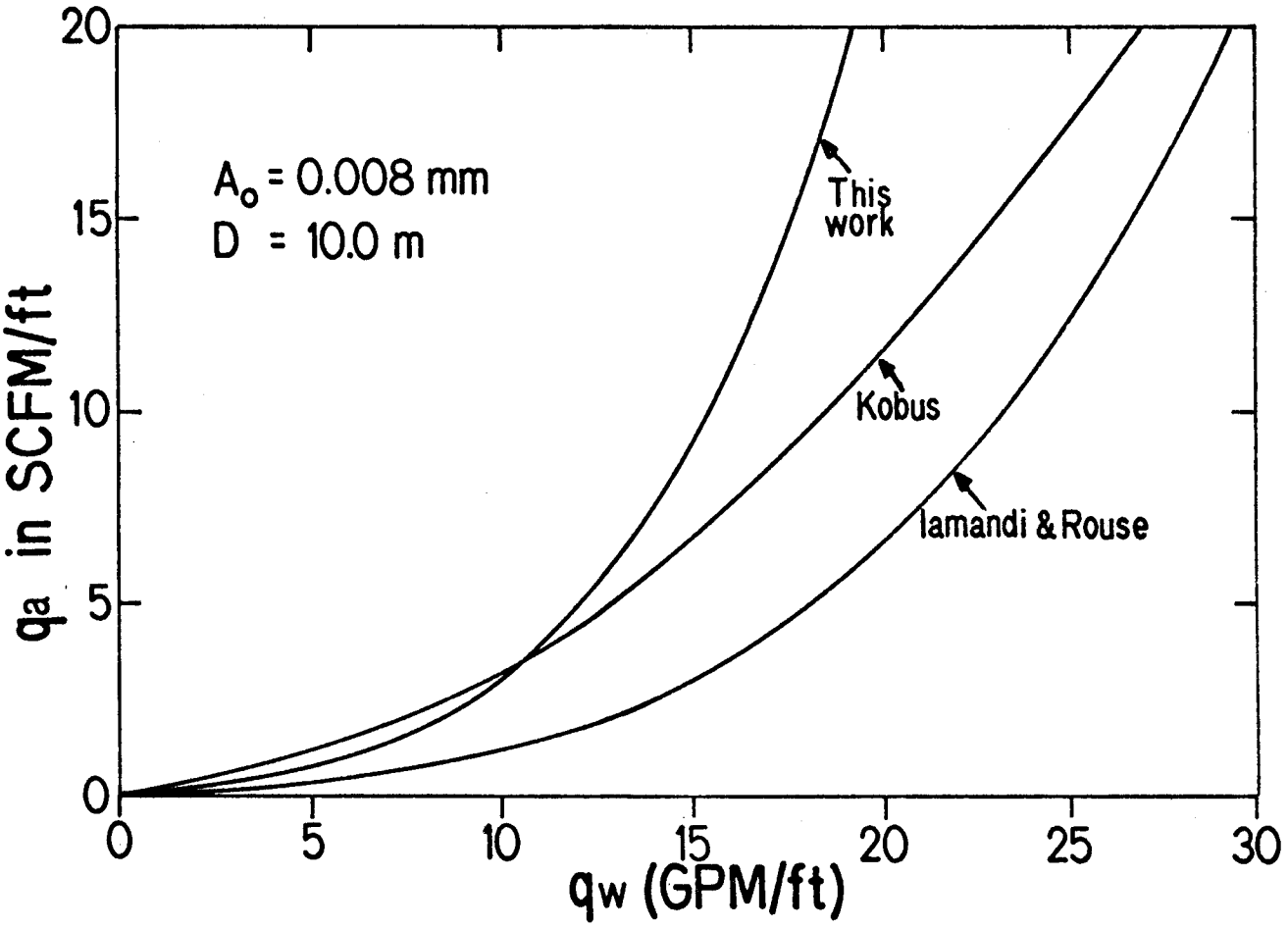

Equation 4-19 is seen to be in fair agreement with Kobus' more accurate result at least over the range of practically significant aeration rates (Kobus' maximum aeration rate was about nine ft^3/min per foot of manifold). At 5 scfm/ft our result is 10% below that of Kobus. By comparison, Equation 4-6 provides a relatively poor estimate over the entire range. Equation 4-19 can be rewritten as

$$q_w = \sqrt{DA_o/2.25}(gq_a)^{1/3} \qquad 4\text{-}20$$

to emphasize the influence of slot width. For our manifold W2, $A_o \simeq .05$ mm, so that for specified q_a and D, Figure 4-10 can be used to scale q_w, that is multiply by the factor $\sqrt{0.05/0.008}$. Then from Equation 4-20, q_w = 30.5 gpm/ft while for Equation 4-10, q_w = 33.9 gpm/ft.

We can specify the aeration and water injection rates to achieve equivalent surface flows. If the overall induced circulation provides a suitable measure of system performance, we can then evaluate the pressure losses for flow through a pipe of specified length, diameter and orifice characteristics. The cost of the required compressor or pump can then be estimated.

5. DISSOLVED OXYGEN VARIATIONS DURING AERATION

We have seen that aeration induced circulations are well described by a few simple equations. We can estimate the time for circulation of fluid in a cell from these results. With this background, it was of interest to determine how dissolved oxygen (D.O.) concentrations varied with aeration rate and other system parameters with the aim of developing a simple model for the time variation of D.O. during aeration. With such a model, we could choose to run the compressors only until the desired D.O. level was attained and then continue aeration on an intermittent basis after the D.O. has fallen off to some predetermined level.

Figure 5-1 shows that the time variation of dissolved oxygen, C, in ppm, was essentially independent of probe position. Here $x/D = 2$ indicates that the probe was at the mid-point of one of the circulation cells (of total extent $x/D = 4$) with measurements for the probe at several water depths, y, and at the mid-plane of the channel $\bar{z} = 0$ or near the wall at $\bar{z} = 14$ cm. The initial D.O. concentration was chemically adjusted to zero for each run as described in the Appendix where other experimental details were presented.

The independence of D.O. on probe position within the circulation cell was not surprising since the aeration rate of 2.48 scfm/ft results in fluid circulation times on the order of tens of seconds while the D.O. buildup is on the order of tens of minutes. However, as shown in Figure 5-2, the D.O. build-up rate is dependent on distance from the manifold.

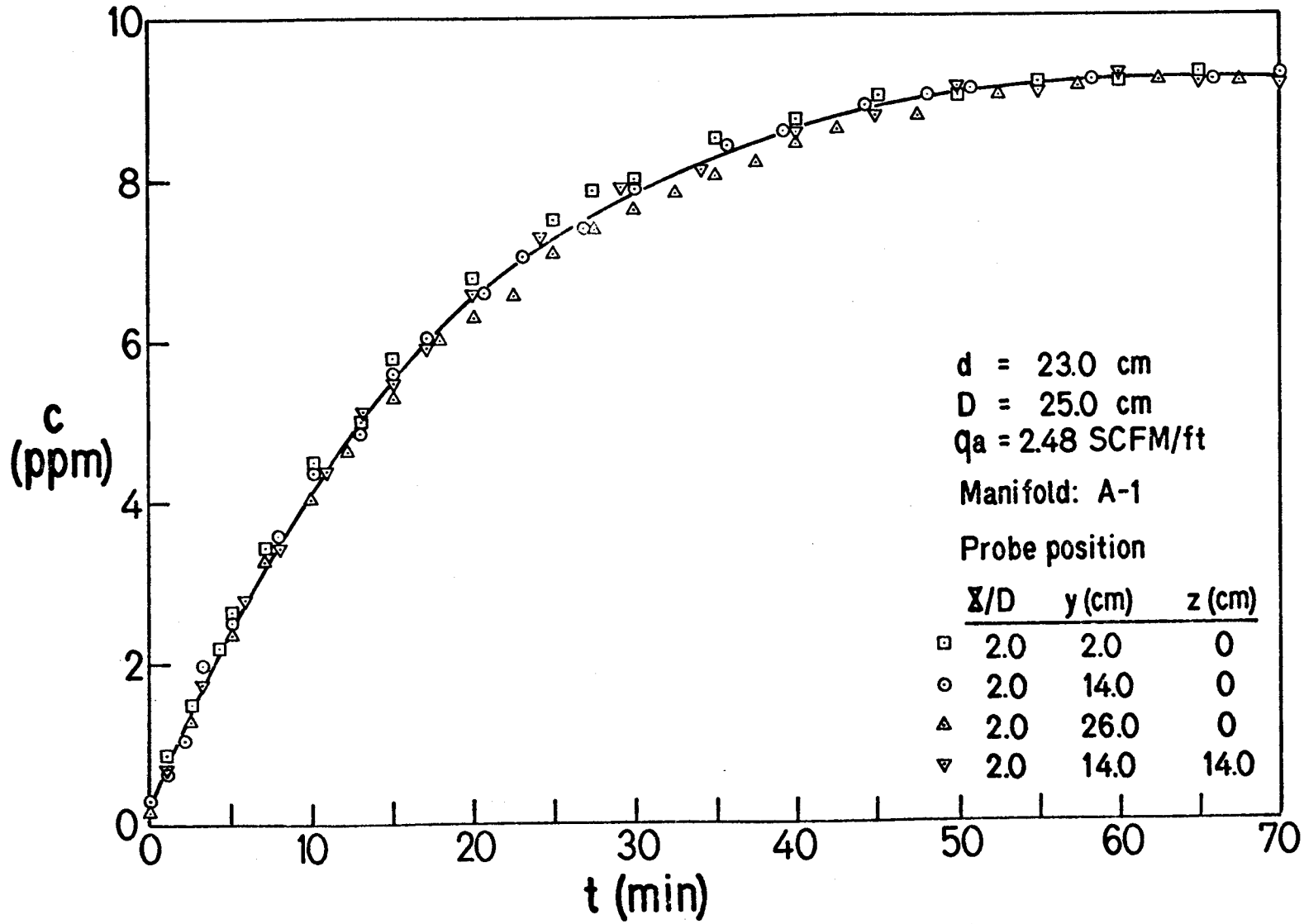

Figure 5-1. Dissolved Oxygen Buildup at x/D = 2 for Several Probe Positions

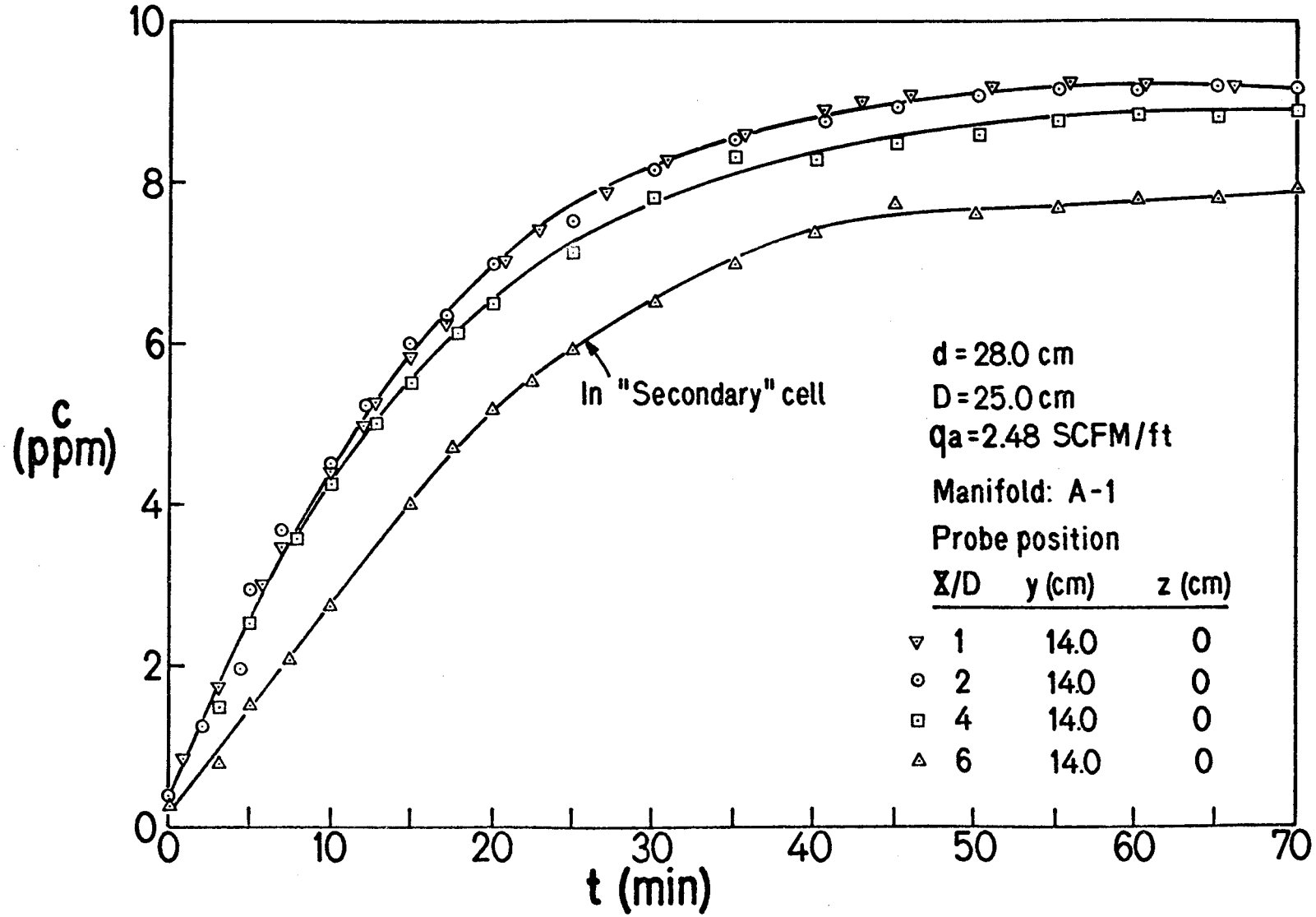

Figure 5-2. Dissolved Oxygen Buildup at Four Values of x/D

Within the cell, that is for probe at x/D = 1 and 2, the results are identical. When the probe is set at the end of the cell, at x/D = 4.0, a somewhat slower build-up of D.O. is observed. With the probe in the "secondary cell" at x/D = 6 the D.O. build-up is substantially slower. While there is transfer of D.O. at the boundary between the primary and secondary cell, it is limited and low velocities in the secondary cell may lead to non-uniformities. Since the secondary cell of Figure 5-2 was constrained within the limited distance between the end of the primary cell and the channel end plate, the particular rate of D.O. increase depends on geometry as well as aeration rate.

The influence of aeration rate on D.O. build-up, for the same conditions as on Figures 5-1 and 5-2, is shown in Figure 5-3. The approach to the equilibrium or saturation D.O. concentration of about 9.2 ppm is clear as is the exponential behavior of the curves. Note that even at the relatively high aeration rate of 3.96 scfm/ft, 40 minutes is required before the final D.O. value is obtained. The results of Figure 5-3 have been re-plotted on Figure 5-4 with the concentration made dimensionless with the saturation D.O., Cs, and initial D.O., C_o, although C_o = 0 for the experiments. The data fall on surprisingly straight lines on this semi-log plot and suggest the utility of the following simple model.

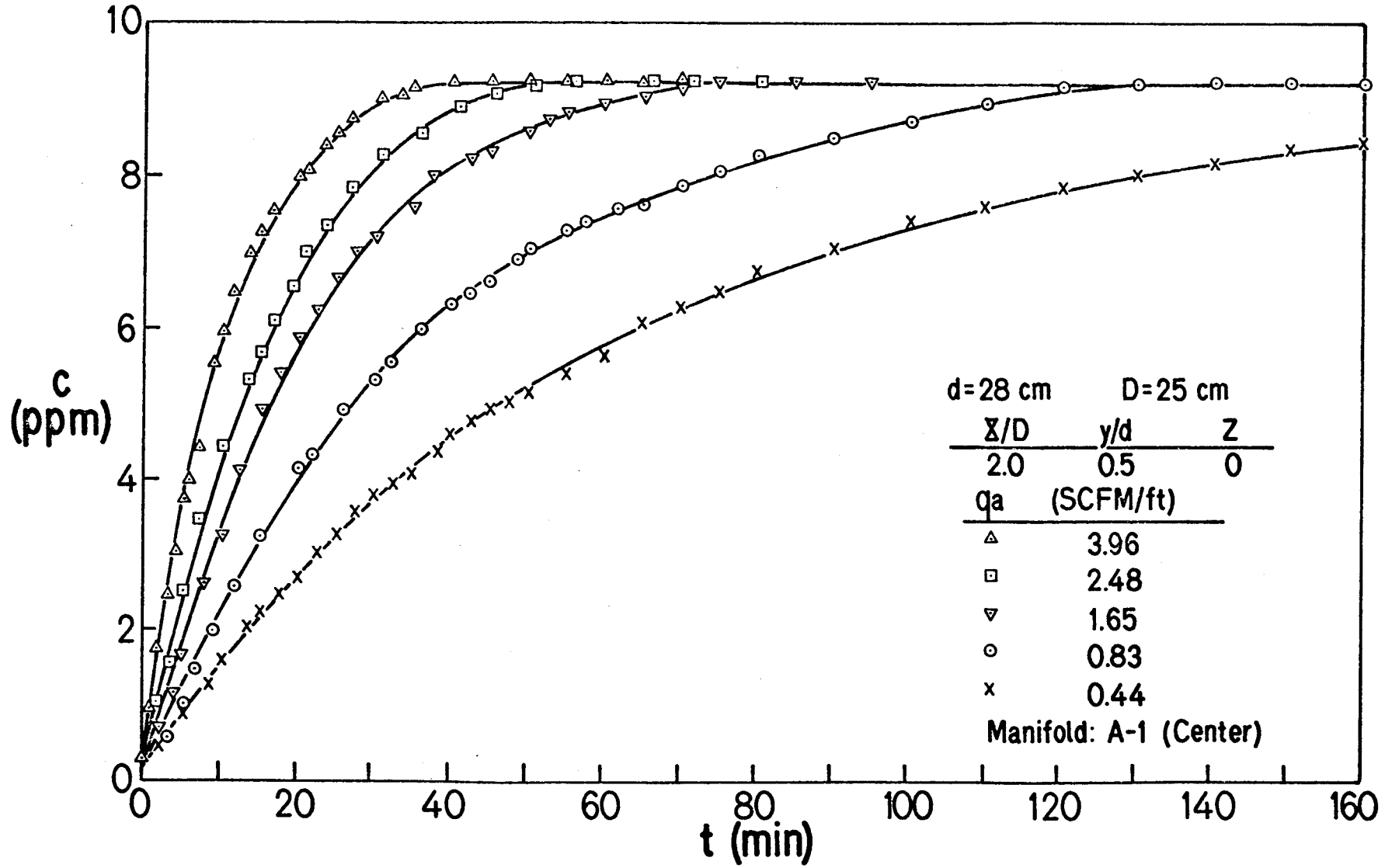

Figure 5-3. Dissolved Oxygen Buildup for a Wide Rate of Aeration Rates

Figure 5-4. Dimensionless D.O. Variation - Figure 5-3 Results

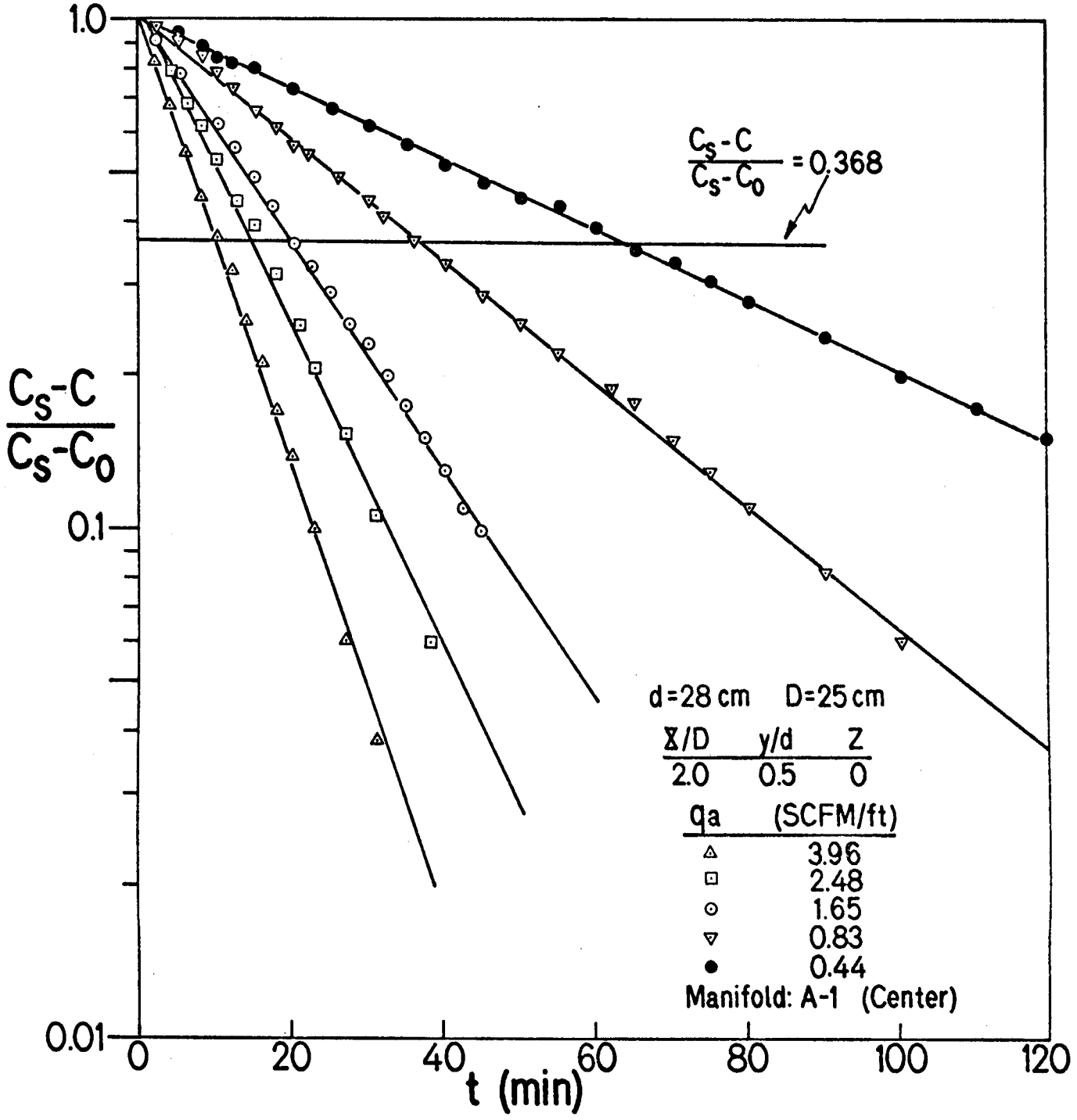

We know that mixing is "ideal" within the cell so that there are no spatial variations in D.O. Then if D.O. build-up is controlled by mass transfer from the manifold air bubbles, for any specified aeration rate and manifold, the mass balance is just

$$v dc/dt = k_f a(C_s - C) \qquad 5\text{-}1$$

where v is the cell volume, a the interfacial area of the air bubbles, and k_f is the mass transfer coefficient which for a slightly soluble gas like oxygen is dependent on the liquid film resistance. Rearranging Equation 5-1 and integrating C_s

$$\frac{C_s - C}{C_s - C_o} = e^{-t/\theta} = \frac{\phi}{\phi_o} \qquad 5\text{-}2$$

where the time constant $\theta = v/ak_f$ and $\phi = C_s - C$ is the dissolved oxygen deficit. The time constant is just the time required for ϕ to reach 36% of its initial value, ϕ_o. Evidently Equation 5-2 provides a useful model in view of the straight lines obtained in Figure 5-3. Of course, the time constant θ decreases with increasing q_a.

Figure 5-5 shows the variation of the time constant with aeration rate and manifold design. For each manifold the slope is the same so that

$$\theta \propto q^{-0.8} \qquad 5\text{-}3$$

Both the interfacial area per unit volume, a/v, and the mass transfer coefficient depend on bubble size and hence manifold design. Manifolds A-1 and A-3 of Figure 5-5 have the same total orifice area, but A-3, with smaller holes, gives a smaller time constant. Use of a porous tube gives substantially lower time constants then the perforated tubes. Remember, however, that variation in orifice size or density had little influence on overall circulation. In practice decreasing orifice size to increase D.O. build-up rate must be balanced against higher system pressure drop or the use of more expensive porous tubing which may be more prone to plugging.

The influence of aeration rate and manifold design on bubble size can be estimated from pertinent literature. Then, with bubble size specified, the mass transfer coefficient may be estimated with well established correlations. We did not attempt a systematic evaluation of the variables that set θ so that no further analysis will be provided here. Eckenfelder's correlation (35) for the overall mass transfer coefficient, $\alpha\, \theta^{-1}$ for air bubbles rising through still water gives $\theta \sim q^{-n}$ where n = 0.8 to 1.0 and $\theta \sim D^{-2/3}$. Limited testing in our shallow depths of 28 to 90 cm did not show any influence of submergence on D.O. build-up rate.

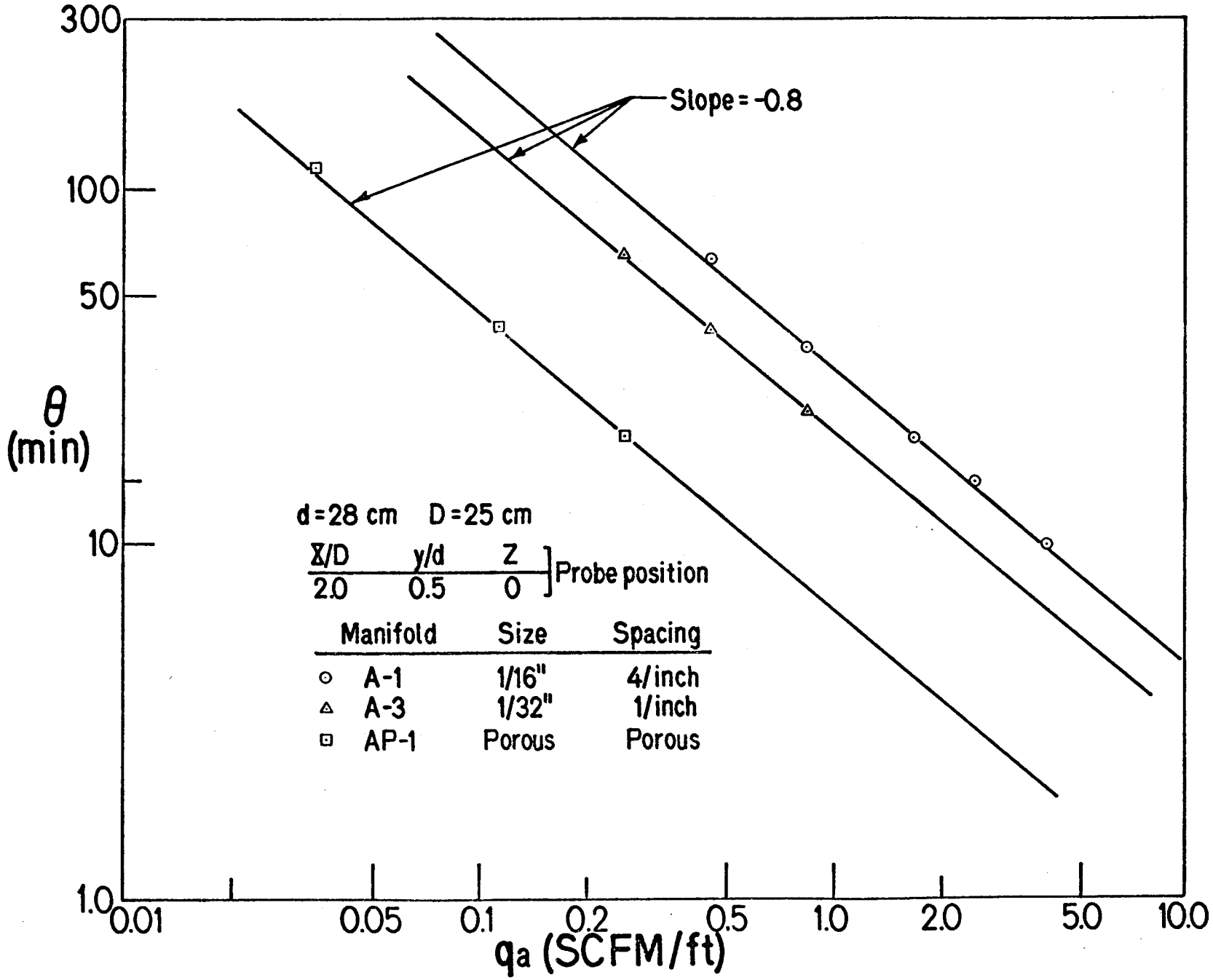

Figure 5-5. Time Constant (from Equation 5-2) Variation with Aeration Rate and Manifold Design

In summary, while our simple D.O. build-up model is quite useful in describing the results of our experiments in shallow water, scale-up to deeper water requires further evaluation of the factors that set the time constant. The verification of uniform D.O. levels throughout the primary cell and the importance of manifold design on D.O. variation, but not overall circulation, are concepts that will remain valid with scale-up.

6. AERATION FROM POINT SOURCES

THE VERTICAL PLUME

The vertical plume induced by aeration from a point source was studied by Baines and Hamilton (49) and later in more detail by Kobus (44). Our experimental studies (43) examined the velocity profiles and circulation cell characteristics to obtain the same kinds of results already described in detail for aeration from line sources.

Kobus (43) used the Gaussian distribution curve,

$$U(r,x) = U_m \exp(-r^2/2\sigma^2) \qquad 6\text{-}1$$

with a linear spread with distance from the analytical origin, x_o, such that

$$\sigma = C(x+x_o) \qquad 6\text{-}2$$

required by similarity. The standard deviation σ is the radial distance from the centerline where $U = 0.606U_m$.

The centerline velocity was given by

$$U_m(x) = (1/C(x+x_o))\sqrt{(-PatmQ/\pi\rho_w U_b)\ln(1-x/H)} \qquad 6\text{-}3$$

where the symbols have the same meaning as in Equation 2-14. The parameters to be determined by experiment are x_o, C, and U_b. Kobus found x_o to be 2.6 ft. independent of air supply rate, for tests with water depths of 2 m and 4.5 m with single orifices of 0.05 to 0.5 cm in diameter at air discharge rates up to 13 ft^3/min. In our experiments with only 2.5 to 3.75 feet of water, x_o was also found to be 2.6 ft. with aeration rates of 1.25 to 8.6 scfm and σ was linear in x. However, our point sources were actually perforated plates with, for example, 96, 1/16" diameter holes spaced uniformly over a circle of 1 5/16" diameter. The rate of spread of the velocity profiles, C, was found to increase with the air discharge rate to 0.15 power as observed by Kobus. Our measurements were limited to 9 scfm since at higher values, high waves and oscillations in our 15 ft. diameter water tank made measurements impossible. We did not attempt to verify Kobus' result that U_b varies with the aeration rate to the 0.15 power. Figure 6-1 shows the variation in centerline velocity with distance above the aeratior for four different aeration rates. These results are observed to be in good agreement with Kobus' result, Equation 6-3, over the mid-range of water depth, where the velocity increases only slowly with x.

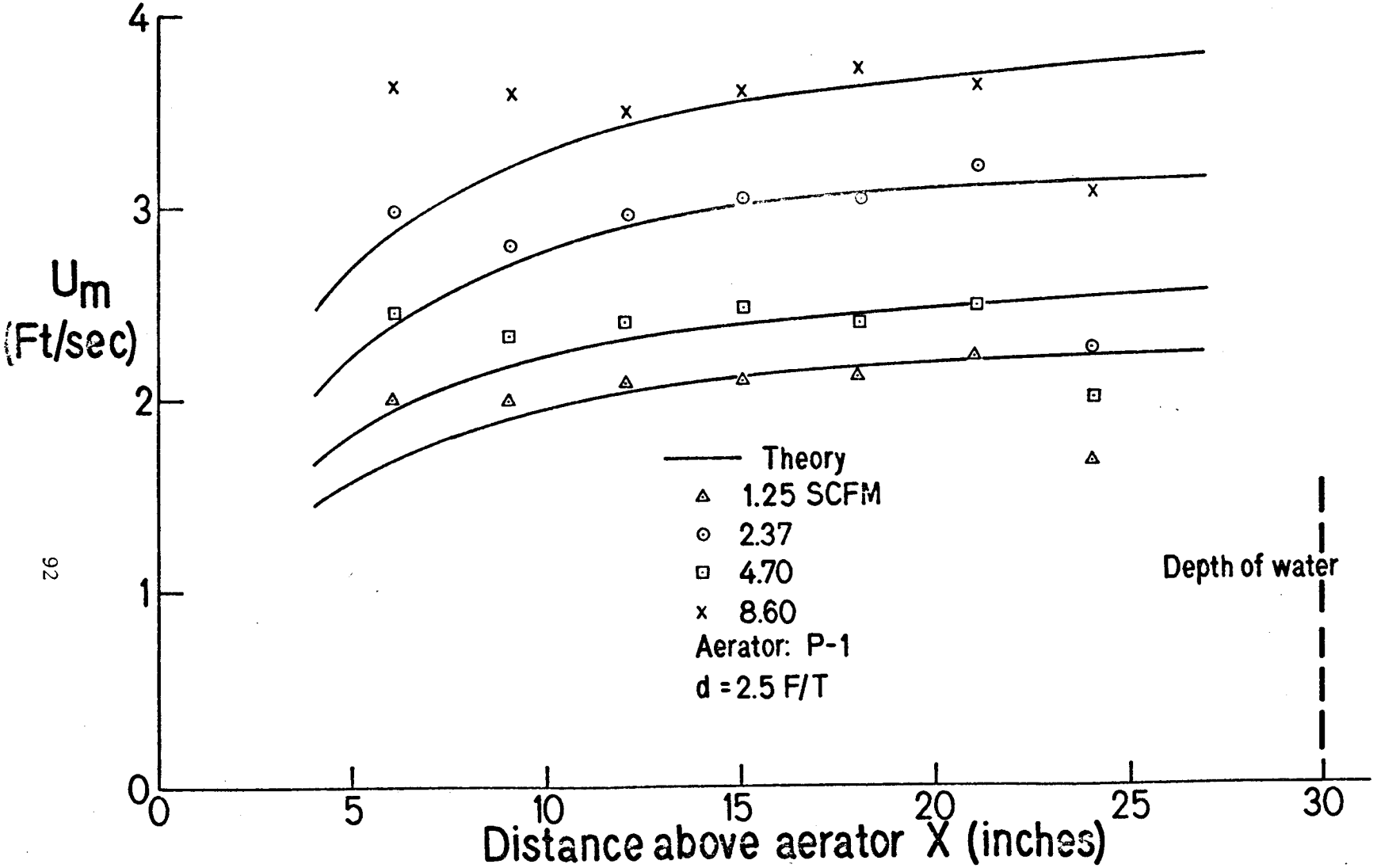

Figure 6-1. Center Line Velocities Above a "Point" Source Aerator at Four Aeration Rates

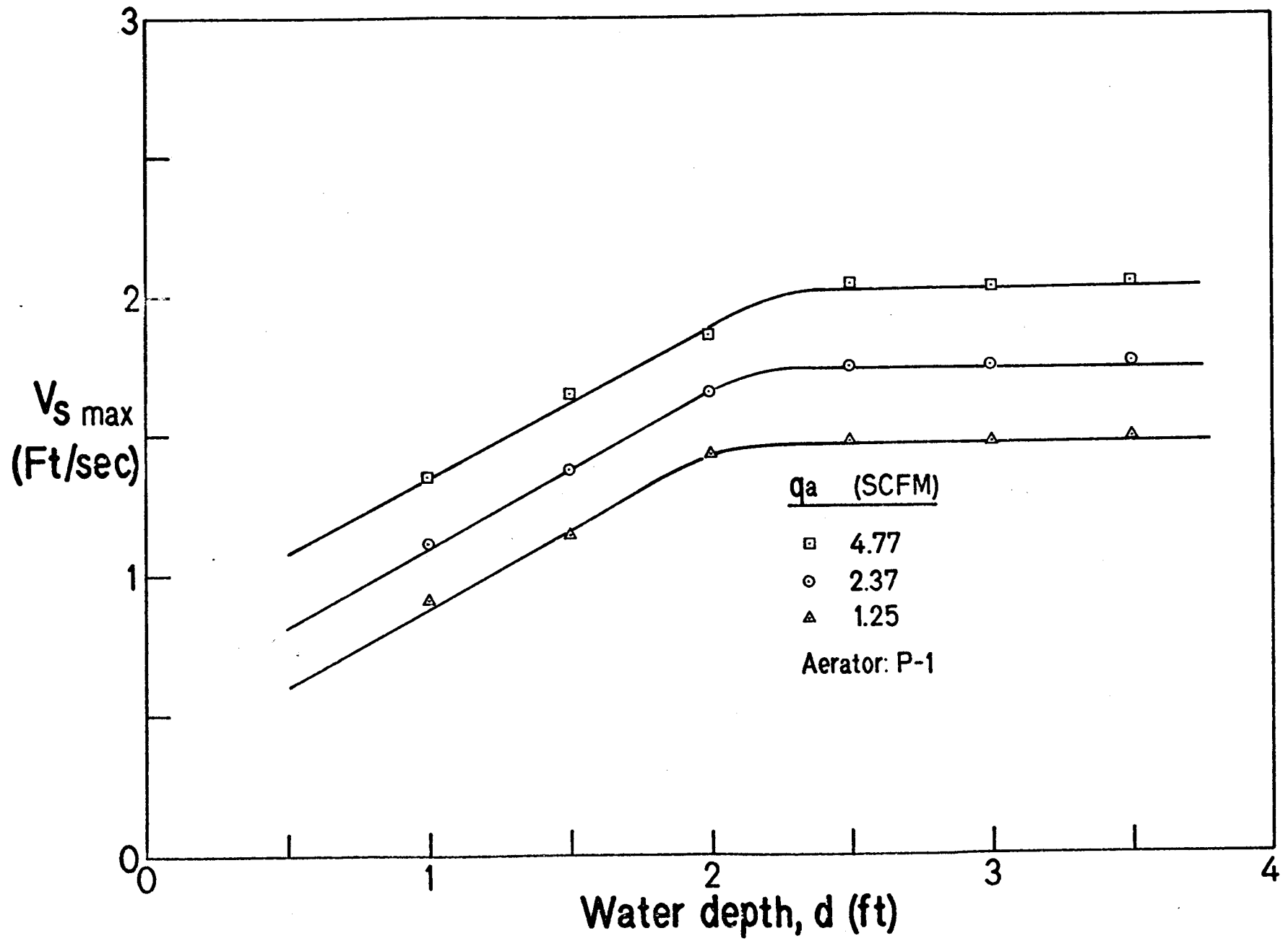

Figure 6-2. Maximum Surface Velocity Variation with Water Depth

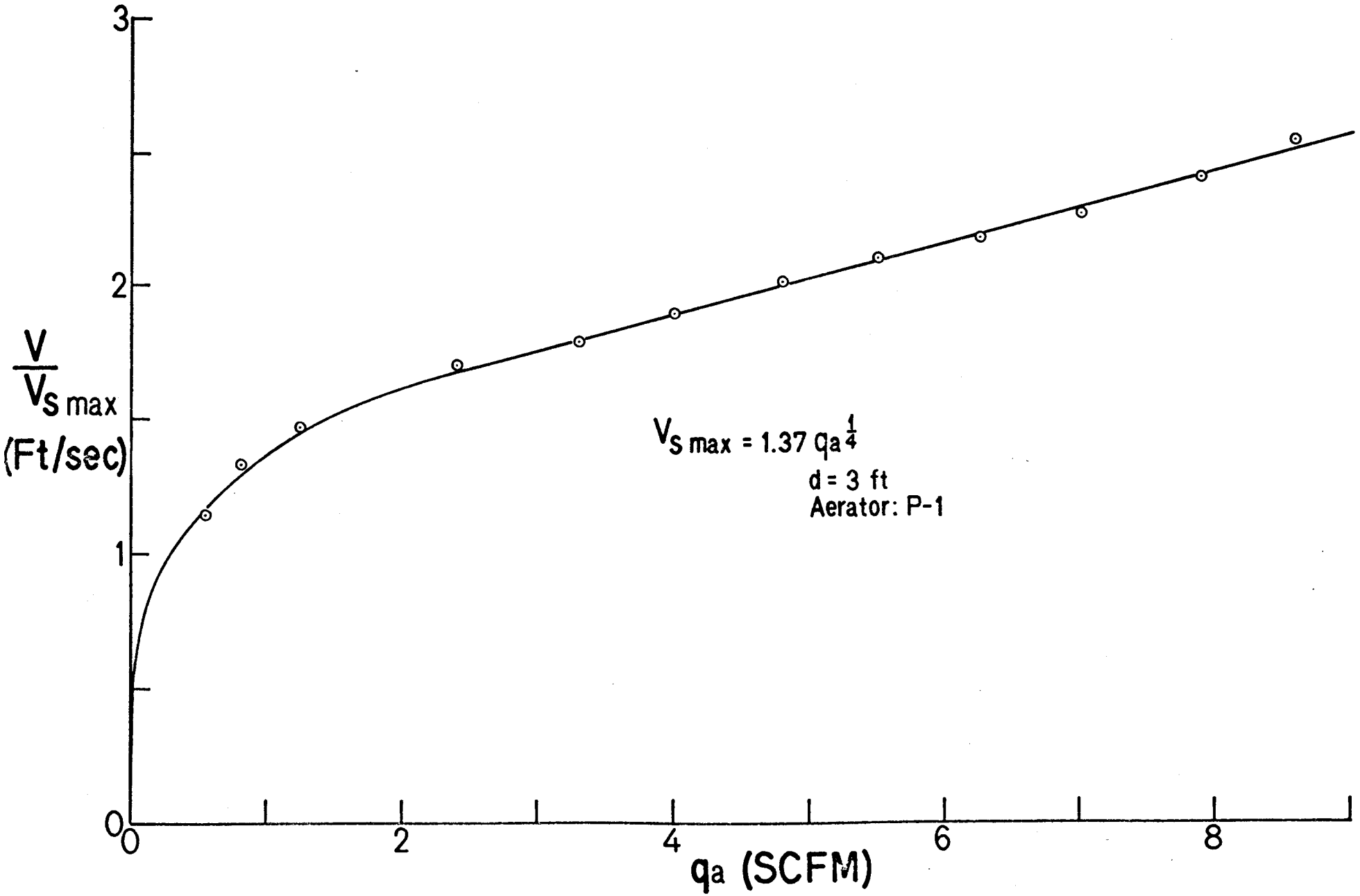

Figure 6-3. Maximum Surface Velocity Variation with Aeration Rate

Although deviations in the vicinity of the aerator and free surface are evident in Figure 6-2, the agreement with Kobus' predictions are surprisingly good in view of the shallow water. Kobus found that centerline velocity varies with aeration rate to the 1/4 power.

In addition to aerator P-1 already described, P-2 consisted of 98, 3/32" diameter holes arranged in concentric circles in a thin plastic plate with a diameter of 1 29/32". Aerators R-1 and R-2 were rings of heavy wall tygon typing with 55, 1/8" holes along the top of a 1" tube bent into a 7 1/2" ID ring and 44 holes of 1/8" along the top of a 3/4" tube bent into a 7" ID ring. For each of these aerators essentially identical velocity profiles were measured at 18 inches above the aerator in 3 feet of water with an aeration rate of 2.37 scfm. While it may have been anticipated that results with single orifices (Kobus) and small circular perforated plates would be quite similar, it is probably not expected that a 7" ring would yield the same profile at only 18" above it. In fact, air bubbles released from the ring move toward the center and form a much smaller column only a few inches above the aerator before spreading with further rise. Hence, our results show that the velocity of the induced flow is independent of aerator design, that is, orifice size, number and geometry, for an apparently wide variation in aerator design. Velocity profiles are also unchanged by aerator elevation above the tank floor. Centerline velocities were found to begin to decay at about 0.7D from the aerator where the influence of the free surface is felt, in agreement with the results for plane jets and line source aeration.

THE RADIAL FLOW

The maximum surface velocity (determined by extrapolation of velocity profiles near the surface) was found to be at five to seven inches from the aerator axis and to remain constant out to a diameter about equal to the water depth. Figure 6-2 shows that the maximum surface velocity V_{smax} becomes essentially independent of depth after a short initial development zone, as expected in view of the vertical velocity variation. Figure 6-3 shows that V_{smax} beyond the region on dependence on depth for very shallow water is given by $V_{smax} \propto (q_a)^{1/4}$, as for the centerline velocity of the vertical plume. For aeration rates from 1.25 to 8.6 scfm, U_{mmax} was found to be about 1.47 times as large as V_{smax}.

The decay of surface velocity with radial position is shown in Figure 6-4. The expected proportionality of V_s to r^{-1} (49 and 54) is observed, as is the initial zone of diameter d, within which $V_s = V_{smax}$. From Figure 6-4, for $0.2 \leq (d/r) \leq 2.0$

$$V_s/V_{smax} = 0.43(d/r) + 1.25 \qquad 6\text{-}4$$

independent of aeration rates. Beyond $(d/r) \simeq 0.2$, the velocity decay is much more rapid to $V_s = 0$ at $(d/r) \simeq 0.15$.

This also explains the very shallow water level of 1 foot since the cell radius was 6 2/3 feet in a tank of 15 foot overall diameter, and the shallow depth was necessary to minimize the influence of the tank walls on measured velocities. Velocity decay for two and three feet of water were found to be in agreement with Figure 6-4, although somewhat more scatter was observed. Then, in practice, the dimensionless surface velocity decay is independent of aeration rate and water depth.

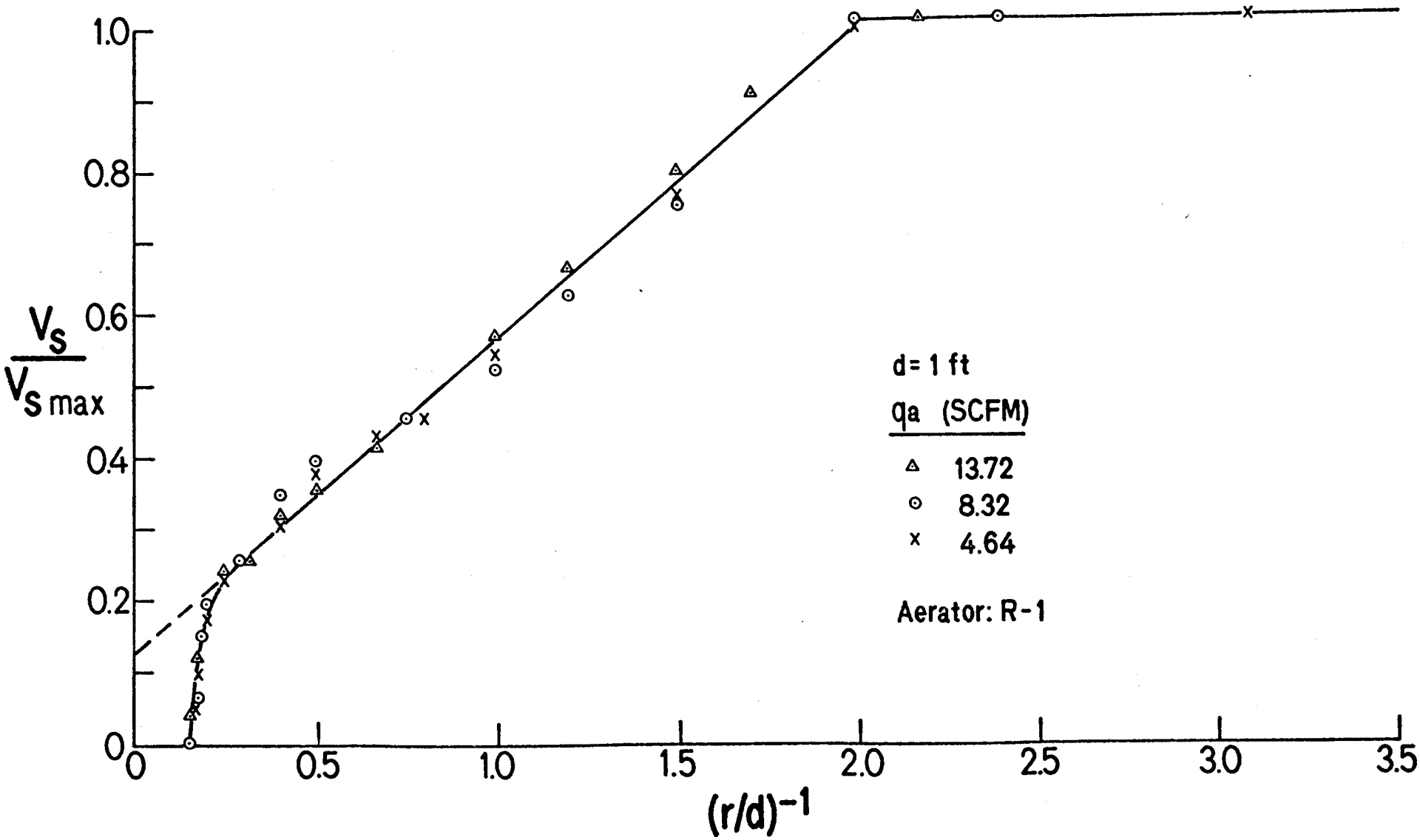

Figure 6-4. Decay of Surface Velocity with Radial Distance from the Source

Figure 6-5 shows a series of velocity profiles at r/d = 2 for a five-fold range of aeration rates with the smallest water depth of one foot. The profiles are observed to be more concave then was the case for line source aeration, but the current thickness is the same for each rate and the bottom currents have constant velocities over a large portion of their extent. These results have been made non-dimensional in Figure 6-6 to show that all of the data fall on a single curve. This was also true at other locations, so that the non-dimensional profile was independent of aeration rate at least over the range shown.

Total water depth does not alter the non-dimensional profile as shown in Figure 6-7 for five depths to three feet. These dimensionless profiles were also independent of the ring or "point" aerator used. Limited testing with a raised aerator confirmed that the surface velocity profile was set by the aerator depth, not the water depth, in agreement with the results for aeration from line sources.

Figure 6-8 shows that when the surface current thickness is used to normalize the vertical position, y, the dimensionless velocity profile is independent of radial position and may be estimated as

$$V/V_s = [1-(y/\delta)]/[1+1.25(y/\delta)] \qquad 6\text{-}5$$

The maximum velocity of the bottom current is approximately equal to $0.2V_s$ for $0.5 \leq r/d \leq 3.0$. The surface current thickness, δ, was found to increase linearly with radial position, independent of aeration rate, such that

$$\delta/D = 0.0513\ r/D + 0.217 \text{ for } 0.5 \leq r/D \leq 6 \qquad 6\text{-}5$$

Figure 6-5. Velocity Profiles for Five Aeration Rates

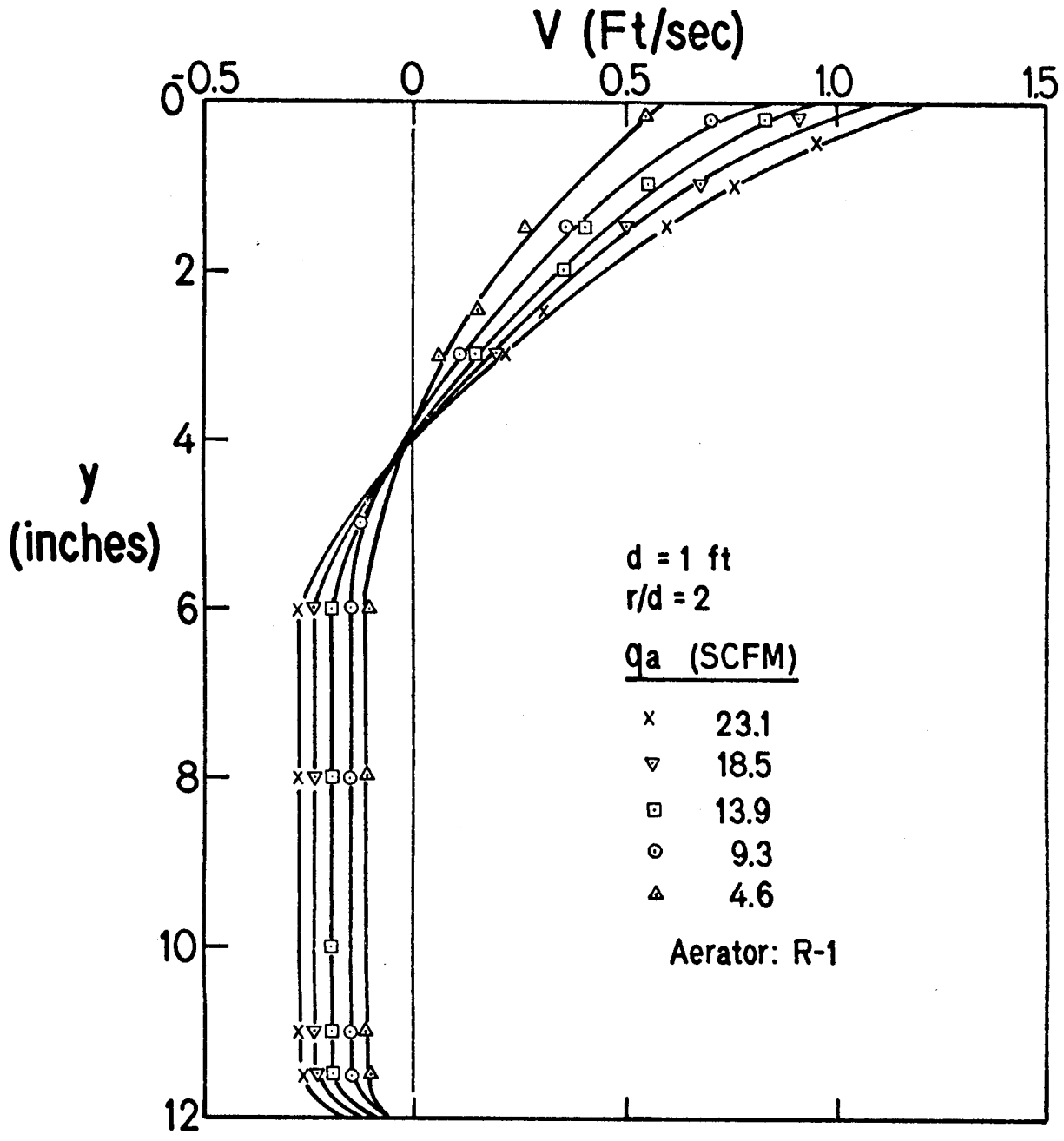

Figure 6-6. Dimensionless Velocity Profiles - Figure 6-5 Results

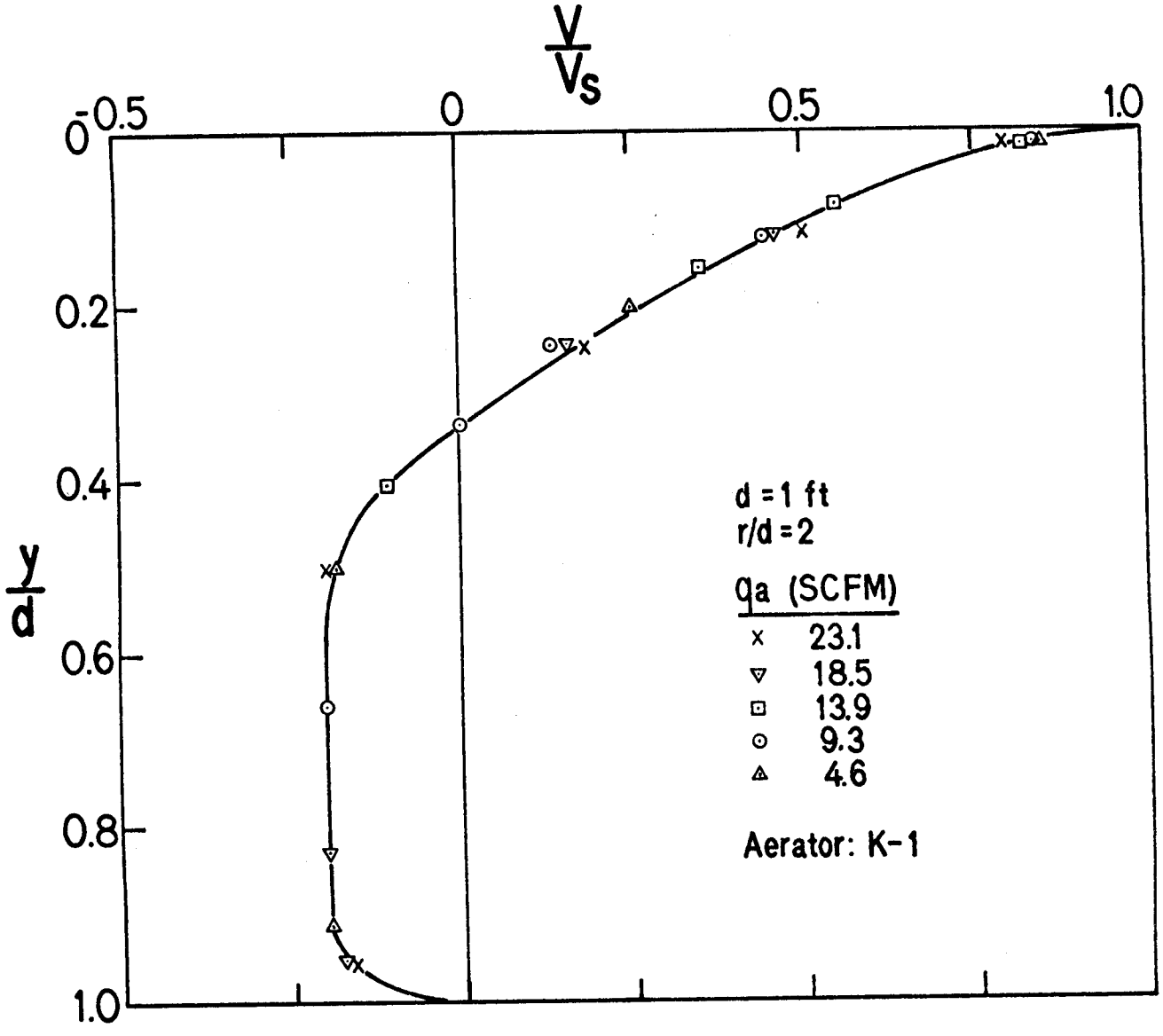

Figure 6-7. Dimensionless Velocity Profiles for Five Water Depths

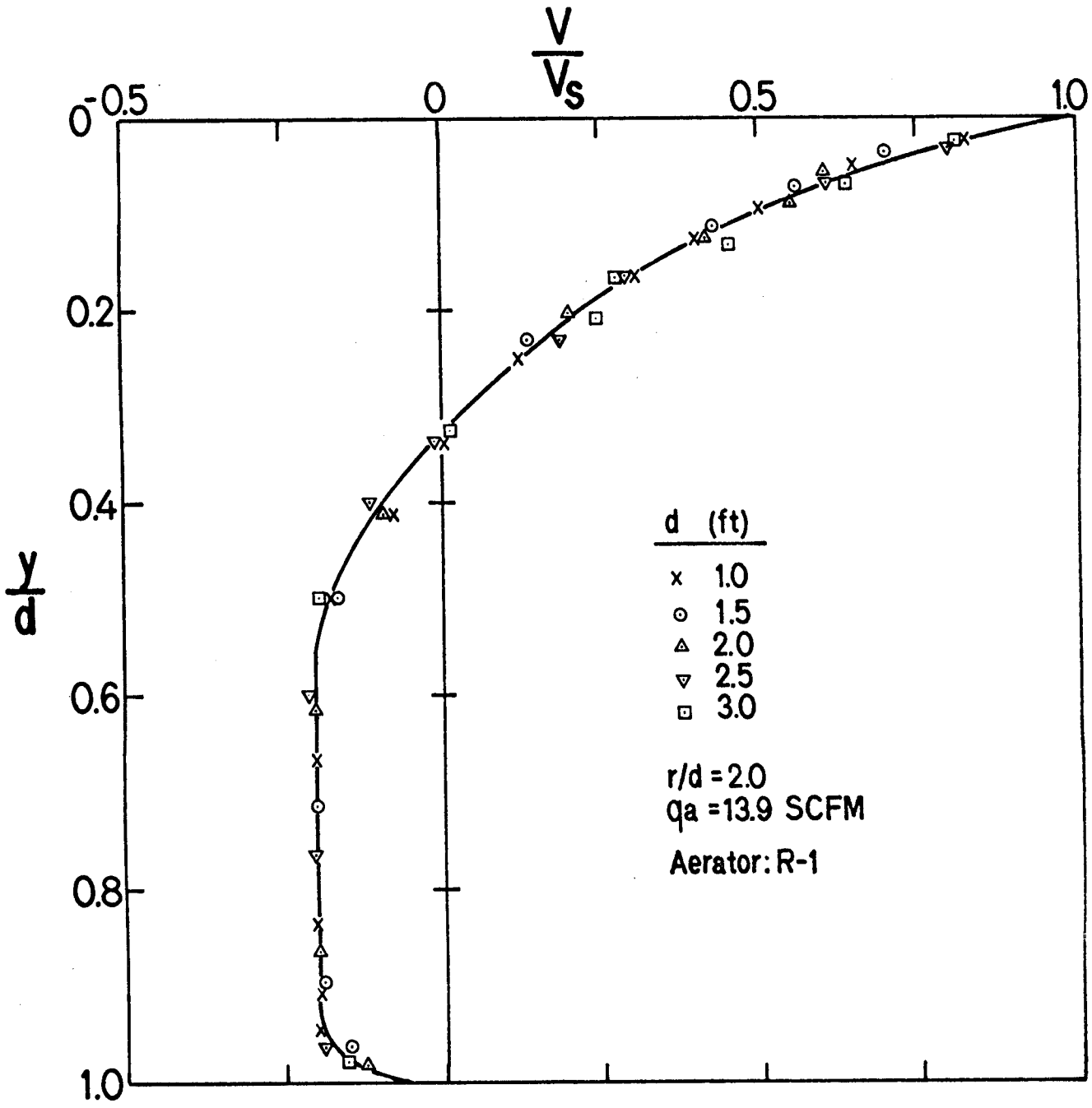

Figure 6-8. Similarity of Dimensionless Surface Velocity Profiles

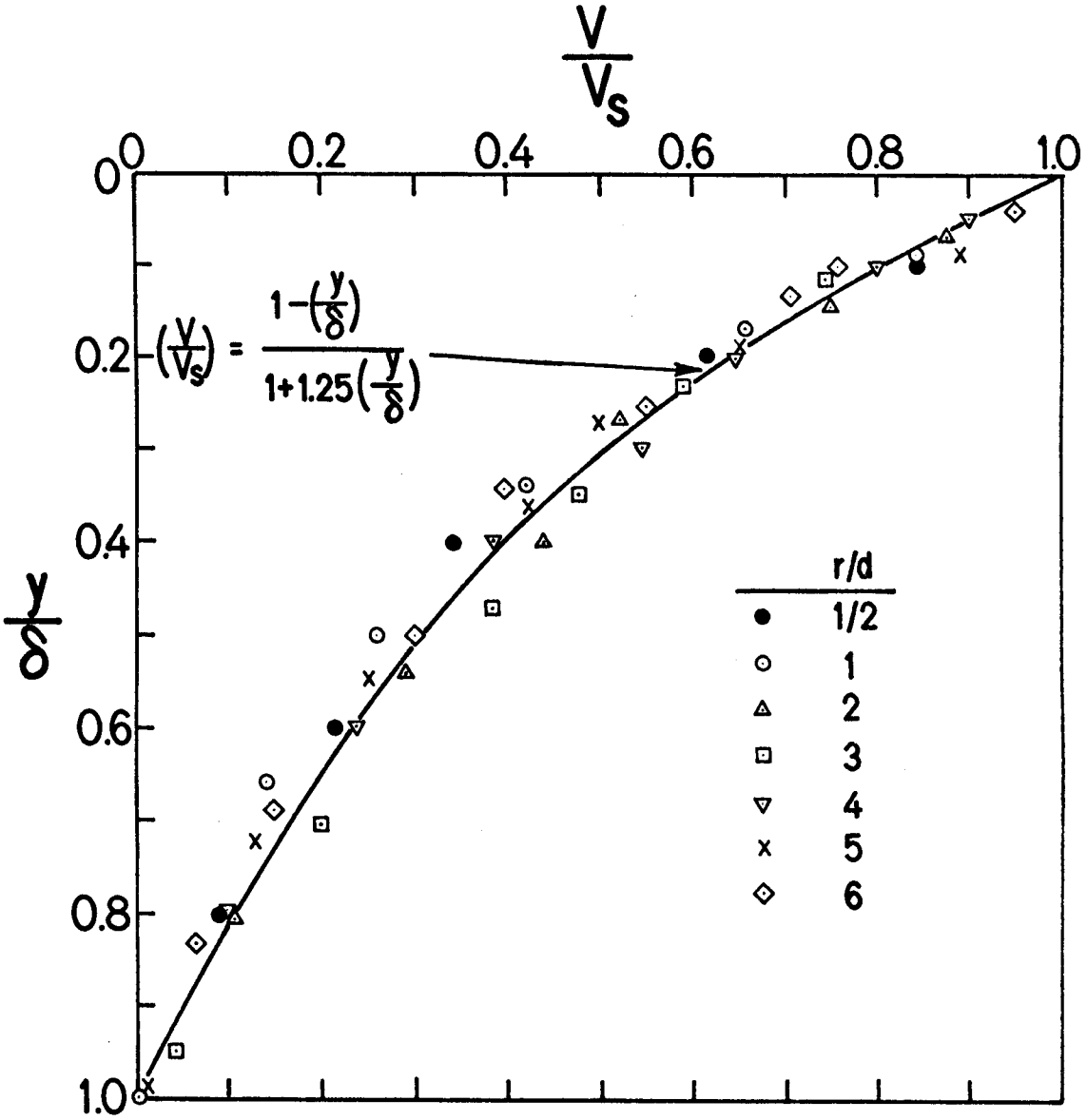

These results are marked contrast to those of Baines and Hamilton (49) who, on the basis of limited data, found δ to be about 5% of the water depth d.

We have seen in Figure 6-4 that V_s reaches zero at (d/r) = 0.15 for a cell size of 6.7d. Because of the limitations imposed by the experimental tank, it was not possible to develop full cells for water depths of greater than one foot, although with water depths of six and nine inches, cells of between six and 7d were observed. Cell size seemed to increase slightly with increasing aeration rate over the range from 4.6 to 19.9 scfm with cell size about 6d at the lowest rate and just over 7d at the highest.

However, experimental uncertainties and the limited size of the tank mask this effect which is certainly not large. Cell size of 7d for a wide range of aeration rates were also confirmed by noting the position at which corks stopped moving towards the wall.

In summary, combining Kobus' result for the vertical plume with our surface velocity profile and cell size estimates, the intensity and extent of circulation induced by point source aeration may be readily determined. Of course, these results may be used to generate efficiency curves of the kind we have presented for line source aeration.

7. RELATED STUDIES - SOME PERTINENT LITERATURE

The work described so far deals only with systems in which the fluid density is initially uniform throughout. It was our intention to extend the study to include initial density stratification, wind induced or other currents, entrainment of bottom sediments and other pertinent subjects. Unfortunately, it was impossible to explore these subjects since the principal investigator left the University and the project was terminated. However, some very preliminary studies of stratified systems were carried out and literature surveys of the other areas were made. These fragments are summarized here with the hope that they will be of some use to others working in this general area.

FLOW IN STRATIFIED SYSTEMS

Our very preliminary experiments with stratified systems were of three kinds:

(1) Low rate aeration from a line source in which the movement of the interface between the dense lower layer and the upper water layer was observed either visually with dyed layers or with conductivity probes.

(2) Intermediate rate aeration which was observed with dyed layers and/or initially vertical dye streaks and photographed, and, in a few cases, measured with conductivity probes.

(3) High rate aeration which was photographed with a motion picture camera beginning with the start of aeration of an initially dye marked lower layer.

Density stratification in which the more dense salt solution underlies fresh water, so that a "step" profile is obtained is usually prepared by pouring the water on to a board floating on the salt solution at a rate chosen to minimize mixing. We found it more convenient in our small tank to add the water layer first, and then slowly inject the salt solution from below up through the bottom of the tank with a horizontal baffle plate set about 1/2 inch above the tank bottom to deflect and contain the injected fluid. The rate of injection was chosen to minimize mixing beyond the end of the baffle plate.

In a few tests linear initial density profiles were prepared. The profiles were as described in (55) by simply moving a series of horizontal rods with a strip at the interface mounted suitably on vertical supports, though a step profile, with conductivity readings used to determine when a sufficiently close approach to linearity has been achieved. An application of the technique is described in (56) and the procedure has been cited in connection with the mixing of chemicals for dissolved oxygen removal. References (57) and (58) discuss several other techniques that have been used to establish specified density profiles.

For low rate aeration using the small porous tube with $q_a \simeq 0.014$ scfm/ft in an initially step stratified system, the air plume carries up the more dense salt solution to form a mound over the aerator with the salt solution flowing out to fill the entire tank. The overall effect is a rise in the level of the dense layer with time with a plume of the progressively less dense salt solution over the aerator. For example, with an initial density difference of 0.002 gm/cc and two equal layers of total height of 30 cm, the dense layer has penetrated halfway into the initially pure water layer after two minutes with about 90% penetration after five minutes. Increasing the initial density difference to 0.005 gm/cc causes only a very minor reduction in the rate of dense layer rise. However, increasing q_a to 0.034 scfm/ft at $\Delta\rho = 0.002$ gm/cc results in about 90% penetration after only two minutes. In all cases there is a tendency for a thin zone (about 1/2 cm thick) of surface pure water to persist for about twice the time required for the penetration to reach about 1/2 cm from the surface. Doubling the initial water height did not alter the rate of penetration when expressed as a fraction of the initial water layer height.

Cederwall and Ditmars (41) comment briefly on the influence of stratification on air bubble system behavior. Complete and partial uncoupling between the plume water and air bubbles at the interface are illustrated. Our observations at very low aeration rates suggest that mixing occurs primarily in the plume "mound" of dense solution over the aerator with relatively uniform density through the salt layer which is smoothly reduced as the more dense layer penetrates up into the water.

At higher aeration rates, the dense solution is carried up over the aerator to spill out much like a turbidity or gravity current over the lower disturbed bottom layer. At even higher rates, the dense solution runs out away from the aerator along the surface before mixing and beginning to drift down into the water layer. Photographs showing the initiation of aeration at about 1 scfm/ft with surging of the dense solution are avialable (59) although the more general references on this subject cited below are of far more value in this regard. Of course, experiments at high aeration rates in small tanks are complicated by end effects and large oscillations in the initial interface and are little more than very brief disturbed illustrations of the flow patterns in full scale systems.

FLOW WITH DENSITY STRATIFICATION

There is a large literature that touches on the kinds of flows encountered in aeration induced circulation in initially stratified systems. An excellent book by Turner (60) includes gravity currents, plumes, and mixing processes among the various topics in a general review. Brooks and Koh (61) considered the influence of stratification on a sewage effluent plume. Cederwall and Ditmars (41) briefly discussed the influence of stratification with specific reference to aeration induced flow. Gay and Hagedorn (62) reported some experimental results for mixing of a stratified system by air injection in which the ratio of energy absorbed to energy input was used as a measure of mixing efficiency and reported as a function of time. Other pertinent references include the work of Brush et al (63). Schijf and Schönfeldt (64) presented an early theoretical treatment of two-layer stratified flow. Keulegan reported detailed studies of the motion of saline fronts (e.g., (65)) with subsequent work by many others (e.g., (66)).

THERMOCLINES AND HEAT EXCHANGE IN LAKES AND RESERVOIRS

The literature on thermocline formation and dynamics is both extensive and increasingly sophisticated. Recent papers by Sundaram and Rehm (67), Huber et al (68), Orlob and Selna (69) and others cover this material while others have presented analysis of simultaneous water quality variations (70) and reservoir modeling (71). An outline of temperature variation in lakes is available in Eagleson's book "Dynamic Hydrology" (72). Recent papers dealing only with heat exchange at the water surface are available (e.g., (73) and (74)).

WIND DRIVEN CURRENTS AND OVERALL CIRCULATION

Wind induced surface currents can counter or enhance aeration induced currents as well as set the overall circulation pattern in lakes and reservoirs. Fortunately, the subject of surface currents induced by wind shear has been thoroughly studied. Keulegan reported detailed results for small closed channels in 1951. Additional results for laboratory channels were later reported by Baines and Knapp(76), Hidy and Plate (77), and Wu (78) with additional results and analysis of wind induced currents reported by Plate (79), Wu (80), and Shemdim (81) and others.

Although the data tend to be scattered at low wind velocities depending on the particular experimental details, Wu (78) shows that the surface velocity increases with wind velocity, U_w, at a decreasing rate from $0.03U_m$ at U_m = 8 ft/sec to about $0.045U_w$ at U_w = 24 to 28 ft/sec with wave breaking occuring at $U_w \simeq 28$ ft/sec. With a typical 10 mph wind (U_w = 14.7 ft/sec), the surface velocity of about 0.6 ft/sec is of the same order of magnitude as that for aeration induced surface currents at typical aeration rates and winds will clearly significantly alter aeration induced surface currents and circulation. Specific comments on the influence of surface currents, which might be wind generated, on aeration induced surface currents is provided by Jones (30) and Basco (31) who, on the basis of limited results, suggested that linear superposition served to combine the velocities.

An early study of the response of a pond to wind was presented by Van Dorn. More recently, Liggett et al (e.g., (83) - (85)) have presented models and numerical results for circulation in homogeneous and stratified lakes. Others (e.g., (86) - (88)) have formulated and solved the problem of lake circulation in a variety of ways.

The references cited, while only a small sample of those available, demonstrate aeration analysis may be supplemented to include the influence of wind driven currents and overall circulation from existing literature. Nevertheless, some controlled experiments would be desireable for the range of surface currents likely to be encountered during aeration.

DESTRATIFICATION EFFICIENCY

Limnologists have long used Schmidt's concept of stability of stratification to represent the energy required to bring a stratified system to the uniform mean temperature. The concept and procedure is described in the books by Hutchinson (91) and Ruttner(92). It is not surprising that the efficiency of artifical destratification, DE, was much later defined in terms of the stability change by Symons et al as

$$DE = \frac{\text{net change in stability from } T_1 \text{ to } T_2}{\text{total mechanical energy input from } T_1 \text{ to } T_2} \times 100$$

and employed to judge the effectiveness of destratification procedures. DE calculations have been carried out for a number of reservoir destratification projects (e.g., Leach et al).

A simple calculation procedure to determine the energy required to mix a stratified lake was presented in reference (89) along with discussion, applications and an estimate of the destratification time. Gay and Hagedorn(62) employed a mixing efficiency defined as the energy absorbed divided by product of the power input and time and correlated the mixing efficiency determined from density profiles measured at various times.

REFERENCES

1. National Academy of Sciences. (1969) *Eutrophication: causes, consequences, correctives*. Proceedings of a Symposium. Washington, D.C.

2. State Water Quality Control Board (1967) *Eutrophication: a review*. Pub#34. State of California.

3. Irwin, W.H., Symons, J.M. and Robeck, G.G. (1966) *Impoundment Destratification by mechanical pumping*. J. Sanit. Eng. Div., Amer. Soc. Civil. Eng. 92 (SA6) 21-40.

4. Riddick, T.M. (1958) *Forced circulation of large bodies of water*. J.Sanit. Eng. Div., Amer. Soc. Civil Eng. 84 (SA4) 1703(1) - 1703(21).

5. Imhoff, K.R. (1969) *Oxygen balance and artificial re-aeration of lake Baldeney and the Lower Ruhr*. pp. 761-781. *Advances in Water Pollution Research*. (Proceedings of the Fourth International Conference - Prague) Pergamon Press.

6. Fast, A. W. (1968) *Artificial destratification by aeration*. Department of Fish and Game. Fish Bulletin 141, p. 97. State of California.

7. U. S. Department of Health, Education and Welfare. Environmental Control Administration. (1969) *Water quality behavior in reservoirs - a compilation of published research papers*.

8. Wirth, T.L. and R. C. Dunst. (1967) *Limnological changes resulting from artificial destratification and aeration of an impoundment*. p.15. Dept. Research Report 22 (Fisheries) Wisconsin Conserv.

9. Johnson, R.C. (1966) *The effect of artificial circulation on production of a thermally stratified lake*. Washington Dept. Fish; Fish Research Papers 2(4): 5-15.

10. Fast, A. W., Moss, B. and Wetzel, R. G. (1973) *Effects of artificial aeration on the chemistry and algae of two Michigan lakes*. Water Resources Research. June. 9,No.3, 624-647.

11. Haynes, R. C. (1971) *Some ecological effects of artificial circulation on a small eutrophic New Hampshire lake.* Ph.D. Thesis in Zoology. University of New Hampshire. August.

12. New Hampshire Water Supply and Pollution Control Commission (1974) *Algae control by mixing, staff report on Kezar Lake in Sutton, N.H.* prepared for the New England Regional Commission.

13. Boyter, C. J. and M. P. Wanvelista. (1973) *Review of lake restoration procedures.* Water Resources Bulletin, 9 No. 3, 499-511. June.

14. Robert S. Kerr Water Research Center (1970) *Induced aeration of small mountain lakes* for Environmental Protection Agency, Project No. 16080, November.

15. Eunpu, F. F. (1973) *Control of Reservoir Eutrophication.* Journal AWWA, pp. 268-274. April.

16. Leach, L. E., Duffer, W. R. and Harlin, C. C., Sr. (1972) *Pilot study of dynamics of reservoir destratification.* Robert S. Kerr Water Research Center, U. S. Department of the Interior, FWPCA. August.

17. Laverty, G. L. and H. L. Nelson. (1970) *Quality improvements by reservoir aeration.* Journal, AWWA 62 711-714.

18. Symons, J. M., Carswell, J. K. and Robeck, G.G. (1970) *Mixing of water supply reservoirs for quality control.* Journal, AWWA 62 322-334.

19. Koberg, G. E. and M. C. Ford, Jr. (1965) *Elimination of thermal stratification in reservoirs and the resulting benefits.* Geological Survey Water-Supply Paper 1809-M.

20. *Artificial destratification in reservoirs.* (1971) Journal, AWWA 579-604. September.

21. Taylor, G. I. (1955) *The action of a surface current used as a breakwater.* Proc. Roy. Soc. A, 231:466.

22. Evans, J. T. (1955) *Pneumatic and similar breakwater.* Proc. Roy. Soc. A, 231:457.

23. Straub, L. G., Bowers, C. E. and Tarapore, Z. S. (1959) *Experimental studies of pneumatic and hydraulic breakwaters.* University of Minnesota. St. Anthony Falls Hydraulic Lab. Technical Paper No. 25, Series B. August.

24. Kurihara, M. *Pneumatic breakwater - Parts I, II and III.* Proceedings of the First, Second and Third Conference on Coastal Engineering in Japan, November 1954, 1955, and 1956 respectively. Available from the Institute of Engineering Research of the University of California at Berkely. Series 104. Issues 4, 5 and 6.

25. Kurihara, M. (1965) *On the study of the pneumatic breakwater in Japan.* Coastal Engineering in Japan. 8:71.

26. Bulson, P. S. (1968) *The theory and design of bubble breakwaters.* Proceedings of the Eleventh Conference on Coastal Engineering. p. 995. London, ASCE.

27. Abraham, G. and Burgh, P. V. D. (1964) *Pneumatic reduction of salt intrusion through locks.* Proc. ASCE 90 #HYI 83-119.

28. Ince. S. (1961) *A guide to the design of air bubblers for melting ice.* Proceedings of the Seventh Conference on Coastal Engineering. p. 600. Published by the Council on Wave Research.

29. Green, J. L. (1961) *Pneumatic breakwaters to protect dredges.* J. Waterways and Harbors Division, Proc. ASCE 87 WW2, 67, May.

30. Jones, W. T. (1972) *Air barriers as oil-spill containment devices.* Society of Petroleum Engineers Journal. p. 126. April.

31. Basco, D. R. (1971) *Pneumatic barriers for oil containment under wind, wave and current conditions.* Proceedings Joint Conference on the Prevention and Control of Oil Spills. API-EPA. June 15.

32. Grace, J. and Sowyrda, A. (1970) *The development and evaluation of a pneumatic barrier for restraining surface oils in a river.* J. Water Pollution Control Federation. p. 2074. December.

33. Rouse, H., Yih, C. S. and Humphreys, H. W. (1952) *Gravitational convection from a buoyancy source.* Tellus 4 No. 3, 201-210.

34. Morton, B. R., Taylor, G. I. and Turner, J. S. (1956) *Turbulent Gravitational convection from maintained and instantaneous sources*. Proc. Roy. Soc. A., 234. pp. 1-23.

35. Lee, S. L. and Emmons, H. W. (1961) *A study of natural convection above a line fire*. J. Fluid Mech. II:353.

36. Yih, C. S. (1951) *Free convection due to a point source of heat*. Proc. of First U. S. National Congress of Applied Mechanics. p. 951. June.

37. Brooks, N. H. and Koh, R. C. Y. (1965) *Discharge of sewage effluent from a line source into a stratified ocean*. Eleventh Congress of the International Association for Hydraulic Research. Leningrad.

38. Turner, J. S. (1973) *Buoyancy effects in fluids*. Cambridge University Press.

39. Brock, R. R. (1970) *Power law solutions for vertical plumes*. J. Hydraulics Div. of ASCE. 96 HY9. p. 1803. September.

40. Schmidt, W. (1941) Z. anglw. Math. Mech.,21. p. 265.

41. Cederwall, K. and Ditmars, J. D. (1970) *Analysis of air-bubble plumes*. Report No. KH-R-24 of the W. M. Keck Laboratory of Hydraulics and Water Resources. California Institute of Technology. September.

42. Provost, R. (1973) *Circulation and flow in water tanks induced by the release of air from a manifold*. M.S. Thesis. Department of Chemical Engineering, University of New Hampshire.

43. Wen, J. D. (1974) M. S. Thesis. Department of Chemical Engineering, University of New Hampshire.

44. Kobus, H.E. (1968) *Analysis of the flow induced by air-bubble systems*. In Proceedings of the Eleventh Conference on Coastal Engineering. London.

45. Schlichting, H. (1968) *Boundary layer theory*. 6th Edition. McGraw-Hill, Inc., New York.

46. Bakke, P. (1957) *An experimental investigation of a wall jet*. J. Fluid Mich. 2, 212.

47. Schwarz, W. H. and Cosart, W. P. (1961) *The two-dimensional turbulent wall jet.* J. Fluid Mech. 10, 481.

48. Baines, W. D. and Knapp, D. J. (1965) *Wind driven water currents.* J. Hydraulics Division. ASCE. 91, #HY2, 205. March.

49. Baines, W. D. and Hamilton, G. F. (1959) *On the flow of water induced by a rising column of air bubbles.* International Association for Hydraulic Research. 8th Congress. Montreal.

50. Iamandi, D. and Rouse, H. (1969) *Jet induced circulation and diffusion.* J. Hydraulics Div of ASCE. 95, #HY2, 589. March.

51. Kobus, H. (1970) *Discussion of previous reference.* J. Hydraulics Div. of ASCE. 96, #HY1, 280. January.

52. Murota, A. and Muraoka, K. (1967) *Turbulent diffusion of the vertically upward jet.* Proceedings of the 12 Congress of International Association for Hydraulic Research. Fort Collins. September.

53. Eckenfelder, W. W., Jr. (1959) *Absorption of oxygen from air bubbles in water.* J. Sanit. Eng. ASCE. 85, SA4, 89.

54. Poreh, M. and Tsuei, Y. G. (1965) *Self simularity in turbulent radial jets and radial wall jets.* Isreal J. Tech. 3, 7-10. #1.

55. Clark, C. B., Stockhousen, P. J. and Kennedy, J.F. (1967) J. Geophys. Res. 72, 1393-1395.

56. Imberger, J. and Fischer, H. B. (1970) *Selective withdrawal from a stratified reservoir.* Report for EPA. Project Number 15040EJZ. December.

57. Cromwell, T. (1959) *Pynoclines created by mixing in an aquarium tank.* J. Marine Research. 18, 73.

58. Mowbray, D. C. (1967) *The use of Schlieren and Shadowgraph techniques in the study of flow patterns in density stratified fluids.* J. Fluid Mech. 27, 595-608.

59. Torrest, R. D. (1973) Annual Report for Project Number A-030-NH. Water Resource Research Center, University of New Hampshire.

60. Turner, J. S. (1973) *Buoyancy effects in fluids.* University Press. Cambridge, England.

61. Brooks, N. H. and Koh, R. C. Y. (1965) *Discharge of sewage effluent from a line source into a stratified ocean.* International Association for Hydraulic Research, Leningrad.

62. Gay, F. T. and Hagedorn, Z., Jr. (1962) *Forced convection in a stratified fluid by air injection.* M. S. Thesis. MIT. Cambridge, Massachusetts.

63. Brush, L. M., Jr., McMichael, F. C. and Kuo, C. Y. (1968) *Artificial mixing of density-stratified fluids: a laboratory investigation.* **Final report** on Research Project B-005-NJ. Water Resources Research Institute, Princeton University.

64. Schijf, J. D. and Schönfeldt, J. C. (1953) *Theoretical considerations on the motion of salt and fresh water.* In proceedings of the International Association for Hydraulic Research Congress. Part 3. Minnesota. pp. 321-333.

65. Keulegan, G. H. (1958) *The motion of saline fronts in still water.* NBA Report 5831. U. S. Department of Commerce. April.

66. Abraham, G. and Vreugdenhil. (1971) *Discontinuities in stratified flows.* J. Hydraulic Research. 9, No. 3 or Publication Number 95. Delft Hydraulics Laboratory.

67. Sundaram, T. R. and Rehm, R. G. (1971) *Formation and maintenance of thermoclines in temperate lakes.* A.I.A.A.J., 9, No. 7, 1322. July.

68. Huber. W. C., Harleman, D. R. F. and Ryan, P. J. (1972) *Temperature prediction in stratified reservoirs.* J. Hydraulics Div. ASCE, 98, No. HY4, 645. April.

69. Orlob, G. T. and Selna, L. B. (1970) *Temperature variations in deep reservoirs.* J. Hydraulics Div. ASCE 96, No. HY2, 391. February.

70. Markofsky, M. and Harleman, D. R. F. (1973) *Prediction of water quality in stratified reservoirs.* J. Hydraulics Div. ASCE, 99, No. HY5, 729. May.

71. Wunderlich, W. O. and Elder, R. A. (1968) *Reservoir modeling for thermal stratification conditions.* Chem. Eng. Progress Symposium, Series 90, 64, 82.

72. Eagleson, P. S. (1970) *Dynamic hydrology.* McGraw-Hill Company.

73. Dingman, S. L. (1972) *Equilibrium temperatures of water surfaces as related to air temperature and solar radiation*. Water Resources Research 8, No. 1, 42. February.

74. Yotsukura, N., Jackman, A. P. and Faust, C. R. (1973) *Approximation of heat exchange at the air-water interface*. Water Resources Research 9, No.1, 118. February.

75. Keulegan, G. H. (1951) *Wind tides in small closed channels*. J. Research of N. B. S.46, No. 5, 358. May.

76. Baines, W. D. and Knapp, D. J. (1965) *Wind driven water currents*. J. Hydraulics Division. ASCE, 91, No. HY2, 205. March.

77. Hidy, G. M. and Plate, E. J. (1966) *Wind action on water standing in a laboratory channel*. J. Fluid Mech., 26, 651.

78. Wu, J. (1968) *Laboratory studies of wind-wave interaction*. J. Fluid Mech., 34, 91.

79. Plate, E. J. (1970) *Wind surface velocities induced by wind shear*. Engineering Mechanics Division. ASCE, 96, No. EM3, 295. June.

80. Wu, J. (1973) *Predicition of near surface drift currents from wind velocity*. J. Hydraulics Division. ASCE, 99, No. HY9, 1291. September.

81. Shendin, O. H. (1973) *Modeling of wind induced currents*. J. Hydraulic Research, II. No. 3, 281.

82. Van Dorn, W. G. (1953) *Wind stress on an artificial pond*. Volume XII, Numver 3, 249.

83. Liggett, J. A. (1970) *Cell method for cumputing lake circulation*. J. Hydraulics Division. ASCE, 96, No. 13, 725. March.

84. Lee, K. K. and Liggett, J. A. (1970) *Computation for circulation in stratified lakes*. J. Hydraulics Division. ASCE, 96, No. HY10, 2089. October.

85. Liggett, J. A. and Lee, K. K. (1971) *Properties of circulation in stratified lakes*. J. Hydraulics Division. ASCE, 97, No. HY1, 15, January.

86. Liu, H. and Perez, H. J. (1971) *Wind-induced circulation in shallow water.* J. Hydraulics Division. ASCE, 97, No. HY7, 923. July.

87. Bennet, J. R. (1974) *On the dynamics of wind-driven lake currents.* J. Phys. Oceanogr., 4, 400. July.

88. Jacobs, S. J. (1974) *On wind-driven lake circulation.* J. Phys. Oceanogr., 4, 392. July.

89. Hogan, W. T., Reed, F. E. and Starbird, A. W. (1970) *Optimum mechanical aeration systems for rivers and ponds.* EPA. Report 16080D00. November.

90. Bulson, P. S. (1961) *Currents produced by an air curtain in deep water.* Dock and Harbour Authority, 42, 15. May.

91. Hutchinson, G. E. (1957) *A treatise on limnology.* Vol. 1. J. Wiley and Sons, Inc., New York.

92. Ruttner, F. (1973) *Fundamentals of limnology.* University of Toronto Press.

APPENDIX

EXPERIMENTAL PROCEDURES AND EQUIPMENT

Channels, Tank and Pool

The initial experiments were carried out in channels of 1 foot (30.5 cm) inside width and 8 feet length (236 cm). One channel A, was 61 cm deep with 1/4 inch clear acrylic plastic sheets for the sides and ends. The other, B, was 130 cm deep with clear acrylic sheet sides, but metal end plates. Channel bottoms were 1/2 inch plywood with several coats of waterproof white epoxy paint. Aluminum angle and strip was used to hold the walls together and clear or white silicone sealer (G.E.) was used for internal seals at edges.

Velocity profiles in radial flow were measured in a circular swimming pool of 15 feet diameter and 4 feet height set up in the chemical engineering laboratory. Velocities in the vertical plume from "point" sources were usually measured in a tank of 2 3/4 ft. width, 3 3/4 ft. length and 4 ft. high with 1/2 inch thick clear acrylic plastic sides and ends and bottom of 3/8 inch aluminum sheet covered with white epoxy paint. Larger channels were easily constructed for use inside the water filled pool, thereby eliminating the need for water proof seals and fixed dimensions. The first of these pool channels, C, was simply 1/4 inch thick clear acrylic parallel plates spaced 1 1/2 feet apart. One end of the 8 foot long by 2 foot high channel was sealed with an epoxy coated plywood panel, the other end was open to the pool. The other pool channel, D, was 12 feet long and 4 feet high with variable width of 1 1/2 or 2 feet.

This channel had one side of 1/4 inch clear acrylic sheet and 1/2 inch thick epoxy coated plywood on the other side. These channels were centered in the pool along a diameter and their sides were braced from the outside. The vinyl liner of the pool served as the channel bottom.

Air Flow System and Aerators

The building air supply was dependable to about 10 cubic feet per minute and capable of delivering up to 25 scfm. When necessary, it was supplemented by a Gast rotary vane compressor (Model 2565). For aeration in the channels the air passed through a prefilter (Wilkerson #1137-4F) and high efficiency filter (Wilkerson #1206-4). A Wilkerson regulator (B2001-4) was used to set the flow to the Brooks O-Ring Seal Flowmeter (Model #1112 A, Size 8, Tube # R-8M-25_4F) with a maximum flow rate of 8.32 scfm and accuracy to 2%. For larger flow rates, a separate larger delivery line with a Wilkerson prefilter and regulator and Brooks O-Ring Seal Flowmeter to 45.9 scfm was used.

The temperature of the metered air was measured with an inline thermometer and pressure was measured just downstream of the rotameters and just upstream of aerators. For the initial experiments, largely with channel A, (42), the manifold was prepared with 1/2 inch schedule 80 PVC pipe of 30 cm length to span the tank width. The orifices were made with a 1/16 inch drill and spaced 4 to the inch along a single line at the top of the manifold. Air entered the manifold from the side at one end to allow the air plume to fill the entire tank width with minimum disturbance to the plume by the feed line.

Later a variety of manifolds were used for linear plumes as summarized in Table A-1. The standard manifold was as described above and is specified in the Table as tube A-1. The same orifice size and spacing was used with tank width of 1 1/2 feet. Two additional manifolds of 1/2 inch PVC pipe were constructed. Tube A-3 had orifices of half the diameter but four times the density as for A-1 for the same total orifice area per manifold. Tube A-5 consisted of five rows of the standard orifice size and spacing, with the rows spaced uniformly over the top half of the manifold. Manifold A-5, a 1/4 inch OD porous tube (Marineland "bubble-wand") was used only for very low aeration rates. Manifolds A-6 and A-7 were prepared from Balson microfiber filter tubes and weighted with loose steel rods to keep them on the tank bottom. All manifolds were sealed at their ends with 1/16 inch thick plastic plate, with orifices to within 1/8 inch of the channel walls.

The aerators used for the pool and tank tests were either "point" sources or rings. Ring R-1 was a 1 inch OD plastic tube formed into a circle of 7 1/2 inch ID, with air input at one position through a tee and 55 holes of 1/8 inch diameter spaced uniformly along the top of the ring. Ring R-2 consisted of 44 1/8 inch holes spaced uniformly along the top of a 5/8 inch plastic tube, 7/8 inches above the pool bottom, formed into a 7 inch ID circle. The tubes of both rings were raised about 1/4 inch from the pool bottom. Point source P-1 consisted of a 1/8 inch thick acrylic plate fastened above the cylindrical cavity of 1 5/16 inch diameter and set 1 3/4 inches above the tank bottom.

96 holes of 1/16 inch diameter were spaced evenly along eleven straight lines. The total diameter of this aerator was 2 13/16 inches. Point source P-2 had 98 holes of 3/32 inch diameter arranged in concentric circles over a circular area of 1 29/32 inch diameter. These holes were drilled in a 1/4 inch acrylic plastic circular sheet of 2 5/8 inch diameter and set above a length of plastic pipe at a total height from the tank bottom of 2 3/4 inches.

Velocity Measurement

Previous studies of aeration induced flow used impeller type current meters. However, they are not suitable for low velocities. Photographic analysis of dye tracers, solid particles, and small gas bubbles, while tedious, will also provide velocity data. We chose to use small pitot-static tubes connected to a very sensitive differential pressure transducer with averaging of the signal for any desired period. This choice allows the collection of accurate reproduceable velocity data with no more than a few minutes of averaging down to low velocities. The technique does require reasonable care and a largely two dimensional character for the flow. That is, the tip of the pitot-static tube must be alligned in the direction of the average velocity. The pitot-static tubes used are listed in Table A-2 (manufactured by United Sensor Corp.) and had the standard right angle tip, except for No. 3. The specific pitot tube used in any experiment was usually chosen to have the minimum length suitable for that experiment.

TUBE	O.D.	LENGTH	ORIFICES		NOTE
			SIZE	SPACING	
A-1	7/8 in	1 ft	1/16 in	4/in	
A-2	7/8 in	1 1/2 ft	1/16 in	4/in	
A-3	7/8 in	1 ft	1/32 in	1/in	
A-4	7/8 in	1 ft	1/16 in	4/in	5 rows
A-5	1/4 in	1 ft		Porous	
A-6	1 3/4 in	1 ft	0.3 Micron	Porous	
A-7	2 1/4 in	1 1/2 ft	0.3 Micron	Porous	

TABLE A-1 MANIFOLD CHARACTERISTICS

No.	Model #	Length	Note
1	PBC-36-G-34-KL	3.0 ft	
2	PBC-24-G-22-KL	2.0 ft	
3	PBC-24-G-22-KL	2.0 ft	Straight
4	PAC-18-KL	1.5 ft	
5	PAC-12-KL	1.0 ft	

TABLE A-2 PITOT TUBES USED IN EXPERIMENTS

The pitot-static tubes had to be mounted to minimize or eliminate movement of the tip and vibration while allowing for flexibility of positioning in two or three directions. For channels A and B, aluminum angle set along both sides of the top of the channel acted as runners for slotted teflon blocks which carried a slide mechanism for positioning across the channel width. This slide carried a vertical track in which a 1/4 inch metal tube could be raised or lowered with the pitot tube attached and braced at the lower end of the 1/4 inch tube. The teflon blocks also carried a wooden platform to which the pressure transducer was securely mounted. Each part of the positioning device could be locked in place. Sketches of the mounting system and channel are available in reference (42).

The pitot tube was connected to 1/8 inch tygon tubing and then 1/8 inch stainless steel tubing with appropriate needle valves and fittings to facilitate filling of the system with water. The transducer, Validyne Variable Differential Pressure Transducer, Model DP-15, with a 0.1 psi diaphragm was sensitive to 0.1%. The transducer was connected to a Validyne Indicator, Model CD-12, which transmits a voltage equivalent to a percentage of the maximum pressure difference from the pitot tube. The great sensitivity of this system required that the position of the plastic connecting tubes between the pitot tube and transducer be fixed to prevent shifting of the zero setting. By moving the transducer with the pitot tube, as described, this problem was largely eliminated. However, re-zeroing was required after vertical movement of the pitot tube.

The output of the Validyne Indicator, with a maximum of ten volts, was connected through an RC averaging circuit either to a digital D.C. voltmeter (Model #242008, United Systems Co.) or to a Bausch and Lomb VOM5 recorder. Transducer signals were often of large amplitude with fluctuations on the order of a second or less (examples are shown in references (42) and (43)) making eyeball averaging difficult. To minimize this source of error a simple RC circuit with a 1000 μf 25 volt electrolytic capacitor in series with a variable resistance box, with a range of 1 to 10^7 ohms, was used. The resistance, R, was increased to increase the time constant, RC, until fluctuations were damped enough to read the mean value of the signal. Time constants were usually chosen to be less than 30 seconds with less than five minutes required for a reading. Details are available in references (42) and (43).

Velocity measurement was essentially the same for each system with a variation in pitot tube size and length as required for maximum stability. But the pitot positioning technique was of necessity different for measurements in the pool. Here a Unistrut channel (1 5/8 x 1 5/8 inches) was set across the top of the pool along a diameter. A teflon block was machined for a slide fit inside the channel and could be pulled from either end to position it as desired along the diameter. The pitot tube was mounted in a slot on a vertical track which was fastened to the block. To move the tube vertically, it was necessary to bring it to the side of the pool and then return it to the desired radial position.

EXPERIMENTS WITH WATER JETS

Studies of water jet induced circulation were carried out primarily in channel A with a few in channel B. Velocity measurement was as described for aeration. To hold the water level constant an overflow drain system was added at both ends of the tank. Each end plate contained two horizontal lines of four threaded holes. Half inch plastic blocks threaded as 90° ells were screwed to pipe nipples extending through one line of end plate holes and were attached to a drain line outside of the channel. The other side of the ells carried 1/2 inch PVC vertical pipe sections cut to the desired water level position. Sets of these level controlling tubes of several lengths were prepared. The overflow water drained to a 20 gallon plastic tank which was connected to the inlet of a pump (Price Pump, Co., Model #E100-100B). The water was pumped through an 11.0 gpm rotameter with flow rate control achieved with values and diversion of part of the flow back to the 20 gallon tank.

The manifold was 1/2 inch PVC pipe with an inlet elbow at one end set flush with the tank bottom along the wall and ground down to be almost the same level as the top of the manifold. Manifold W-1 had four 1/16 inch orifices per inch over the full length, but gave a very nonuniform vertical velocity profile especially at higher flow rates, and was not used for measurements. Manifold W-2 had eight 1/16 inch orifices per inch and resulted in a symmetrical vertical velocity distribution across the channel as described in the main text.

DISSOLVED OXYGEN MEASUREMENTS

Dissolved oxygen concentrations were obtained with a Chemtrix, Type 30 D.O. Meter and Chemtrix Oxygen probe. The probe was mounted as were the pitot tubes and could be positioned anywhere in the channel although usually it was set along the centerplane at half the water depth. Meter operation followed standard procedure with temperature measurement and compensation.

To simplify data interpretation, D. O. in the fresh tap water used to fill the channel was removed by adding anhydrous sodium sulfite and $CoCl_2.6H_2O$ as catalyst at concentrations of eight and five mg/liter respectively per ppm D.O. These chemicals were added separately from a pressurized injection tank through a distributor moved slowly over the channel to achieve uniform distribution and removal of D.O. in the channels. The distributor was 1/2 inch PVC pipe with 1/16 inch holes spaced four per inch along a single line, and connected to the pressurized tank with flexible tubing. In addition, a mixing device consisting of horizontal rods was moved through the tank after chemical addition to assure uniform concentration.

Air flow rate was measured with the Brooks 8.32 scfm rotameter and two smaller Gilmont flow meters (Size No. 3 and 5). After chemical removal of tap water D.O., the air flow rate was set as desired and a stop watch started. D.O. readings were taken periodically until a steady (or nearly constant) final reading was reached. D.O. measurements were found to be of excellent reproducibility for duplicate experiments on different days.

VISUALIZATION

Injection of a dark colored dye (gentian violet or methylene blue at 1/2 gm liter) from a pressurized tank through hypodermic tubing (0.023 inch ID) was useful to define the limits of the circulation cell and general characteristics of the flows. Mounting was as for the pitot tube for flexibility or with the hypodermic hand-held.

Spherical plastic particles modified so that they were almost neutrally buoyant were prepared to enhance flow visualization for motion pictures. They were useful in defining the limits of the circulation cell, the strong vertical flow above the manifold and more generally showing the highly turbulent and time varying nature of the flows. In some cases, the times of transit of a particle along the surface from above the manifold to the end of the cell were compared with calculated times from velocity decay laws with good agreement. Some preliminary attempts at flow visualization with hydrogen bubble generation were soon abandoned because of the highly turbulent nature of the flows.